Realistic forests and the modeling of forest–atmosphere exchange

E. J. Bannister[1,2], A. R. MacKenzie[1,2], and X. -M. Cai[2]

[1] Birmingham Institute of Forest Research (BIFoR), University of Birmingham, Edgbaston, Birmingham, B15 2TT, United Kingdom.

[2] School of Geography, Earth and Environmental Sciences, University of Birmingham, Edgbaston, Birmingham, B15 2TT, United Kingdom.

Corresponding author: Rob MacKenzie (a.r.mackenzie@bham.ac.uk)

Key Points:

- Forests are becoming increasingly fragmented. Patchy landscapes and non-ideal weather complicate the interpretation of observations.
- Turbulence-resolving models can capture scalar transport, plant movement, varied atmospheric conditions, and site-specific structure.
- Models capturing forests more realistically will simulate fluxes better but need targeted observations and new parametrizations.

Abstract

Forests cover around 30% of the Earth's land area but are becoming increasingly fragmented. In many parts of the world, edge effects dominate most of the forested area. Inhomogeneous landscapes and non-ideal weather conditions generate fluid dynamical features that cause observations to be inaccurately interpreted, biased, or over-generalized. We discuss progress towards capturing the complicated reality of forests in turbulence-resolving models. Scalar transport does not necessarily follow the flow in complex terrain, meaning scalar quantities are rarely at equilibrium around patchy forests, and significant scalar fluxes may form in the lee of forested hills. Gaps and patchiness generate significant spatial fluxes that current models and observations neglect. Atmospheric instability, driven by differential heating of the canopy, increases the distance over which fluxes adjust at forest edges. For deciduous forests, the effects of patchiness differ between seasons; eddies reach further into rougher, leafy canopies. Air parcel residence times are likely much lower in patchy forests than homogeneous ones, particularly around edges. However, the modeled probabilities of gusts are sensitive to the model setup, including any stochastic element. Eulerian parametrizations now allow researchers to investigate forest chemistry and particle deposition in the turbulent flow. The reconfiguration of plants under wind loading can be captured efficiently by modifying the velocity dependence of the aerodynamic drag. Future challenges include: (i) targeted observations in patchy landscapes; (ii) developing parametrizations of turbulent transfer applicable to larger scales; (iii) developing numerically efficient improvements to model forest structure; and (iv) simulating a greater range of weather conditions.

Plain Language Summary

Plants live by an intricate set of exchanges with the atmosphere. They draw carbon dioxide from the air—while being buffeted by the wind—and release water vapor, oxygen, pollen, and a variety of organic compounds. These exchanges are especially intricate in forests, where microbes and animals add to the quantity and variety of exchanges. Forests' patchwork structures mean that certain trees may experience profoundly different climates to others only meters away. These exchanges are made yet more complicated by the fragmentation of forests by human activity. This review of the computational modeling of exchanges between forests and the air focuses on practical ways to improve the realism of the modeling. No model can recreate all the exchanges in detail. However, capturing more of the edges, gaps, and patches in real forests, as well as non-ideal weather conditions, will improve our understanding of forest-atmosphere exchanges. This will aid scientific understanding and policy making for forest ecology, meteorology and climatology, and air and water quality.

1 Introduction

1.1 Fragmentation and forest–atmosphere interactions

Forests around the world are becoming increasingly fragmented (Bogaert et al., 2011; Fahrig, 2003; Riitters et al., 2000; Taubert et al., 2018). Only about half of the world's remaining forest area, mostly in the Amazon and the Congo Basin, lies more than 500m from the nearest edge (Haddad et al., 2015). In much of the Northern Hemisphere, forests are small and patchy because they are located close to areas where large populations of humans have lived for centuries. As an extreme example, approximately three-quarters of English woodland lies less than 100 m from the nearest edge (Riutta et al., 2014). Extensive edges, including internal

edges around clearings, alter how forests interact with the surrounding environment. Edge regions are different to the forest interior both in their mean local climate (e.g., less humid) and in the range of meteorological extremes they experience (Crockatt & Bebber, 2015; Magnago et al., 2015). Edge-region climate slows woody-debris decomposition (Crockatt & Bebber, 2015), increases transpiration (Kunert et al., 2015), and affects the carbon budget (Froelich et al., 2015; Schmidt et al., 2017). Local climatic changes affect the forest ecology by favoring certain plant species (e.g., Bertrand et al., 2020; Zellweger et al., 2020) or altering the habitats of forest-dwelling animals (Pfeifer et al., 2017). Internal fragmentation from logging and road building facilitates the spread of invasive plant species through forests (Mortensen et al., 2009; With, 2002). Forest edge and patch environments are important ecologically and make up an increasingly large fraction of the total forest ecosystem. The variation in energy balance, water balance, and ecology across different forest structures implies differing exchange of momentum, and of scalar quantities transported with the flow such as CO_2, water vapor, biogenic volatile organic compounds (BVOCs), and anthropogenic and biological aerosol particles.

It is more difficult to measure forest–atmosphere exchange in patchy forests than in large, intact ones. For chemical species for which sufficiently fast sensors exist, eddy covariance is the standard method for investigating forest–atmosphere exchange at an ecosystem scale (Aubinet et al., 2012; Baldocchi et al., 2001; Hicks & Baldocchi, 2020; Oliphant, 2012). The technique assumes certain conditions about the surface and the flow, for example, that the forest is horizontally homogeneous below height of the instruments and that the flow is stationary. Around forest edges and in other complex terrain, these assumptions are seldom satisfied even approximately, causing the estimates of exchange to be inaccurate or biased. This is a well-documented problem (Baldocchi, 2008; Stoy et al., 2013; K. Wilson et al., 2002) which remains unresolved despite sophisticated efforts to refine the eddy-covariance technique (Aubinet et al., 2010) or to correct measurements collected during problematic weather conditions (Acevedo et al., 2009; Wharton et al., 2017). This problem is becoming increasingly relevant as forests become patchier and more fragmented.

1.2 The scope of this review

Researchers typically approach modeling forest–atmosphere interactions from one of two directions. The first focuses on the effect of forests on the atmosphere, for example, on leaf boundary layers (Schuepp, 1993a) and evapotranspiration (Katul et al., 2012) at small time and space scales, and on climate feedbacks at larger time and space scales (Bonan et al., 1992; Rap et al., 2018; Spracklen et al., 2008). The second approach focuses on the effect of the atmosphere on vegetation, such as on plant biomechanics (Gosselin, 2019; De Langre, 2008, 2019; Vogel, 2009) or water use efficiency (Schymanski & Or, 2016) at small scales, to ecosystem changes at larger scales (Canadell & Raupach, 2008; Norby et al., 1999; Zohner et al., 2020). While these approaches overlap, researchers use different techniques depending on the physical process and scale of interest. In this review, we concentrate on models of forest–atmosphere interactions across length scales of up to a few kilometers and time scales of up to several hours. We refer to this as the ‘fragment scale’, which approximately corresponds to the ecological scales from ‘individuals’ to ‘patches’ (Scholes, 2017) and the meteorological micro– and γ–mesoscales (Stull, 1988).

At the fragment scale, we can consider forests as cohesive units, which may exist as isolated fragments or as part of a larger whole. In approximately homogeneous canopies, one expects a certain amount of statistical homogeneity in the flow of air and the forest structure. However, forest patchiness and challenging weather conditions induce non-random fluid dynamical phenomena that violate the assumptions of eddy covariance and are not easy to constrain in parametrizations for larger scale models. Recent reviews have discussed the modeling of land–atmosphere interactions more generally (Fisher & Koven, 2020), flow in vegetation canopies (Belcher et al., 2012; Brunet, 2020), and ecological processes such as evapotranspiration (Katul et al., 2012). We supplement these reviews by focusing on practical steps to improve numerical models of forest–atmosphere exchange, particularly as tools to interpret field observations in real-world patchy landscapes and challenging weather conditions. Developments in theory, computational capacity and observational networks offer the potential to improve scientific understanding and policy across forest ecology, meteorology and climatology, air and water quality, and land management. Section 2 summarizes the main fluid dynamical phenomena relevant to forests and the representation of forests in numerical models. Readers from a micrometeorological background may wish to skim read sections 2.1–2.4. We discuss four main topics in the remainder of the review: (i) the realities of forest structure and its representation in numerical models (section 3); (ii) developments in the theory and modeling of scalar transport around patchy forests (section 4); (iii) incorporating atmospheric phenomena such as stability, air parcel residence time, and non-passive scalar quantities into high-resolution models (section 5); and (iv) modeling the effect of wind on forests, accounting for processes such as plant reconfiguration (section 6). We conclude in section 7 and provide recommendations for further research.

2 Flow in and around forests

2.1 Definition of terms

We use right-handed Cartesian tensor notation, with the Einstein summation convention, and indices (i, j, k) take values (1, 2, 3) respectively. For example, u_i is the velocity in the x_i direction, with i = 1, 2, 3 representing the streamwise (x), spanwise (y) and vertical (z) directions. We denote $x=(x, y, z)$, $(u¿¿1, u_2, u_3)=(u, v, w)¿$, and time as t. For a resolved quantity, ϕ, $\langle\phi\rangle$ denotes a spatial average and $\overline{\phi}$ denotes a time average such that $\phi(x,t)=\langle\phi\rangle(t)+\phi''(x,t)$ and $\phi(x,t)=\overline{\phi}(x)+\phi'(x,t)$. We refer to the quantities $\phi''(x,t)$ and $\phi'(x,t)$ as the 'dispersive' and 'turbulent' quantities, respectively, which reflect local departures from the space and time averages. The n^{th} moment, where n is a positive integer, is given by $\langle\phi'^n\rangle$. The standard deviations of the velocity components are $\sigma_{u_i}=\langle u_i'^2\rangle^{\frac{1}{2}}$, the mean turbulence kinetic energy (TKE) $¿\frac{1}{2}\langle\overline{u_i'^2}\rangle^{\frac{1}{2}}$, skewness $Sk_{u_i}=\langle u_i'^3\rangle/\langle u_i'^2\rangle^{\frac{3}{2}}$, kurtosis $Kt❑_{u_i}=¿\langle u_i'^4\rangle/\langle u_i'^2\rangle^2$, and the friction velocity, $u_¿=\left(\langle\overline{u'w'}\rangle^2+\langle\overline{v'w'}\rangle^2\right)^{\frac{1}{4}}$.

Forests are located in the atmospheric boundary layer (ABL), the layer of atmosphere that is directly influenced by the Earth's surface. Figure 1 presents a schematic of the idealized structure of the daytime ABL. The top of the daytime ABL, at height z_i, caps the mixed layer, within which variables such as humidity and potential temperature are approximately

constant with height. The lowest 10% or so of the ABL is known as the atmospheric surface layer (ASL), analogous to the 'inner region' in wall boundary layers. Above rough surfaces, such as forests and urban areas, the ASL can be further divided into the inertial sublayer (ISL) and the roughness sublayer (RSL) (Raupach et al., 1991). Within the ISL, the turbulent fluxes of momentum and scalar quantities are approximately constant with height. These constant fluxes are used as scaling parameters in a set of relationships known as Monin–Obukhov similarity theory (MOST) (Foken, 2006; Monin & Obukhov, 1954; Stull, 1988). MOST is widely used in surface-layer parametrisations for numerical weather prediction and climate modeling (Hari Prasad et al., 2016; Skamarock et al., 2008). The RSL extends from the ground up to around 1.5–5 times the mean height of the obstacles h_c, known as the blending height. The lowest part of the RSL, from the ground to $z=h_c$, is the canopy layer, in which obstacles and air are intimately intermingled. In neutral atmospheric conditions, turbulent structures that scale with the mean canopy height h_c control the exchange of momentum and scalar quantities between air and the surfaces of the obstacles. The friction velocity u_* can be interpreted as a measure of the mean velocities of the turbulent eddies. It is often used as a shorthand for ASL turbulence, with higher values indicating more turbulent conditions. However, u_* is only clearly defined in the ISL. Around forests, the complexity of the flow means that u_* alone provides limited information about the turbulence (Wharton et al., 2017)

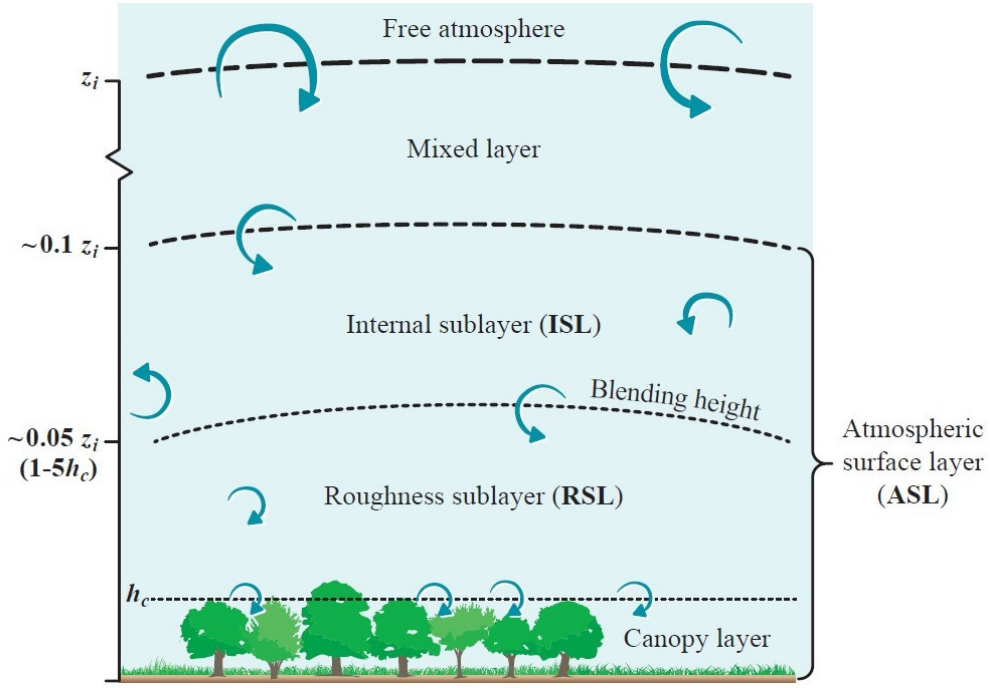

Figure 1. Sublayers of the daytime atmospheric boundary layer (ABL) over a forest. The figure follows the classification in Oke (1988) for an urban boundary layer. The height of the mixed layer, which typically accounts for around 90% of the daytime ABL height, is suppressed to aid presentation. The variables z_i and h_c denote the height of the ABL and the mean height of the forest, respectively.

2.2 Representing forests in numerical models

Early models of flow in vegetation canopies accounted for the presence of the plants through empirical drag terms based on spatially averaged velocity measurements (Cionco, 1965; Inoue, 1963). In the 1970s and 1980s, researchers developed a more formal basis for the plants' presence, often referred to as the 'double-average method', which proceeds directly from the transport equations (Finnigan, 1985; Raupach et al., 1986; Raupach & Shaw, 1982; N. R. Wilson & Shaw, 1977). This is achieved using a volume average operation such that, for a resolved quantity ϕ,

$$\langle \phi \rangle (x,t) = \frac{1}{V} \iiint \phi (x+r,t)\, dr. \quad (1)$$

The spatial average in equation (1) is over a volume that (a) includes multiple trees and plants, but (b) is small compared to the distance over which the structure of the forest varies. The vertical resolution is high in order to properly resolve the flow gradients (Finnigan & Shaw, 2008). Around the same time, researchers applied similar procedures to investigate mass transfer in engineering applications (Howes & Whitaker, 1985; Whitaker, 1973). Because plant elements occupy a small proportion of the available volume, no distinction is typically made between the 'superficial' averaging operation (including air and plant elements in the average) and the 'intrinsic' average (within the body of fluid only), although this distinction can be important in urban areas (Schmid et al., 2019). The averaging operation is followed by a time average sufficient to capture the dominant scales of motion. Applying the two operations to the continuity and momentum equations, ignoring the Coriolis force and the momentum transfer from viscosity, gives

$$\frac{\partial U \square_i}{\partial x_i} = 0, \quad (2a)$$

$$\frac{\partial U_i}{\partial t} + U_j \frac{\partial U_i}{\partial x_j} = \frac{-\partial P}{\partial x_i} + \frac{g}{\theta_0} \langle \overline{\theta}_v \rangle \delta_{i3} - \frac{\partial \langle \overline{u_i' u_j'} \rangle}{\partial x_j} - \frac{\partial \langle \overline{u}_i \text{ overline } \{\{u\} \text{ rsub } \{j\}\} \rangle}{\partial x_j} + f_i, \quad (2b)$$

where P is the kinematic pressure, g is the gravitational acceleration, θ_0 is a reference temperature, θ_v is the virtual potential temperature, and δ_{i3} is the Kronecker delta (non-zero when i = 3). Capital letters denote the double-averaged quantities, which we refer to as the mean quantities—e.g., the mean streamwise velocity component U. The term $-\partial \langle \overline{u}_i \text{ \{overline \{u\}\} rsub \{i\} } \rangle / \partial x_j$is the dispersive flux of mean momentum, which accounts for spatial correlations in the time-averaged velocity field. The dispersive flux is usually assumed to be low in homogeneous forests and is therefore typically disregarded in numerical models (Patton & Finnigan, 2012). However, recent evidence suggests that the

dispersive fluxes of momentum and scalar quantities can be significant around patchy forests (see sections 3.3 and 4.3).

The aerodynamic drag of the forest (per unit mass of air) is accounted for through the term f_i (m s^{-2}) on the right-hand side of equation (2b). This term is the net sum of (i) the form drag from pressure differences either side of each plant element, and (ii) the viscous boundary layers that develop over each plant element,

$$f_i = -\left\langle \frac{\partial \overline{P}''}{\partial x_i} \right\rangle + \nu \left\langle \frac{\partial^2 \overline{u}''}{\partial x_j \partial x_j} \right\rangle, \quad (3)$$

where ν is the kinematic viscosity of air. This term is usually parametrized as spatially distributed drag, which we discuss in section 3. See Finnigan (2000) and Finnigan & Shaw (2008) for more detailed discussion of the double-average method.

Researchers have adopted various approaches to find approximate solutions to the double-averaged equations, including first-order analytical closure (Finnigan et al., 2015, and references therein), modified gradient-diffusion theory (Zeng & Takahashi, 2000), Reynolds-averaged Navier–Stokes (RANS) solvers (Boudreault et al., 2015; Brunet, 2020, and references therein; Katul & Albertson, 1998), and large-eddy simulation (LES) (Shaw & Schumann, 1992). Direct numerical simulation (DNS) has recently been used for small, idealized plant canopies (Sharma & García-Mayoral, 2020b, 2020a). However, the computational expense of DNS means it can still be employed only for relatively low Reynolds number (*Re*) flow and that it remains unsuitable for fragment-scale investigations around forests. Of these techniques, LES has emerged as the most popular method for investigating fragment-scale exchange around forests, although analytical closure schemes and RANS remain popular for situations that do not require the turbulence to be resolved. Using LES, a low-pass filter is applied to the momentum equations, where the spatial filter is analogous to the volume average in equation (1). This divides the flow into numerically resolved motion larger than the spatial filter, and smaller sub-grid scale (SGS) motion, which must be parametrized (section 3.5). The main advantage of LES is that the largest scales of motion are expressly resolved, allowing visualization and term-by-term analysis of the turbulent flow of air that is impossible to achieve using observations or physical models.

2.3 The turbulence structure around forests

As air moves through a forest, momentum is transferred from the flow to the aerial parts of the plants and trees. This reduces the streamwise wind speed throughout the depth of the canopy and a region of high wind shear forms around the crown top. The shear region is evidenced by an inflection in the mean streamwise wind-speed profile, which is approximately exponential within the canopy and logarithmic above it (Finnigan, 2000; Raupach et al., 1996). A secondary maximum in the streamwise wind speed sometimes occurs in the trunk space, especially near edges and in forests with sparse understories (Dupont et al., 2011). The high shear around the crown top generates Kelvin–Helmholtz-type instabilities, which in turn generate coherent large eddies around the tops of the trees, analogous to the dominant processes in a plane mixing layer (Raupach et al., 1996). Using the analogy of vorticity thickness in a mixing layer, Raupach et al. (1996) reduce canopy turbulence to a single length scale, $L_s = U_{h_c} / (\partial U / \partial z)_{h_c}$, where U_{h_c} is the mean streamwise

velocity component U at $z=h_c$. The shear length scale L_s, which equates to around $0.5h_c$ for medium density vegetation, provides a rough estimate of the diameter of the dominant turbulent eddies. It is difficult to determine the value of L_s exactly for real forests because dU/dz varies quickly with height around the crown top (i.e., d^2U/dz^2 is not easily defined).

The presence of the trees and plants affect the flow statistics in distinctive ways. The second-order moments $\langle\overline{u'^2}\rangle$, $\langle\overline{w'^2}\rangle$, $\langle\overline{u'w'}\rangle$ and the TKE increase with height within plant canopies, but are roughly constant above the canopy (Brunet, 2020; Raupach et al., 1996). The turbulent velocity components u' and w' are more correlated and skewed in the RSL than they are in the ISL above, where many velocity statistics display approximately Gaussian behavior. Streamwise and vertical skewness (Sk_u and Sk_w) are approximately zero in the ISL but take values $0.5 \le Sk_u \le 1$ and $-1 \le Sk_w \le 0$ in forests (Amiro, 1990; Kruijt et al., 2000; Lee & Black, 1993; Raupach et al., 1996; Villani et al., 2003). The values of Sk_u and Sk_w may be higher, absolutely, at forest edges (Dupont & Brunet, 2008a). The association of positive Sk_u and negative Sk_w values indicates that turbulent transfer is dominated by strong but infrequent downward penetrations of air into the canopy, known as 'sweep motions' ($u'>0$ and $w'<0$). Frequent upward motions of low-momentum air from within the canopy, known as 'ejections' ($u'<0$ and $w'>0$), also account for a large proportion of the turbulent transfer (Shaw & Patton, 2003), although sweep motions contribute more to the total transfer of momentum around the crown top (Raupach et al., 1996; Shaw & Tavangar, 1983). Together sweep motions and ejections account for between 60% and 80% of the exchange of scalar quantities from homogeneous forest canopies to the atmosphere aloft (Gao et al., 1989). The greater magnitudes of the skewness statistics around forest edges reflect the significant differences in momentum and scalar exchange in patchy and gappy forests as compared to homogeneous canopies.

The mixing-layer analogy—where the turbulence is dominated by shear generated eddies around the crown top—has proved remarkably robust in forests and other vegetation. However, current understanding of canopy turbulence is far from complete, particularly around patchy forests. Further LES studies and targeted observations will help to reveal to what extent three-dimensional structures dominate the turbulence, to what extent the mixing-layer analogy breaks down when the canopy is patchy, and the density of trees that is required for the flow to transition from boundary-layer to mixing-layer-type flow (mixing-layer behavior has been observed at low densities). The impact of atmospheric stability and precipitation on fragment-scale forest–atmosphere exchange is also poorly understood. For good reason, modeling studies have typically sought 'canonical' dynamical behavior that occurs in different types of vegetation. However, this has usually meant neglecting buoyancy and other challenging weather, despite their significant impact on both the forest ecology and the flow dynamics (see section 5.1). For further discussion of plant-canopy turbulence see Finnigan (2000) for flow statistics and technical background, Bailey & Stoll (2016) and Finnigan et al. (2009) for the emergence of coherent fluid structures, Belcher et al. (2012) for scaling analysis in complex terrain, and Brunet (2020) for historical background and a review of recent studies in homogeneous plant canopies.

2.4 Flow adjustment around forest edges

Figure 2 presents a schematic of the statistical patterns in momentum transfer that emerge as the flow adjusts around the edges of a small forest in neutral atmospheric conditions (Belcher et al., 2003, 2012; Dupont & Brunet, 2008a, 2009).

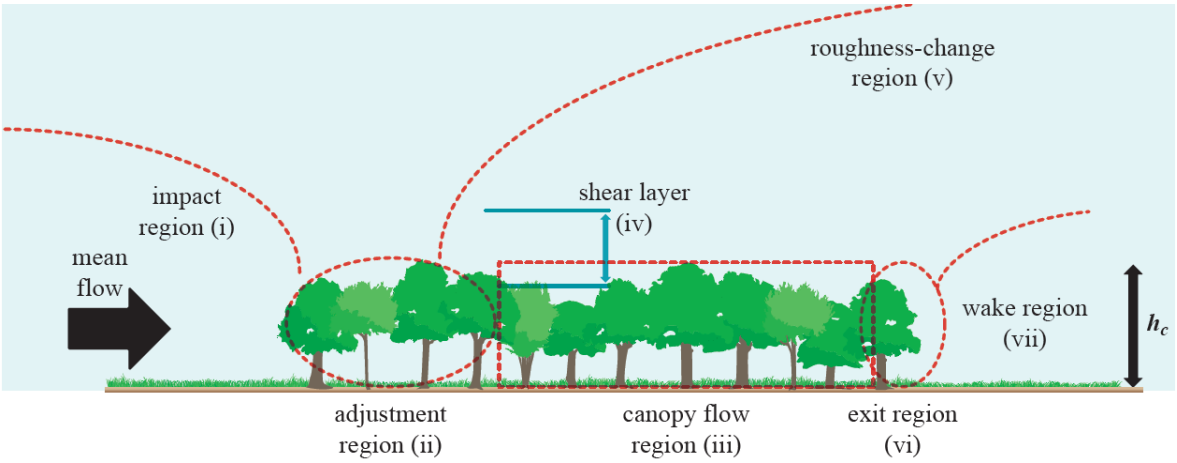

Figure 2. Dynamical flow patterns around a small forest in neutral atmospheric conditions. Each pictured tree represents approximately three trees in the streamwise direction. Figure after Belcher et al. (2003) and Dupont and Brunet (2009). The stylized edge profile of the schematic forest is discussed in section 3.2.

In the *impact region*, (i) in Figure 2, the forest acts as a step-change in porosity, inducing a pressure gradient to slow the flow. Just downstream of the forest edge is the *adjustment region*, (ii) in Figure 2, in which the drag from the trees decelerates the flow over a distance x_A proportional to a canopy drag length scale $L_c = 1/C_d a(z)$ (Belcher et al., 2003, 2012; Rominger & Nepf, 2011), where $a(z)$ ($\mathrm{m^2\ m^{-3}}$) is a height-dependent function of local plant density, and C_d is a dimensionless drag coefficient. The length scale L_c emerges from quasi-inviscid solutions to the momentum equations in one-dimensional flow. It can be interpreted as a distance constant over which the velocity and drag adjust to balance the pressure gradient (Finnigan & Brunet, 1995). At the edge of homogeneous canopies, assuming constant shear, and neutral atmospheric conditions, $L_c \approx L_s U_{hc}^2 / 2u_*^2$. Because L_c is inversely proportional to the plant density, the flow adjusts more quickly with increasing forest density, provided the density varies on scales greater than the volume averaging operation. The length scale L_c is only an approximation for three-dimensional flow around real forests, for which the variables C_d and $a(z)$ may not be clearly defined (sections 3 and 6). Nonetheless, numerical simulations, field observations and flume experiments of vegetation canopies show the adjustment distance x_A downstream of a forest edge is indeed proportional to L_c, with $x_A \approx 4$–$6L_c \approx$ 8–$10h_c$(Belcher et al., 2012; Morse et al., 2002; Rominger & Nepf, 2011; Yang, Raupach, et al., 2006).

In the *canopy-flow region*, (iii) in Figure 2, the flow is fully adjusted to the presence of the forest. The *canopy-shear layer* (iv) is characterized by the shear-generated turbulent eddies that exchange most of the energy, mass and momentum between the forest and the atmosphere. These eddies are generated by processes analogous to those in a plane mixing layer (Raupach et al., 1996). Downstream of the adjustment region, an internal boundary layer may begin to develop above the trees, known as the *roughness-change region* (v). If

there is low vegetation or a large clearing in the lee of the forest, an *exit region* (vi) forms, within which mean wind speed increases, with a corresponding downwards flow, over a streamwise distance 1–2h_c. A *wake region* (vii), in which the flow recirculates, may form in the lee of relatively dense forests (Cassiani et al., 2008). The formation and strength of the recirculation depends on the density on the forest, but appears to be relatively independent of its foliage distribution (Ma et al., 2020).

2.5 The edge regions in context

Simple geometric considerations show that the area of forest subject to edge effects, the 'edge region', is surprisingly large. Among two-dimensional shapes with the same area, a circle has the shortest perimeter, i.e., we can consider it the most compact shape in terms of its edge to area ratio. By approximating the plan of a forest stand as a circle, we obtain a lower limit to the area of the edge region from the annulus of widthx_A, where x_A is the flow's adjustment distance. The lower limit for the ratio R_0 of the area of the edge region to the total stand area is therefore

$$R_o = \frac{x_A(2r - x_A)}{r^2} = \frac{\pi . x_A\left(2\sqrt{\frac{A}{\pi}} - x_A\right)}{A}; r \geq x_A > 0, \quad (4)$$

where A is the area of the forest stand and r is the radius of the equivalent-area circle. Taking $R_0 > 1/2$ in equation (4) shows the edge region comprises over half the forest stand where $\sqrt{A/\pi} < (2+\sqrt{2})x_A$, i.e., where $A < (6+4\sqrt{2})\pi x_A^2$. Because most forest stands are not even approximately circular, the area subject to edge effects is substantially larger than this minimum. As a conservative heuristic for non-circular forests, we suggest edge effects dominate an area 25% greater than the area of the equivalent-area circle, therefore, where $A < 1.25 \times (6+4\sqrt{2})\pi x_A^2 \approx 46 x_A^2$. Taking $x_A \approx 8 h_c$—the lower end of reported values of x_A—provides a rule-of-thumb that edge effects dominate in forest stands where $A < 3000 h_c^2$. Since forested areas are usually reported in hectares and canopy heights in meters, a dimensional version of the rule-of-thumb is

$$A(ha) < 0.3\left[h_c(m)\right]^2. \quad (5)$$

For example, for a mature forest with a canopy height of 20 m, edge effects dominate for patches whose area are less than 120 ha. In many parts of the world (Haddad et al., 2015), edge effects dominate most of the forested area.

3 Beyond idealized forest structures

3.1 The drag parametrization and its simplifications

The aerodynamic drag f_i in equations (2) and (3) is typically parametrized[1] by spatially averaging the localized drag from the individual plant elements as

$$f_i = -C_d a(z)|U|U_i, \quad (6)$$

where $|U| = (U_j U_j)^{\frac{1}{2}}$ and the drag coefficient C_d is usually specified as a constant, with values ranging from 0.1–0.5 (Table A1). This parametrization, which we refer to as the 'distributed-drag method', assumes the aerodynamic drag from the forest increases with the square of the velocity, as is the case around bluff bodies (Shaw & Schumann, 1992; N. R. Wilson & Shaw, 1977). The viscous component of the drag is usually neglected in the approximation of f_i because form drag dominates in high-*Re* flow through forests (Thom, 1971). The local forest density $a(z)$ is typically assumed to be a function of the plant area density (PAD), the total one-sided plant area per unit layer volume (m^2/m^3). The plant area index (PAI) is the PAD integrated over the height of the forest h_c, i.e., PAI $= \int_0^{h_c} a(z)dz$. Figure 3a shows $a(z)$ derived using the parametrization by Lalic and Mihailovic (2004), as employed by Yan et al. (2020), among many others. The Lalic and Mihailovic parametrization is flexible, covering a broad range of densely packed, even-aged monocultures, but it is less suitable for discontinuous canopies, uneven-aged forests, and 'standards with coppice' forest forms, which have multiple modes of leaf density. Other vertical profiles of $a(z)$ are typically scaled or generated empirically from published PAI values. However, some studies have specified $a(z)$ using field measurements (Dupont et al., 2011) or terrestrial laser scans of forests (Schlegel et al., 2012) – see Table A1 for a summary of the various techniques used. The canopy drag length scale permits an alternative expression for the PAI of a forest: PAI $= h_c a(z) \approx a$, so that PAI $\approx h_c / C_d L_c$. This is only a rough approximation, because it assumes the plant area is evenly distributed in all directions. Modeling studies have used PAI values in the range 1–8, with most studies concentrating at the low-to-medium end of the range (Table A1). The relative scarcity of studies using PAI > 5 is surprising given that values in tropical and conifer forests often fall in the range 8–12 (Fleischbein et al., 2005; Lefsky et al., 1999).

[1] This parametrization is based on the aerodynamic drag equation, used in fluid mechanics and engineering applications. In the fluid mechanics literature, the drag equation (per unit mass) is usually written with a factor of ½, which originates from the formula for the kinetic energy of the fluid in front of the body. By meteorological convention, the factor of ½ is included in the drag coefficient and does not appear expressly here.

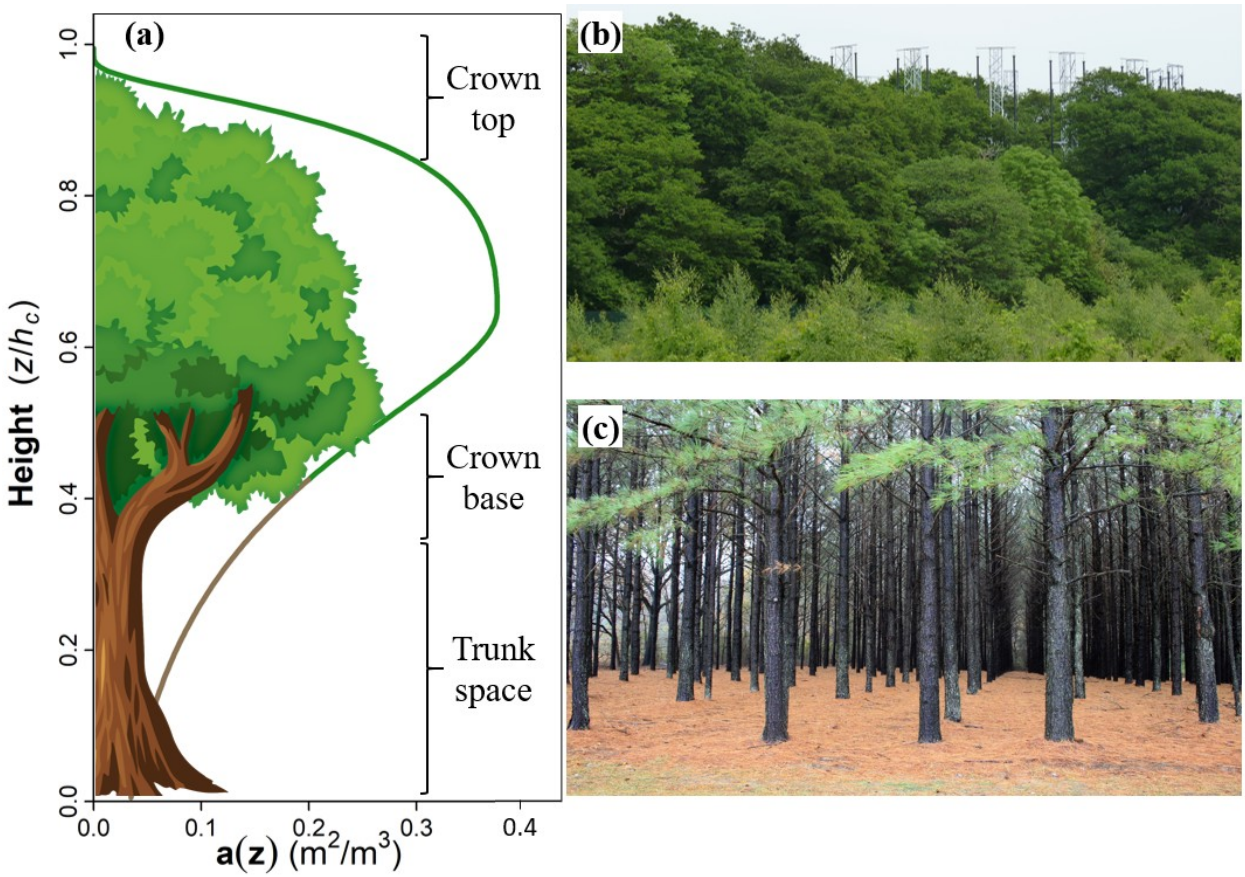

Figure 3. (a) Vertical profile of PAD, $a(z)$, calculated using the formula derived by Lalic and Mihailovic (2004; (b) the southern edge of the oak-dominated woodland at the Birmingham Institute of Forest Research (BIFoR) free-air carbon dioxide enrichment (FACE) facility belonging to the authors' institute; and (c) open trunk space of an even-aged *Pinus taeda* monoculture plantation.

The distributed-drag method was introduced in the 1970s and remains the starting point for numerical investigations of forest–atmosphere exchange in the turbulent ASL. The approach accurately resolves the mean flow around bluff bodies and through homogeneous forests (Yang et al., 2006). However, it poorly reproduces higher-order flow statistics around forests and in other vegetation canopies (Dupont & Brunet, 2008a; Ma & Liu, 2019; Pan, Chamecki, et al., 2014). It also makes several unrealistic assumptions about the canopy structure, which are especially relevant when forests are patchy. First, while the drag force is time dependent, the local foliage density $a(z)$ varies only with height, if at all. The forest is therefore assumed to be horizontally homogeneous at each height, reducing the forest morphology to a single dimension (z). In reality, forest canopies comprise a patchwork of openings of many shapes and sizes, formed by senescence, disease, and windthrow (Hirons & Thomas, 2018; Whitmore, 1989) as well as human activities (Figure 4). These gaps are significant ecologically and structurally. The floras of the northern temperate forests, for example, include many species that depend on gaps and patchiness (Fox, 1977; Tinya et al., 2009; White, 1979).

A second assumption underlying the distributed-drag method is that forest edges are structural continuations of the main body of the canopy (Dupont & Brunet, 2008a; Kanani-Sühring & Raasch, 2015; Ma et al., 2020). Unless the forest has been recently disturbed, this assumption is unrealistic because many trees and understory plants grow into the light to maximize the leaf area available for photosynthesis, thereby forming an almost closed edge (see the example in Figure 3b). Failing to account for the true structure of forest edges strongly overestimates the penetration of air into the forest (Schlegel et al., 2012, 2015), and neglects the possibility of dispersive fluxes of momentum and scalar quantities (Boudreault et al., 2017; Q. Li & Bou-Zeid, 2019). Third, even where $a(z)$ is treated as varying with height, most studies represent the plant area as being distributed very densely in the tree crowns and sparsely in the trunk space (Figure 3a). This is a reasonable approximation for certain forests, such as unthinned conifer plantations (Figure 3c), but a poor approximation for forests with extensive understory growth.

3.2 Modeling forest patchiness

At which scale do canopy gaps begin to matter? As regards light penetration, Zhu et al. (2015) propose three categories of gap sizes in temperate forests: 'small' $0.49 \lesssim R_{O_d/h_c} \leq 1$; 'medium' $1 \lesssim R_{O_d/h_c} \leq 2$; and 'large' gaps, $2 \lesssim R_{O_d/h_c} < 3.5$, where R_{O_d/h_c} is the ratio of the opening's diameter (O_d) to the mean height of the trees surrounding the gap. Openings with diameters such that $R_{O_d/h_c} \geq 3.5$ are considered clearings with their own edges. Small openings, such that $R_{O_d/h_c} \leq 0.49$ are not treated as gaps, because they remain in shade for much of the day.

Regarding the flow of air, it is not clear at which size a canopy opening is a 'pore', in that the filtering operations smooth out its effect on the flow, and at which size it is a 'gap', in that it induces non-random dynamical effects. Determining a numerical threshold between pores and gaps is not possible using observations alone because of the difficulties inherent in obtaining spatially-representative velocity observations in forests (Finnigan, 2000; Finnigan & Shaw, 2008), and is not straightforward even using idealized LES models, because the threshold likely to be around the scale of, or smaller than, the spatial filter. We propose, as a first approximation, that openings with horizontal diameter greater than to the shear length scale ($O_d \geq L_s$) can be considered 'gaps', because they are likely to induce fluid dynamical effects on the scale of the dominant turbulent eddies. Openings where $O_d \ll L_s$ can be considered 'pores' in that they have only wake-scale effects on the flow and contribute little to the overall TKE budget (Finnigan, 2000; Raupach et al., 1996; Raupach & Shaw, 1982). The length scale L_s is most soundly defined in homogeneous, dense vegetation canopies, so this is only rough approximation for patchy forests. Because $L_s \approx 0.5h_c$, this dynamical definition of canopy gaps corresponds to the minimum size of the 'small gaps' proposed by Zhu et al. (2015), which they determined with respect to light penetration rather than fluid dynamics.

Figure 4. Openings in various forest canopies. In-canopy (a) and aerial (b) views of the BIFoR FACE facility, situated in a mature deciduous woodland in the United Kingdom (Hart et al., 2020). The FACE infrastructure is sited in natural gaps in the forest canopy. Note the variation in foliage color and density in (b), which was caused by insect herbivory during an outbreak of the European winter moth; (c) canopy openings in the understory layer of a tropical rainforest in Suriname; (d) canopy openings in the understory layer of a boreal forest in British Columbia, Canada.

A few studies have modeled patchiness at the stand level and below. Bohrer et al. (2009) use a virtual canopy generator (Bohrer et al., 2007) to simulate three-dimensional deciduous canopies, including gaps smaller than a tree crown. The heterogeneity caused turbulent fluxes to become spatially correlated in some parts of the forests, such as stronger and more frequent ejection events occurring over shorter trees. Bohrer et al. (2009) also show that canopy gaps affect the flow differently depending on season. In winter, when deciduous forests are sparse, heterogeneity in the forest canopy causes the dominant turbulent eddies to penetrate less deeply into the canopy relative to the homogeneous case. This decreases the forest's roughness length z_0

, a common measure of surface roughness, and the displacement height h_d, which reflects the height of the bulk sink of momentum. By the end of spring, however, when the PAI is higher, gaps in the forest canopy cause the dominant turbulent eddies to penetrate further into the canopy, and the values of z_0 and h_d to increase. In other words, in winter, the flow perceives a patchy forest as smoother than a homogeneous one but, after spring leaf-out, it perceives a patchy forest as rougher. This probably results from there being a smaller density contrast between the gaps (high eddy penetration) and full canopy cover (low eddy penetration) in winter, as well as lower wind speeds in spring. It is not clear why Bohrer et al. (2009) focused on spring rather than summer as their leaf-out season, since, for deciduous forests, spring is a time of rapid change in terms of weather and canopy structure. The changes to the values of z_0 and h_d induced by the transitions in canopy morphology are relevant to large-scale atmospheric models, which employ these parameters to represent forests' effect on the atmosphere. Bohrer et al. (2009) propose that variables such as the maximum PAI and the fractional area of gaps may be used in regional models to adjust the parameterized values of z_0, h_d and the eddy penetration depth, each of which may vary by around 25% in patchy forests relative to homogeneous forests of the same density. Maurer et al. (2015) find that varying z_0 and h_d seasonally, as a function of the canopy structure, produces more precise and less biased estimates of u_c than models taking constant values of those parameters.

Schlegel et al. (2015, 2012) use LES to simulate flow around a clearing, with the forest structure derived using terrestrial lidar observations. Small-scale plant heterogeneity creates sustained upwards motion in denser patches of forest and downwards motion in clearings and large gaps. In patchy urban areas (treated as porous media), where a patch is larger than x_A, the mean streamwise velocity component fully adjusts to the change in density induced by the patch, creating a strong vertical velocity component at the upstream edge of edge patch (Bannister et al., 2021). The lidar measurements of Schlegel et al. (2012, 2015) show that, even in a forest dominated by Norway spruce and Scots pine, the edges are dense throughout the height of the forest. This assumption is less realistic still for tropical and deciduous broadleaf forests, which often have dense understory layers in which the PAD is similar to that of the crown layer (Schneider et al., 2019; Zhao et al., 2011). Schlegel et al. (2012, 2015) show the flow does not penetrate closed edges as easily as may appear in homogeneous models. TKE and Reynolds stresses decay faster behind closed edges and strong cross flows may develop. Away from the edges, large gaps and clearings deflect the flow downwards, creating advective fluxes within the forest air space (Queck et al., 2016). Boudreault et al. (2017) use lidar measurements (outlined in Boudreault et al., 2015) to generate a three-dimensional forest structure, which they use in an LES model of flow across a forest edge. Compared to a homogeneous edge, the gaps induce variations in the flow, for example, the streamwise (U) and vertical (W) velocity components respectively vary by around 20% and 5% of their spatial means at $z=0.5h_c$. The turbulent momentum fluxes are likewise higher in the heterogeneous case, for example σ_w varies by around 40% of its spatial mean, because air is forced through patches of low density.

3.3 Dispersive fluxes of momentum can be significant

Spatial correlations in the time-averaged statistics, the term $-\partial\langle\overline{u}_i$ {overline {u}} rsub {i} $\rangle/\partial x_j$ in equation (2b), are usually excluded from analyses of forest–atmosphere exchange (Kaimal & Finnigan, 1994; Patton & Finnigan, 2012). This is a reasonable assumption in homogeneous, idealized canopies in which these dispersive fluxes are small (Moltchanov et al., 2011). However, investigations in model canopies show that inhomogeneities in the structure can generate large dispersive fluxes, particularly around edges (Harman et al., 2016; Moltchanov et al., 2011, 2015). Boudreault et al. (2017) show that spatial variability in forest canopy structure induces dispersive fluxes that account for 10–70% of the total variances of U and W at the upstream edge of the forest, across a streamwise distance of x/h_c=¿ 0–8 ≈ 0–x_A. Here, the dispersive momentum fluxes and skewness are greater than their turbulent counterparts, for example, with the dispersive flux of momentum accounting for ¿50% of the total momentum flux. Away from the edges, gaps and other patchiness decrease the efficiency of momentum transfer at the crown top. This suggests gap-induced flow phenomena interfere with the mixing-layer-type coherent structures that form around the tops of the trees. Bailey et al. (2014) observed a similar result in row-structured versus homogeneous trellis-trained crops. This interference is probably strongest when the structural inhomogeneities are of a size ≈L_s, so that the vortices shed around them are of a similar scale to the coherent structures that develop around the crown top. In a more idealized example, Q. Li & Bou-Zeid, (2019) use LES to show that very rough, heterogeneous surfaces—comprising cuboids of various dimensions and orientations—affect the dispersive fluxes of momentum and scalar quantities more than the turbulent components of the fluxes. As in Boudreault et al. (2017), Q. Li & Bou-Zeid, (2019) show the dispersive components can comprise most of the total momentum flux. Ignoring these dispersive fluxes may mean ignoring over half of the total momentum flux by focusing only on deviations from the time average and neglecting spatial deviations. Real forests channel air into gaps and patches, creating spatially coherent structures whose contributions can be as large as those induced by turbulence.

3.4 Resolved trees

The difficulties involved in incorporating realistic structure into the distributed drag approach, discussed above, raise the question of whether it is possible to resolve the forest directly in numerical and physical models. Poggi et al. (2004) approximate plants as rigid circular cylinders in a wind-tunnel model, finding the wakes in the lee of the vegetation stems perturbed the dominant mixing-layer type eddies at the crown top. Yue et al. (2007) model corn plants as stems surrounded by leaves, applying a distributed drag parametrization at the leaf points and, at the stem points, a force calculated as drag around a cylinder. Böhm et al. (2013) modeled trees as cylindrical trunks below spherical crowns in a wind tunnel. They conclude similarly to Poggi et al. (2004) that the partially coherent wakes of the bluff canopy elements modify the dominant eddies at the crown top, and that flow within the canopy divide into wake and non-wake regions. Yan et al. (2017) performed high-resolution LES studies of a regular array of bluff elements, specified similarly to the wind-tunnel model of Böhm et al. (2013). In a series of separate simulations, Yan et al. (2017) configure the trees as (a) entirely bluff bodies; (b) solid trunks

with the crown represented as distributed drag; and (c) as entirely distributed drag. The spatially averaged flow statistics were quite similar across the three cases, with slightly higher turbulence in the shear layer using the bluff-body representations. As an interesting alternative, Schröttle and Dörnbrack (2013) use LES to simulate flow around 16 Pythagoras trees[2], treated as immersed boundary layers with the outer tree branches 3.35 K warmer than their surroundings. They show the thermally driven vortices from the trees, of diameter roughly h_c and turnover time of ~30 s, interfere with the shear-generated coherent structure at the tops of the trees. However, the study was a method prototype, and its results reveal little about real forests.

For the time being, because of the computational expense of simulating turbulent flow, resolving forest structure directly remains out of reach for field-scale investigations of forest–atmosphere exchange. For example, Yan et al. (2017) use an extremely high resolution model to discretize the trees ($dx = dy = 0.03\,h_c$), which severely constrains the number of trees that can be simulated. Further, treating the trees as bluff bodies does not account for plant reconfiguration, may overestimate the scales of vortical wakes behind tree crowns, and excludes the possibility of resolving the cooperative waving motion that occurs in real vegetation. There are no theoretical limits to the number of trees that can be included in wind-tunnel models. However, it is difficult to include canopy exchange and other ecological processes in physical models. It is also challenging to maintain flow with sufficiently high *Re* values around forests, for which higher values are needed than in many engineering applications (Gromke, 2018). Results from bluff-body models may be useful to derive drag parametrization schemes for use in larger scale simulations. Böhm et al. (2013) provide a strong starting point by identifying that wake-scale TKE in bluff-body canopies is around 1/5 L_s (the mixing layer hypothesis eddy scale) rather than 1/100 to 1/10 L_s typical of vegetation canopies. This implies momentum is transferred more efficiently in vegetation than in canopies of bluff bodies.

3.5 Resolution and domain size

Scientists continually face a trade-off between scale and resolution. This choice is particularly relevant to fluid modeling because of the extreme computational expense of simulating turbulence. LES of fragment-scale interactions around forests currently use around 10^6–10^7 cells (e.g., Ma et al., 2020), although Patton et al. (2016) deployed some 4×10^9 cells in an enormous computational effort. In practice, this means LES models simulating turbulence in a horizontal domain of a few square kilometers currently have a horizontal grid resolution of 2–10m. Computing capacity is expected to increase with time for the foreseeable future, although LES resolution has increased more slowly than the general semiconductor capacity predicted by Moore's law (Bou-Zeid, 2014). This raises the question of whether the extra capacity should be applied towards increasing the resolution or the size of the simulated domain. In many fluid applications, the answer to this question is 'both'. However, the distributed-drag method requires the averaging volume to be much larger than the individual plant elements so that their presence is accounted for statistically. For mature forests, where the tree trunks can have diameters of a

[2] A type of fractal constructed iteratively from a right-angled triangle with squares erected on each of its sides.

meter or more, increasing LES resolution further than the current maxima makes little physical sense without a formal re-think of the averaging operations.

Increased computational capacity could be used more productively (i) to increase the simulated ABL height, thereby increasing the total amount of resolved TKE (Grylls et al., 2020), (ii) to increase the size of the simulated domain, (iii) to include a wider range of physical and chemical processes, or (iv) to account for plant movement. Each of these points is discussed below. The workhorse spatial resolution remains, then, a forest volume of up to tens of cubic meters accounted for by a single grid cell, and the smallest resolved eddies ≈ 5 m in diameter. This implies a need for robust SGS schemes if LES simulations are to be useful. Although LES has become popular over the last few decades, development of SGS schemes has been slow (Moser et al., 2021). The most widely used SGS parametrization is the Smagorinsky scheme, in which closure is achieved using empirical arguments and theory (Smagorinsky, 1963). This scheme assumes the turbulence is isotropic, which is not the case in forests (and in many other ASL applications). Recently, more suitable schemes have been developed by determining the minimum energy dissipation needed to balance the turbulence production at SGS scales (Gadde et al., 2021; Rozema et al., 2015), but these schemes have not yet been widely adopted. While, as we argue above, blindly increasing the grid resolution is likely to achieve little, improving SGS schemes for forest applications is an important line of future research. Eddies larger than the plant elements lose TKE to heat and fine-scale TKE, which short cuts the usual eddy cascade that is assumed by Kolmogorov's –5/3 law (Finnigan, 2000). Shaw & Patton (2003) show this effect can be accounted for in LES using a TKE cascade term, without the need for extra modifications to account for wake-scale kinetic energy transfer. However, the effect of this short cut to fine scales has not been tested in patchy vegetation canopies, with moving plants, or with a view to determining its impact on scalar exchange across the boundary layers of leaves.

4 Scalar quantities in complex terrain

The desire to understand forest–atmosphere scalar exchange is a major motivation for measuring and modeling forests at all. Important scalar quantities in forest ecology include: temperature; trace gases such as CO_2, water vapor, ozone, and volatile organic compounds (VOCs); ultrafine particles (UFP); litter fragments; soil particles; insect and animal detritus; and spores and pollen. In this section we focus on the numerical modeling of species that can be approximated as being passive and massless. These include CO_2, as well as other gases and UFPs whose lifetimes are longer than the longest air parcel residence times (Bannister et al., 2021; Janhäll, 2015; Kanani-Sühring & Raasch, 2015; Petroff et al., 2008). Other scalars, such as litter, animal detritus, and certain pollens, are much larger and must be treated differently (section 5 below). For a resolved scalar quantity ϕ, the conservation equation (neglecting molecular diffusion) is

$$\frac{\partial \phi_i}{\partial t} + U_j \frac{\partial \phi_i}{\partial x_i} = \frac{-\partial \tau_{j\phi_i}}{\partial x_j} + S_{\phi_i}, \quad (7)$$

where $\tau_{j\phi_i}$ is the SGS scalar flux (this term is not present when the equation is not spatially filtered). The term S_{ϕ_i} is a source/sink accounting for the emission, deposition, and production or

destruction of the scalar quantity. Equation (7) can be double filtered into mean, turbulent and dispersive components, as for equation (2).

4.1 A one-dimensional view

Edburg et al. (2012) provides an excellent case study for exchange in a homogeneous forest. The authors use LES to simulate a sparse (PAI ¿ 1), continuous, homogeneous forest in which the bulk of the PAD in concentrated between $z/h_c \approx$ 0.3–0.8. They simulate passive scalars as being emitted from the ground at a constant flux rate, and from the canopy using a height-dependent source, $S_\uparrow = Q_{h_c} \exp\left(-\alpha a(z)\right)$, where Q_{h_c} is a specified flux at the crown top, and α is an attenuation coefficient, which accounts for the flow's response to the forest density (Cionco, 1978). They simulate scalar deposition onto the plants through a sink term $S_\downarrow = -v_\phi a(z) \phi_l$, where v_ϕ is the bulk dry deposition velocity, accounting for a combination of aerodynamic and stomatal resistances, and ϕ_l is the resolved local scalar concentration. Scalar concentrations in the lower two-thirds of the canopy are much higher for scalars with ground sources than for those with canopy sources. The turbulent fluxes of scalar quantities are high throughout the depth of the canopy for ground sources of scalars. However, for canopy sources, the magnitudes of the turbulent fluxes decrease sharply towards the ground. Scalar quantities with canopy sources are stirred by the large turbulent eddies near the tops of the trees, whereas ground sources of scalars require intermittent turbulent motions to permeate the entire canopy depth. Scalars emitted from the canopy are therefore more evenly mixed throughout the forest and have shorter residence times compared with those emitted from the ground.

4.2 Scalar adjustment around forest edges

4.2.1 Single source models

We retain the terminology from section 2 (Figure 2) to help summarize recent investigations of scalar transport around forest edges. A simple conceptual model considers a scalar field, with a uniform ground source, adjusting when the flow enters a homogeneous forest. Scalar quantities accumulate in the adjustment region at the upstream edge of the forest (region (ii) in Figure 2) over a streamwise distance $x \approx$ 9–12$L_c \approx 2\,x_A \approx$ 16–20h_c. Here, concentrations of the scalar quantity can be several times higher than in the upwind air before it enters the forest. This pattern appears consistent across field observations of heat transport around forest edges (Klaassen et al., 2002), and in RANS (Sogachev et al., 2008) and LES (Kanani-Sühring & Raasch, 2015; Ma et al., 2020) models of flow around idealized forests.

Turbulent fluxes of scalar quantities above the adjustment region are 1.2–3.8 times larger than the surface source rate, and are therefore compensated by horizontal fluxes from elsewhere in the forest (Kanani-Sühring & Raasch, 2015). The location of the peak scalar concentrations and turbulent fluxes is dictated by (a) the adjustment of the flow and (b) streamwise turbulent scalar transport. The mean and turbulent fluxes are of the same order, with the turbulent component more influential in sparser forests. Concentration peaks are more pronounced in denser forests and are located closer to the upstream edge, for example, at $x \approx$ 9–12$L_c \approx 8\,h_c$ for PAI $\approx h_c / C_d L_c$

= 8 but $x \approx$ 5–6$L_c \approx 14\,h_c$ for PAI = 2. Forest succession and management, both of which can change PAI will, therefore, greatly influence scalar concentration gradients close to edges. This is because denser forests impose more drag on the flow than sparser ones, which suppresses turbulent mixing and causes the flow to adjust more quickly, i.e., the canopy drag length scale L_c is reduced. Turbulent scalar fluxes are greater in magnitude and located closer to the edge with increasing density. The magnitude of the fluxes increases with increasing wind speed but, because the turbulent components w' and ϕ' vary inversely with increasing wind speed, the locations of the fluxes do not change.

4.2.2 Models with multiple sources and sinks

Single source models provide good conceptual templates for certain processes around forests, such as the encroachment of pollutants from surrounding areas, or the release of isoprene, which is overwhelmingly from sunlit leaves in the canopy (Sharkey et al., 1996). However, most scalars have multiple sources and sinks, whose distribution varies temporally and spatially. Recent work has attempted to tackle this complexity in idealized settings. Kanani-Sühring & Raasch (2017) extend their 2015 work to investigate scalar transport in the exit and wake regions of forests, regions (vi) and (vii) in Figure 2, respectively. They simulate three scalar source distributions: the ground, the canopy, and the ground plus the canopy. Scalar accumulates in the wake region over a distance $x/L_c \approx$ 0.5–1 downstream of the trailing edge of the forest, with peak concentrations 10–75% larger than those at a reference point far downstream. Turbulent transport accounts for around half the total scalar transport. The locations of the highest concentrations and turbulent fluxes do not vary with wind speed. Higher concentrations occur at lower wind speeds, but the magnitudes of the turbulent fluxes do not change. In the wake region, the magnitudes of both the concentrations and turbulent fluxes increase non-linearly with forest density. For example, the magnitude of the turbulent fluxes for forests of PAI $\approx h_c/C_d L_c =$¿ 8 are around two and half times those of forests with PAI = 2.

Ma & Liu (2019) adapt the Community Land Model (CLM) Version 4.5 (Oleson et al., 2013) to create a multi-layer canopy model, 'MCANOPY', which simulates one-dimensional transport of water vapor, heat, and CO_2 in the soil-forest-atmosphere system. Ma & Liu (2019) couple MCANOPY to the LES mode of the Weather Research and Forecasting model (WRF) version 3.9 (Skamarock et al., 2008), with a horizontally and vertically uniform forest represented through the drag parametrization in equation (6). Due to computational constraints, the authors did not evaluate the performance of the coupled-LES over simulation times of more than a few hours. The stand-alone version—which includes a vertical turbulent mixing parametrization (Katul et al., 2004)—simulates most variables well when evaluated against observations from a walnut orchard (Patton et al., 2011). However, MCANOPY failed to simulate observed humidity gradients within the canopy, which the authors attribute to large−scale processes in the observations, such as the advection of humid air, which were not captured in their model. Ma et al. (2020) use MCANOPY to investigate scalar transport around forest edges, simulating three different forests by varying $a(z)$ equation (6) (with constant PAI). They specify two scalar configurations: (i) constant flux sources at the ground and at $z/h_c =$¿ 0.3, 0.6 and 0.9; and (ii)

using MCANOPY coupled to WRF-LES. The lowest CO_2 concentrations coincide with the canopy sink, with the depth of the region of low concentration increasing with distance from the upstream edge. Strong turbulent fluxes occur above the end of the adjustment region at $x \approx x_A$, and $z \approx 1.5 h_c$, agreeing with the results of Kanani-Sühring & Raasch (2015). Ma et al. (2020) attribute this flux to scalar-rich air being swept upwards by the mean and turbulent components of the flow (σ_w^2 is high in this region). Horizontal and vertical advection, which eddy covariance measurements do not usually account for (Aubinet et al., 2010), dominate CO_2 transport in the adjustment region. The patterns of scalar concentrations and fluxes are most complicated in the adjustment region where they are influenced by the strong turbulence, the inflow concentration from the surrounding environment, and the distribution of the sources and sinks within the forest. In mesoscale simulations over a forested area, including a vegetation canopy with a simple radiation scheme improved the simulated velocity fields compared with simulations based on land-use information alone (Yan et al., 2020).

4.3 Dispersive fluxes of scalar quantities

There have been no studies of the influence of small-scale variations in forest structure on scalar transport. A particular unknown is whether gaps and other patchiness induce dispersive fluxes of scalar quantities, i.e. spatial correlations between time-averaged scalar fields and velocity components. Wind-tunnel measurements in idealized plant canopies found the dispersive scalar fluxes to be small (Legg et al., 1986). However, recent studies in urban areas and generalized porous media suggest the dispersive fluxes of scalar quantities should not be dismissed out of hand. Philips et al. (2013) use LES in an urban canopy to show that scalar dispersion of a scalar quantity is sensitive to the geometry of the obstacles surrounding the source (they observe a plume's evolution directly, rather than investigating time-averaged quantities). Q. Li & Bou-Zeid, (2019) show the dispersive fluxes of scalar quantities do not always follow the flow of momentum, with obstacle geometry typically affecting dispersive fluxes of momentum more than those of scalars. The authors attribute this difference to the physical mechanisms involved. The air's velocity decreases before it reaches the upstream face of an obstacle, and therefore pressure affects momentum transfer away from surfaces. However, the air must touch an obstacle's surface to deposit or take up scalars, so scalar transport is much more spatially confined. LES studies of ABL flow over homogeneous surfaces indicate dispersive fluxes of heat are modulated by two broad flow regimes. The first is where surface heterogeneities, such as unevenly heated ground, drive the dispersive fluxes. The second is where dispersive fluxes are driven by turbulent coherent structures in high-shear conditions (Inagaki et al., 2006; Margairaz et al., 2020).

4.4 Topography and passive scalar quantities

Topographical effects on forest–atmosphere exchange are not random and can introduce notable horizontal fluxes that are not captured by eddy covariance or smoothed out by time averaging. In heavily populated regions, forests are overwhelmingly confined to land of marginal agricultural value, which often means sloping land (Sabatini et al., 2018). The effect of topography on forest-atmosphere interactions is therefore of wide applicability. Finnigan et al. (2020) review

boundary-layer flow in hilly terrain, including sections discussing flows around vegetated hills. We refer readers to their paper for a thorough overview of topographical effects on forest–atmosphere exchange. Before moving on, however, we highlight a remarkably consistent picture of scalar transport around forested hills that has emerged from recent studies. In the lee of a forested hill, an in-canopy recirculation region (ICR) may form within the forest, particularly when (a) the hills are steep, so there is a large pressure gradient at the upstream slope; and (b) in tall, dense forests, in which there is little mixing of high momentum air from above the forest with that near the forest floor. Another ICR may form at the foot of the slope at the upstream side of the hill. The ICRs result from a balancing act between the aerodynamic drag, the pressure perturbation induced by the hill, and the shear stress induced by the forests. A helpful scale to interpret flow in hilly terrain is the hill half length, L, defined in Finnigan and Belcher (2004) as a quarter of the wavelength of the topography. The ICR upstream of the hill occurs at $x/L \approx -¿1$ to 0 , and another in the lee of the hill at $x/L \approx$ 2–4 (Figure 5) (B. Chen et al., 2019; Ross & Harman, 2015). Forests absorb lots of momentum, meaning ICRs are more common in forested landscapes than in those with low vegetation, and may form in the lee of even gentle hills (Finnigan & Belcher, 2004; Patton & Katul, 2009). Both the forest density, through its effect on the canopy drag length scale L_c, and the absolute height of the canopy influence the likelihood of ICRs forming. In 'shallow' canopies, where $h_c/L_c < 2(u_¿/U_{h_c})^2 \approx 0.2$ (Poggi et al., 2008), not all of the momentum is absorbed by the foliage and ICRs are less likely to form than for 'deep' canopies, where $h_c/L_c \gg 0.2$.

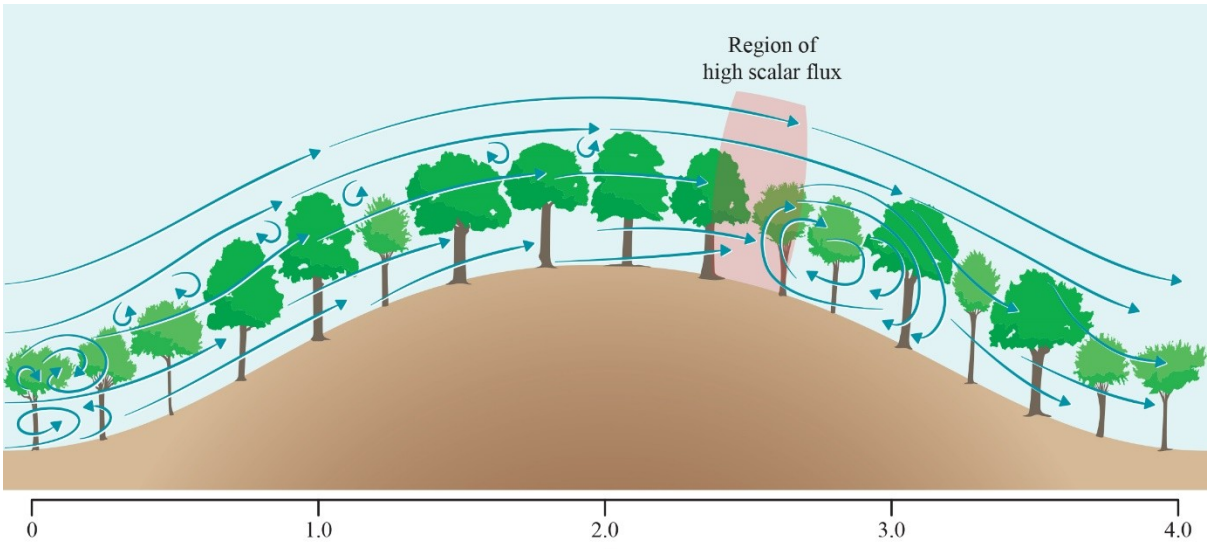

Figure 5. Schematic of scalar flux over a forested hill. A region of high scalar flux occurs around the in-canopy recirculation region in the lee of the hill. This region acts as a chimney for air parcels leaving the forest air space.

Figure 5 shows the region of strong vertical fluxes of scalar quantities forms between the crest of the hill and the upstream edge of the lee ICR. This result appears robust across models, despite their differing treatments of the physics (B. Chen et al., 2019; Katul et al., 2006; Ross &

Harman, 2015). Scalar fluxes around the lee ICR are stronger for ground sources of scalars than for canopy sources, because the topography affects the flow and turbulent mixing more near the forest floor (Ross & Harman, 2015). In models for which multiple sources and sinks are specified, the net effect of the sources depends on the balance of the individual transport terms. Chen et al. (2019) propose two pathways by which air parcels leave the forest: (i) the 'local' pathway, where ejection events transport air parcels out the forest, approximately vertically; and (ii) the 'advection' pathway, where parcels are transported horizontally until they encounter and are entrained into the lee ICR, before turbulent fluxes eject them from the forest. The local and advection pathways, respectively, dominate air parcels moving from the upper and lower parts of the forest air space. The whole forest air space contributes air parcels that leave via the advection pathway, although sources from the forest floor contribute a greater proportion of the total escape. This region acts as a chimney for air parcels leaving the forest. This behavior is amenable to observational testing but has not been verified by field measurements. Zeri et al. (2010) observed higher CO_2 concentrations around a forested hill when the wind blew from certain directions, which they attributed to CO_2 accumulating in the lee. However, the accumulation region fell just outside of the observational area, so the authors could not investigate this behavior further.

4.5 Conclusions about passive scalar transport in patchy forests

Scalar processes remain far less well understood than velocity adjustment and momentum transport, in terms of both the fundamental flow statistics (Shralman & Siggia, 2000) and in geophysical applications around forests (Bou-Zeid et al., 2020; Katul et al., 2013). For example, one would expect the adjustment of the flow to the presence of the forest to dictate patterns in scalar transport, such as the location and magnitudes of their fluxes. Scalar fluxes appear to adjust more slowly than momentum as the flow meets the forest, but the patterns in scalar transport are not always intuitive. Scalars are represented in models through the source term S in equation (7) as either a concentration or flux boundary condition. In numerical models specifying flux boundary conditions, such as those discussed in the previous two subsections, one would expect scalar quantities to be slave to the flow because no additional length scales are introduced in the model. Based on Sogachev et al. (2008), Belcher et al. (2012) suggest scalar concentrations and fluxes ought to reach equilibrium after a distance of $x \approx 2\,x_A$ downstream of the edge, where the value of x_A decreases with increasing forest density. Following this reasoning, we expect the fluxes of scalars to adjust more rapidly in denser forests. However, Kanani-Sühring and Raasch (2015) find the opposite: scalar fluxes adjust more slowly with increasing PAI, $x/x_A \approx 2$ for sparse forests, where PAI $\approx h_c/C_d L_c =$ ¿1–2, and $x/x_A \approx$ 3–4 for forests with PAI = 4.5–8. The relative size of sparse and dense patches of heterogeneity in forests may also affect scalar concentrations. For example, for flow through idealized porous media, maximum scalar concentrations occur in sparse patches where the patch size is less than the adjustment distance x_A, but in the dense patches where the patch size is greater than x_A (Bannister et al., 2021). Given the abundance of edges in contemporary forested landscapes, scalar concentrations and fluxes will be out of equilibrium for much, perhaps even most, of the world's forests.

There are potential ecological consequences of the patterns in scalar transport. For example, the simulations of Ma et al. (2020) indicate the air can be a few degrees warmer at the upstream edge of the forest. If this temperature variation is correct, a forest edge in the prevailing wind direction may provide a very different habitat to forest only tens of meters away (Zellweger et al., 2020). Turbulent fluxes of scalar quantities adjust slowly around patchy forests and in other complex terrain. For example, turbulent fluxes of water vapor and CO_2 respectively adjust over distances $x \approx 30\,h_c \approx 38\,L_c$ and $x \approx 60\,h_c \approx 76\,L_c$ downstream of a forest edge (Ma et al., 2020). This amounts to some 500–1000 m for mature forests, which again suggests scalars are rarely at equilibrium in patchy landscapes. However, it is difficult to generalize beyond these broad observations because the results are sensitive to the model configuration. For example, Ma et al. (2020) find CO_2 accumulates in the adjustment region, but water vapor accumulates downstream in the canopy flow region. This difference probably results from the authors' treatment of each species. They specify a ground source of CO_2 across the whole domain, with a sink in the upper canopy, but multiple sources of water vapor, with ground sources either side of the forest and a second larger source in the upper canopy.

5 Adding more atmospheric physics and chemistry

5.1 Atmospheric stability

Air in the ASL is, on average, statically unstable during the day and stable at night (although the true dynamics are more complicated (Stull, 1991)). The mixing-layer model of canopy flow described in section 2 assumes near-neutral conditions, with the dynamics controlled by the high shear in the mean wind velocity around the tops of the trees. However, in strongly stable or unstable conditions, the velocity shear can be much less influential (Brunet & Irvine, 2000; Lemone et al., 2019). As the ABL becomes more unstable, the turbulence structure around forests transitions from a shear-driven to a convection-driven regime, i.e. thermal cells govern the flow dynamics, and the mixing-layer type turbulence becomes less prominent (Dupont & Patton, 2012; Lemone et al., 2019; Mahrt, 2000). Conversely, when the ABL is stable, the buoyancy of the air dampens vertical motion. Mixing-layer type coherent structures may still develop around a forest, but they are smaller and less frequent than those that form in near-neutral conditions (Dupont & Patton, 2012). ABL turbulence is generally more intermittent—variable in space and time—in stable conditions (Mahrt, 2014). In very stable conditions, fluxes of scalar quantities are driven by an interaction of mesoscale phenomena, such as gravity waves and nocturnal jets, and the local turbulence. This interaction is observed in the large, intermittent variations in temperature and CO_2 concentration around forest that occur when extended calm periods are interrupted by short bursts of intense turbulence (Aubinet, 2008; Heinesch et al., 2007; Wohlfahrt et al., 2005).

Simulations of flow around idealized forests in non-neutral conditions are beginning to add detail to this general picture. Patton et al. (2016) used LES to investigate the entire ABL over an interactive forest canopy, across five stability classes (near neutral to free convection). In strongly unstable conditions, thermal plumes may bubble up from the forest floor or the canopy top, and the vertical profiles of the atmosphere in the RSL approach those predicted by MOST.

As stability decreases from near neutral to free convection, the dominant turbulent structures around the forest change from shear layer vortices to thermal plumes, and momentum and scalar fluxes become less correlated. It is not clear whether this transition is gradual, with shear and thermally driven structures coexisting, or sudden, with a flip between regimes upon reaching a stability threshold. Nascent research indicates the transition may be sudden (Brunet, 2020). In unstable conditions, scalar quantities are transported predominantly by thermal plumes—also observed in field measurements (Dupont & Patton, 2012)—and the velocity variances, momentum stresses, and momentum transport efficiency decrease as the atmosphere becomes less stable.

Around forest edges, TKE and momentum transfer are much higher in unstable conditions than when the ABL is approximately neutral, and the flow takes longer to adjust upon meeting the canopy (Ma & Liu, 2019). In the adjustment region, the skewness of the streamwise Sk_u and vertical Sk_w velocity are smaller in magnitude in unstable conditions than in neutral conditions, indicating sweep motions do not penetrate as easily into the forest canopy when the air is buoyant. In neutral conditions, CO_2 accumulates in the adjustment region at the upstream edge of the forest, and water vapor in the canopy flow region, but these patterns largely vanish in unstable conditions.

In stable conditions, wind shear at the crown top is higher than in unstable or neutral conditions, and momentum penetrates less deeply into the forest (Chaudhari et al., 2016; Nebenführ & Davidson, 2015; H. B. Su et al., 2008). Within the forest, turbulence is much weaker and more intermittent than in neutral or unstable conditions, and the pressure transport term of the TKE budget becomes more significant with increasing stability (Nebenführ & Davidson, 2015). In open forests, intermittent turbulence, driven by shear in the air aloft, may penetrate into the canopy and dramatically alter the distribution of scalars (Wharton et al., 2017). These intermittent events in stable conditions are not well understood and are seldom resolved well by numerical models because they do not result from resolved shear generated turbulence at the microscale or MOST theory used in larger scale models. They are thought to result from nonturbulent 'submeso' motions, which fall between the scale of the largest turbulent ABL eddies (~O(100 m)) and the smallest γ–mesoscale(~O(2 km)) (Mahrt, 2014). There is some evidence that parametrizations of submeso motions may be possible by analogy with 'self-organized criticality', the tendency of dynamical systems to organize their microscopic behavior to be scale independent (Cava et al., 2019). However, this remains an active area of future research, requiring careful comparison between numerical model results and observations (Sun et al., 2015).

The atmospheric stability within the forest itself often differs to that of the surrounding atmosphere. For example, on a sunny day, warm convective thermals may form above a forest, while the air within it remains stable (Ramos et al., 2004; Stull, 2006). At night, the situation is reversed when the forest crown loses heat through radiative cooling, forming a capping layer of very stable air around the tops of the trees that can decouple the forest air space from the surrounding atmosphere (Nebenführ & Davidson, 2015; Paul-Limoges et al., 2017; Xu et al., 2015). The decoupling is sensitive to site-specific meteorological conditions, such as local temperature gradients (Alekseychik et al., 2013; Russell et al., 2016). The capping layer forms

around the tops of the trees, below the height of the instruments at many long-term observational sites. In these conditions, eddy-covariance measurements are difficult to interpret because CO_2 and other scalars can accumulate within the canopy, and the measured turbulent flux is unrepresentative of the forest as a whole (Aubinet, 2008; Massman & Lee, 2002). In hilly terrain, the decoupling can trigger drainage flows, transporting CO_2, heat, and water vapor to and from forests (Finnigan et al., 2020; Sun et al., 2012; Wharton et al., 2017; Xu et al., 2015). Drainage flows and other below-canopy transport contribute a large proportion to the total scalar transport in certain meteorological conditions, such as during stable nights with weak winds (McHugh et al., 2017; Paul-Limoges et al., 2017).

A tricky further challenge to modelers is dealing with the localized heat sources that form within a forest. During the daytime in direct sunlight, broad leaves may be 20 ^{o}C warmer than their surroundings (Monteith & Unsworth, 2008; Schuepp, 1993b; Vogel, 2009) and can therefore act as highly localized heat sources. We are not aware of direct investigations the effect of these sources, but LES of unevenly heated generic surfaces suggests thermal heterogeneities drive the local mean flow in certain weather conditions. In these conditions, the dispersive fluxes of heat account for more than 40% of the total sensible heat flux at $z=¿$ 100 m and up to 10% near the surface (Margairaz et al., 2020). This behavior is difficult to constrain in models because the locations of sunflecks (brief periods of high photon flux density) change quickly depending on branch movement (Way & Pearcy, 2012). The radiative properties of the leaves may even vary between the sun and shade sides of a tree (Vogel, 1968). One possible starting point is to combine the modeling approaches of thermal transfer in urban areas (e.g. Martilli et al. 2002; Salamanca et al. 2010) and radiation transfer in vegetation (Ma and Liu 2019). For example, the leaves of the forest may be represented using a probability density function (PDF) of small, flexible, surfaces with high absorptance, and the trunks through a PDF of vertically aligned cylinders of varying thickness and low absorptance.

5.2 Air parcel residence times

Once a molecule enters a forest from outside, or is released from a leaf or the soil, it is mixed within the forest air space. This is easiest to visualize in terms of the stretching and dissipation of small air parcels. During the passage of these air parcels, the molecules or particles contained within may react or deposit on surfaces. The local turbulence affects the parcels' residence times, which in turn affects the forest's ecology—e.g. influencing chemical signaling (Szendrei & Rodriguez-Saona, 2010) and VOC chemical processes (e.g., Pugh et al. 2011; Batista et al. 2019), or varying the likelihood of nutrients (Fowler et al., 2009) or fungal spores (Norros et al., 2014; Pan, Chamecki, et al., 2014) being deposited. The lifetimes of some VOCs emitted by forests are in the order of tens of minutes, similar to the residence times parcels moving from close to the ground (Wolfe et al., 2011). Reactive scalar quantities emitted from the ground are therefore more likely to be chemically transformed within the forest than scalars emitted in the tree crowns. Numerical models are powerful tools for investigating air parcel residence times because the flow can be studied from either a Lagrangian or Eulerian point of view. The Eulerian specification of the flow focuses on specific locations in space through which the air flows with

time, whereas the Lagrangian specification follows an individual air parcel as it moves through space and time.

The initial vertical position of an air parcel affects its residence time, with parcels 'released'[3] near the ground having much longer residence times than those released higher in the forest canopy (Edburg et al., 2012; Fuentes et al., 2007). Estimates of parcel residence times vary from a few seconds for parcels moving from the crown, to around 30 minutes for parcels moving from the forest floor, with spatially averaged values in the order of a few minutes (Edburg et al., 2012; Fuentes et al., 2007; Gerken et al., 2017; Hart et al., 2020). The density and morphology of vegetation influences air parcel residence times. For example, in a short, trellis-trained crop, parcel residence time increases with canopy PAI, other than for parcels released high in the canopy (Bailey et al., 2014). Residence times increase with increasing PAI, because mixing-layer-type eddies and TKE do not penetrate as deeply into the canopy (Gerken et al., 2017). Air parcels remain in the canopy for longer when they are released from approximately the height at which most of the plant area is located. For example, for parcels released in the upper canopy, residence times are longer for top-heavy PAI profiles, such as pine plantations, than for forests with more plant area lower down. We expect longer residence times in stable atmospheric conditions, such as at night or on overcast days, because turbulent mixing is suppressed. We are not aware of any investigations into stability effects on parcel residence times in forests. Observations and RANS simulations in urban areas indicate parcel residence times generally increase with increasing atmospheric stability, although they also heavily influenced by the wind velocity and the geometry of local obstacles (Mavroidis et al., 2012).

The next challenge is to explain quantitatively how forest canopy turbulence affects air parcel residence times. As rough approximation in homogeneous forests, Gerken et al. (2017) propose that the parcel residence time (τ) is proportional to the reciprocal of the friction velocity, i.e. $\tau \propto 1/u_*$. Unfortunately, this relationship is unlikely to hold even approximately in patchy landscapes. As an illustration, we simulate flow across a continuous homogeneous forest (Case 1) and a small, homogeneous forest patch (Case 2). Case 1 and Case 2 are represented using the drag parametrization in equation (6), with the transport equations solved using LES (see Appendix A for numerical details). Figure 6 presents two-dimensional evolutions of Sk_u and Sk_w for each case. In the adjustment region of the forest in Case 2, the mean wind velocity is higher than in the homogeneous forest in Case 1. More importantly, around the forest edges in Case 2, the velocity statistics are highly non-Gaussian, evidenced by the clear patterns in Sk_u and Sk_w in Figure 6b and d relative to Case 1 (Figure 6a and c). The friction velocity u_* is a global quantity that is only well defined in the ISL where the shear stress $\overline{u'w'}$ is approximately constant with height. Therefore, although the value of u_* may not differ greatly between forests in the same weather conditions —e.g., $u_* \approx 0.5$ m s^{-1} for both cases here— residence times are likely to be much lower in patchy forests than homogeneous ones, particularly around edges.

[3] Studies looking at particle residence times in plant canopies often adopt a Lagrangian point of view.

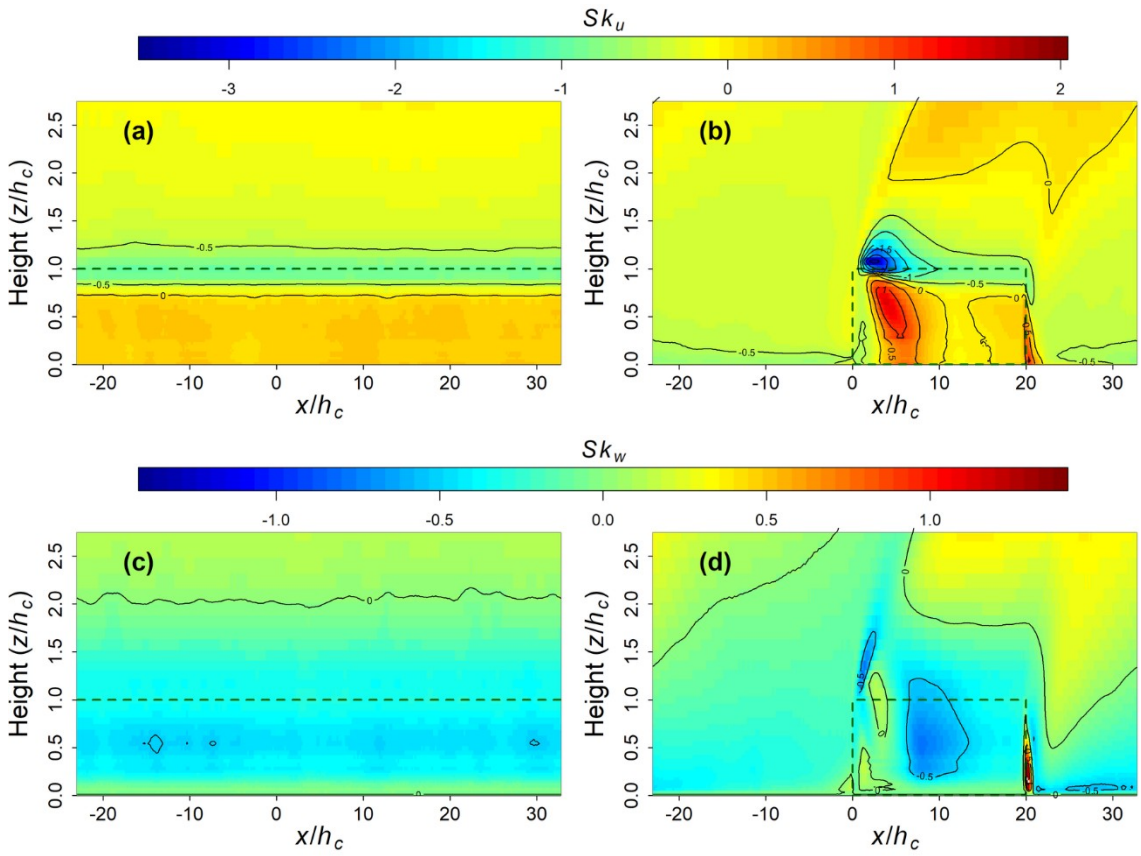

Figure 6. Two-dimensional evolutions of streamwise velocity skewness Sk_u for (a) Case 1 and (b) Case 2; and vertical velocity skewness Sk_w for (c) Case 1 and (d) Case 2. The green dashed line shows the presence of the forest. The *x*-axis is scaled so that 0 coincides with the upstream edge of the forest for Case 2. The figures for Case 1 (a, c) can be considered snapshots of a large homogeneous forest.

5.3 Modeling in-canopy chemistry and particle deposition

Fragment-scale investigations of forest–atmosphere interactions are often motivated by questions concerning trace gas exchange, usually representing the species of interest as passive scalars (see section 4). However, the behavior of many biologically important gases and particles cannot be approximated in this way. For example, many pollens and spores have substantial mass and are subject to inertial forces different to those on a trace gas molecule (see, e.g., Hinds, 1999; Seinfeld & Pandis, 2016). Freshly nucleated UFPs, resulting from the oxidation of BVOCs (Kulmala et al., 2001, 2007), are produced in high number concentrations around forests and may coagulate (Dal Maso et al., 2002; Kulmala et al., 2001; Pierce et al., 2012). These processes introduce physics requiring a different mathematical approach to that for fluid flow or particle growth/evaporation (Jacobson, 2005; Seinfeld & Pandis, 2016; Spracklen et al., 2006). Chemical transformation and particle deposition around vegetation are important aspects of atmospheric science that deserve their own reviews. Here, we highlight recent work in which some of these processes are captured efficiently in high-*Re* models.

5.3.1 Modeling in-canopy chemistry

BVOCs are ecologically important in forests (Niinemets, 2010; Visakorpi et al., 2018) and influence air quality, meteorology, and the climate through their interactions with oxidants such as O_3 and OH (Fuentes et al., 2000; Lelieveld et al., 2008; Peñuelas & Staudt, 2010; Rap et al., 2018; Richardson et al., 2013). Studies investigating BVOC chemistry in forests are usually interested in time and space scales that are too large for the turbulent flow to be resolved by DNS, LES or RANS, requiring the turbulent exchange to be parametrized (Ashworth et al., 2015; Bryan et al., 2012; Forkel et al., 2006; B. Wang et al., 2017). These parametrizations are usually based on K–theory, which is flawed around forests and other rough surfaces (Monteith & Unsworth, 2008). Model predictions of BVOCs and their oxidation products can be very sensitive to the turbulence parameterization used (Bryan et al., 2012; Makar et al., 2017). It is therefore important to make the parametrizations as robust as possible.

Fragment-scale LES models can simulate counter-gradient transport and are therefore likely to be indispensable tools in developing chemistry parametrizations that scale to large space and time resolutions. Due to the complexity of the task, there have been few attempts to investigate forest chemistry while resolving turbulence. However, the urban literature is an excellent source of relevant techniques (e.g., Bright et al., 2013; Buccolieri et al., 2018; Khan et al., 2020; Kwak et al., 2015; Liao et al., 2014; Zhong et al., 2016, and references in each).

One possible path is to couple chemistry models to LES, a technique which has recently been used to investigate chemical transformation, transport, and deposition of air pollutants in realistically shaped urban areas (Khan et al., 2020). However, the computational expense of the coupled approach heavily restricts the resolution of the domain and the number of chemical species that can be investigated in each run. Another approach is to model chemistry inside a forest air space using ‘box models’, which treat the air space as a fixed volume into which species are emitted and are able to react. Box models require the characteristics of the turbulence to be specified a priori, such as through an exchange velocity between the box and its surroundings. This simplification allows computing resources to be reallocated to more complex chemistry or particle microphysics than is possible when the turbulence is highly resolved using RANS or LES. Box models are widely used to model street canyon chemistry (Holmes & Morawska, 2006; Fabio Murena, 2012; Zhong et al., 2016) and have been used for one-dimensional investigations of forest–atmosphere exchange and BVOC chemistry across large homogeneous canopies (Ashworth et al., 2015; Pugh et al., 2011). In patchy landscapes, multiple boxes would be required to account for the fluid dynamical regions that form around forest edges and clearings. The urban literature offers a precedent for dividing air spaces into dynamical regions. For example, models of street canyon chemistry have used multiple boxes to represent the ‘compartmentalization’ of fluid dynamical phenomena such as counter-rotating vortices (Kwak & Baik, 2014; F. Murena et al., 2011; Fabio Murena, 2012; Zhong et al., 2016, 2018).

5.3.2 Modeling particle deposition in forests

Many studies of scalar quantities (Poggi et al. 2006) and particles (Aylor and Flesch 2001) in vegetation adopt a Lagrangian stochastic modeling (LSM) approach, which requires the vertical profiles of turbulence statistics to be specified a priori. However, around patchy forests, determining a priori vertical profiles is extremely difficult because the dynamics are so spatially varied. There have been a handful of attempts to incorporate non-Gaussian turbulence in an LSM framework, with varying success (e.g., Reynolds, 2012). More recently, several groups have adopted an Eulerian specification of the flow field to model particle deposition. Around patchy forests, Eulerian models offer the advantage of resolving the velocity statistics directly down to the scale of their grids. This does not necessarily affect the predictive ability of the models around vegetation. For example, Gleicher et al. (2014) simulated more accurate concentrations of spores in a homogeneous maize canopy using an Eulerian LES model than using their equivalent LSM. However, an inherent difficultly using LES is that canopy deposition occurs at spatial scales much finer than the spatial filter and therefore must be parametrized. One method is to include a sink term in the conservation equation,

$$S = E_\phi \alpha \phi_l |U|, \quad (8)$$

where α is the attenuation coefficient (see section 4.1), ϕ_l the resolved local particle concentration, and E_ϕ the efficiency of particle deposition (Friedlander, 2000; M. Lin et al., 2012; X. Lin et al., 2018). Pan et al. (2014a) use a similar approach, modifying the deposition model in Aylor and Flesch (2001) to generate a sink term linked to PAD,

$$S = E_\phi (P_x + P_y) a(z) \phi_l |U|. \quad (9)$$

This formulation considers the distribution of the forest density directly though the incorporation of PAD, as $a(z)$, and the projection coefficients P_x and P_y, which respectively account for the PAD facing the streamwise and spanwise directions. Ground deposition of particles can be modelled using a surface flux boundary condition. We contrast the formulations in equations (8) and (9) with the sink term for a passive scalar used by Edburg et al. (2012), $S = -v_\phi a(z) \phi_l$ (v_ϕ is the dry deposition velocity), which does not account for wind speed (section 4.1). Lin et al. (2018) and Pan et al. (2014a) use slightly different formulations for the deposition efficiency E_ϕ based, respectively, on a parametrization of molecular diffusion and on observations of particle impaction onto cylinders (similar approaches are common when investigating particle deposition onto fibers (Friedlander, 2000)). The deposition efficiency term E_ϕ accounts for the momentum and size of the particles, so that equations (8) and (9) are solved separately for each particle size, with the only difference between the solutions resulting from the approximation of the deposition efficiency (the same is true for the surface-flux parametrization representing ground deposition).

The mechanisms of particle deposition, and hence deposition velocities, are highly size-dependent for the size ranges of particles commonly encountered in forests (Litschike & Kuttler, 2008). Lin et al. (2018) found the deposition velocity decreased sharply with increasing particle

size for the range of sizes they investigated (diameters 10–50 nm). Pan et al. (2014a) investigate size indirectly through the ratio of the particle settling velocity w_s to the friction velocity u_*, with 'light' particles having $w_s/u_* \approx 0.04 \ll 1$, and 'heavy' particles $w_s/u_* \approx 0.2$. They show, for large values of w_s/u_* (heavy particles) and sources near the ground, few particles escape the canopy, reflecting their empirical observation that plant diseases initiated deep within a canopy move upward to the canopy top before spreading. Unsurprisingly, more particles are deposited in denser vegetation (Branford et al., 2004), particularly at $z \approx h_c$, and therefore lower concentrations of particles occur deep in the canopy. The rate of dry deposition generally increases with increasing turbulence because the thickness of the quasi-laminar boundary layers around plant elements is reduced, therefore increasing the probability of impaction (Fowler et al., 2009). However, the rate at which particles are deposited depends on the tree species. Studies of urban trees indicate deposition onto conifers is more efficient than onto broadleaf trees (L. Chen et al., 2017; Pace & Grote, 2020). Beyond these general observations, there appears to be no clear dependence of fluxes or deposition of fine particles on broad-brush measures of the canopy morphology (Katul et al., 2011; X. Lin et al., 2018). Deposition patterns appear to depend strongly on the complex arrangement of plant area in forests and other plant canopies (Fowler et al., 2009).

A future task, straddling in-canopy chemistry and trace-gas deposition, is to investigate how forest patchiness and more complicated weather conditions affect the rate of deposition and stomatal uptake of trace gases. For example, particle impaction can be several times higher in unstable conditions versus stable ones (Chiesa et al., 2019; Fowler et al., 2009; Pryor et al., 2008). This suggests leaf related removal by forests is likely much lower at night than measurements taken during the day would suggest; impaction is much lower in stable, nocturnal conditions and the stomata are mostly closed at night. Local atmospheric stability gradients, such as from patchy heating from sunlight, may produce apparent fluxes when particles and gases trapped in stable conditions are eventually released in convective plumes (Chiesa et al., 2019). Most models of spore dispersal in forests, including those cited above, consider only dry deposition, which is a major simplification in many climates where forests are found, and pay little attention to the resuspension of deposited particles. However, the rates of particle removal by rain and resuspension by depend on species composition and the local meteorological conditions, such as the frequency and intensity of rainfall events (L. Chen et al., 2017). Airborne fungal spore concentrations in forests are generally higher in wet conditions (Crandall & Gilbert, 2017), which are physiologically favorable to certain fungal species such as *Ganoderma* spp. (Stępalska & Wołek, 2009). Air vortex rings, which can carry dry-dispersed spores away from the host plant, form around the impact site when raindrops hit plant surfaces, (S. Kim et al., 2019). This process, which is not accounted for in current models, is likely significant in the transmission of fungal spores because particles transported by the air vortices can reach beyond the laminar boundary layer around plant surfaces, enabling long-distance transport in the turbulent flow.

6 Forest structure and wind

6.1 Adaptation to wind loading

Wind affects all aerial parts of forests on time and space scales from those of the smallest eddy to those of climate variation and tree lifetimes. Many plants respond to wind by reducing their surface area to minimize drag, and therefore lower the likelihood of damage from wind loading. On longer timescales, plants may apportion biomass in such a way as to acclimate to wind direction and intensity, a process known as thigmomorphogenesis. Figure 7a, for example, shows a hawthorn tree on the Isle of Wight, UK that has undergone thigmomorphogenesis to minimize drag from the prevailing south-westerly wind. Other examples of wind adaptation include the different root architectures of trees growing in windy environments compared with sheltered trees (Cucchi et al., 2004; Nicoll & Ray, 1996; Ramos-Rivera et al., 2020), trees at the upstream edge of a forest having stiffer wood than those further inside the stand (Brüchert & Gardiner, 2006; Cucchi et al., 2004), and trees exposed to high winds developing lower crown densities, comprising a smaller number of smaller leaves (Telewski, 2009; Telewski & Pruyn, 1998). This adaptation is a trade-off for the trees, with increased resistance to wind loading and other environmental stresses coming at the expense of slower growth (Hirons & Thomas, 2018). For further background on the permanent response of trees to wind loading, see, for example, Telewski and Pruyn (1998), Telewski (2009), Hirons and Thomas (2018).

Figure 7. (a – left) A wind modified hawthorn (*Crataegus monogyna*) on the Isle of Wight, UK; and (b – right) leaves of a cottonwood (*Populus deltoides*) curling in high wind.

On shorter timescales, trees and other plants reconfigure elastically to reduce drag forces in high winds, which is visible in the everyday observation of leaves curling (e.g., Figure 7b) and tree branches thrashing in high wind. At the stand level, this reconfiguration is evident from coherent 'honami' waves passing through a field of wheat (Inoue, 1955; Maitani, 1979), from wavelet analysis of pine plantations (Schindler et al., 2012), and in video footage of forests taken above the crowns (Harper, BIFoR FACE site, private communication 2021). At low wind speeds, the movement of individual leaves dominates foliage reconfiguration, with the erratic movement of branches, known as 'buffeting', dominating at higher speeds (Tadrist et al., 2018). The size, type and shape of the leaves determines their behavior in wind, even at low speeds. Leaf fluttering is not simply a by-product of the leaves' flexibility, which alone would tend to increase their drag

through flapping in the manner of flags (Virot et al., 2013). Instead, the leaves of many tree species curl up to form cones and cylinders, which become tighter with increasing wind speed (Vogel, 1989).

6.2 Plant reconfiguration and drag

The distributed-drag method accounts for the average aerodynamic drag the plants impose over some spatial scale larger than individual twigs and leaves. There is nothing in the formulation that accounts for the detailed morphology and mechanics of plants and trees. There would be no difference between the treatments of a forest and a sponge of the same dimensions and porosity. Plant reconfiguration is particularly relevant to patchy forests because the flow is constantly adjusting and readjusting as it moves across gaps and clearings. Capturing this reconfiguration directly in fragment-scale models is currently unworkable because of the computational expense of simulating the motion of flexible bodies in turbulent flow. However, it may be partly captured by modifying the drag parametrization in equation (6). For example, one could consider the PAD, represented in $a(z)$ in equation (6), as varying with velocity (Speck, 2003), or replace the drag coefficient C_d, with a shape factor that varies with the flow (Gaylord & Denny, 1997). However, these approaches require a detailed three-dimensional knowledge of the forest structure and its response to wind loading. A more empirical approach is to proceed from the observation that reconfiguration leads to a lower increase of drag with velocity than could be expected by assuming $a(z)$ and C_d both take constant values (Vogel, 1989). Therefore, instead of having the drag $f_i \propto U^2$, we have $f_i \propto U^{2+B}$, where B is known as the Vogel number (De Langre, 2008; Vogel, 2020). B therefore acts as an empirical modification to equation (6) to account for the variation of $a(z)$ and C_d with velocity. Negative values of B imply that, because of reconfiguration, plant drag increases with velocity more slowly than the usual assumption of velocity squared. Where the plants do not reconfigure, $B \to 0$ and the drag increases approximately with the square of the velocity.

There have been no numerical studies of this instantaneous reconfiguration in forests, but researchers have studied the effect in other vegetation canopies. Pan et al. (2014a) use LES to model the reconfiguration of a wheat canopy. They maintain the quadratic dependence of drag on velocity in the drag parametrization in equation (6), accounting for plant reconfiguration using a velocity-dependent drag coefficient $C_d = (¿U \vee ¿A_v)^B$, where A_v is a velocity scale related to the shape and rigidity of the plants. They calculate values of $A_v = ¿$ 0.29 m s^{-1} and $B = -0.74$ by fitting experimental data to the Reynolds averaged momentum balance equation for airflow through a uniform canopy. Using the variable C_d, their LES model simulated flow with more accurate higher order statistics than the same model with a constant C_d value (with similar performance with respect to the mean velocities, momentum transfer and TKE). Using a variable C_d value also improved estimates of momentum transport by sweep motions penetrating the canopy. In similar work, Pan et al. (2014b) show plants reconfigure more at higher flow velocities, reflecting the results of lab investigations on isolated plants (Tadrist et al., 2018). In both Pan et al. (2014a, 2014b), the absolute values of Sk_u and Sk_w increase with a more negative Vogel number—i.e. simulating more reconfiguration—as did the ratio of sweeps to ejections. To

see why, taking $B=-0.74$ from Pan et al. (2014a) gives $f_i \propto U^{1.26}$ in equation (6) rather than $f_i \propto U^2$. This change slows the rate at which the drag force increases with increasing velocity, leading to a greater the contrast of TKE inside and above the canopy. The decrease in the velocity exponent also increases the frequency and strength of sweep motions because strong events ($u^{'}>0$) penetrate further into the canopy. The canopy drag length scale L_c increases when the value of C_d is smaller because stronger events are able to penetrate further into the forest before drag halts their progress.

There are no published values of B that are immediately applicable to high-Re models of forest–atmosphere exchange. Field studies of plant reconfiguration typically focus on time-averaged adaptation over long time intervals, although measurements in poplar crowns show C_d values decrease with increasing wind speed across averaging periods as short as 1 s (Koizumi et al., 2010). Pan et al. (2014b) ran simulations using $B=$¿ 0, $-$¿2/3, $-$¿1, and $-$¿4/3, finding that a non-zero Vogel number improved the agreement of the simulations with flume observations, with the greatest fidelity obtained using $B=-$¿ 1. Other estimates for B include $-1<B\leftarrow 2/3$ from biomechanics theory (Gosselin et al., 2010). $B\approx -1$ appears to be a robust measurement for poroelastic structures, including forests and other vegetation canopies (Gosselin, 2019 and references therein). As a starting point, we suggest 0 and $-$¿1 as approximate upper and lower bounds for the Vogel number B.

6.3 Parametrizing plant reconfiguration

6.3.1 Stochastic drag forcing

The product $C_d a(z)$ in equation (6) is typically approximated as a smoothly varying function of height, with C_d taken as constant. However, Finnigan & Shaw (2008) raise the important point that the dominant large eddies around forests have diameters in the order of $L_s \propto h_c$ (Bailey & Stoll, 2016; Raupach et al., 1996). To resolve the structure of these eddies in numerical models, the vertical filter needs to be much smaller than h_c, for example, a filter of $h_c/25$ is taken in the model in Appendix A. At this resolution, we can no longer assume $a(z)$ is a smooth function—for example, notice the structural variation of the forest understories in Figure 4. Finnigan & Shaw (2008) propose representing $C_d a(z)$ through a stochastic variation overlaying a smooth background trend, thereby introducing a stochastic forcing into the resolved momentum equations.

To illustrate this argument, we retain the Case 2 forest from section 5.2, for which $C_d a(z)$ is uniform throughout the domain (see Appendix A for numerical details). We define a Case 3, which is of the same dimensions and mean density as Case 2. However, for Case 3, $C_d a(z)$ varies randomly in space throughout the forest by $\pm 2\%$ of the value for Case 2, a small variation in comparison to the natural variation of forests. The random spatial variation of $C_d a(z)$ is almost imperceptible in the mean variables and second-order statistics such as the TKE and kinematic turbulent momentum flux. However, Figure 8a shows the streamwise velocity skewness Sk_u at

the upstream edge of the forest ($x/h_c \approx$ 0–5) is less negative for Case 3 than it is for Case 2. The value of Sk_u above the forest is more negative for Case 3 than it is for Case 2. The streamwise velocity kurtosis Kt_u at the upstream edge of the forest ($x/h_c \approx$ 0–5) is smaller for Case 3 than it is for Case 2 within the forest, and larger for Case 3 than it is for Case 2 above the forest (Figure 8b). These statistics indicate the small stochastic forcing in Case 3 decreases the coherence of the flow at the upstream edge—i.e., the upstream edge behaves less like a bluff body than the homogeneous Case 2—leading to fewer lulls in the streamwise velocity within the forest but more lulls just above the canopy. We do not generalize these results further because Cases 2 and 3 are highly idealized. But they support the conclusions of Dupont & Brunet (2008a) and Pan, Chamecki, et al. (2014), for example, that the probability distribution of gusts indicated by higher-order statistics are particularly sensitive to the model setup, including any stochastic element.

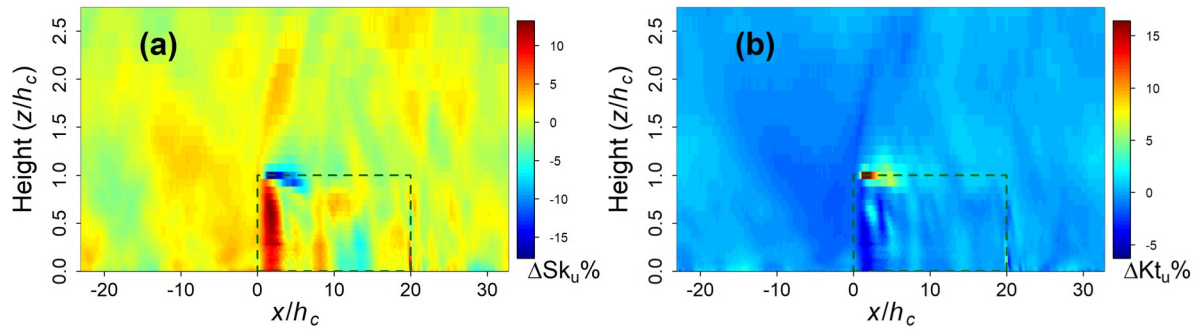

Figure 8. (a) Percentage difference in Sk_u; and (b) Kt_u between Case 2 and Case 3, as a total of the maxima for Case 2. The changes are induced by the stochastic variations in $C_d a(z)$ for Case 3. The green dashed line shows the presence of the forest. The *x*-axis is scaled so that 0 coincides with the upstream edge of the forest for each case. ΔKt_u is around 25 % for a few resolved cells in (b). These values are suppressed to 15% to aid presentation.

6.3.2 Waving plants and biological backscatter

Velocity spectra of airflow around forests and other vegetation canopies often contain peaks that correspond to plant movement (Cava & Katul, 2008; Dupont et al., 2018; Finnigan, 1979a, 1979b). This indicates that energy is transferred in two directions—the flow perturbs the plants, but the plants also perturb the flow. This effect is usually ignored in models at the fragment scale and above on the assumption (usually implicit) that the turbulent structures generated by plant movement are much smaller and less energetic than the dominant mixing-layer eddies. However, this neglects the possibility of resonant effects occurring when the passage frequency of the dominant eddies approaches the natural frequency f_0 of the moving plants, as has been observed in crops (Py et al., 2006). Trees near the edges of forests, such as in patchy landscapes and around clearings, are more susceptible to resonance effects than those further inside forest stands (Dupont et al., 2018).

Accounting for this two-way transfer of energy is not straightforward at the fragment scale. Dupont et al. (2010) use LES to model a crop canopy as a poroelastic continuum, with plant movement incorporated into the momentum equations as small mechanical oscillations of rigid stems. Other researchers had previously developed models coupling wind flow and plant swaying in a similar way, but with analytical solutions obtained from simplified velocity statistics rather than through LES (Gosselin & de Langre, 2009; Webb & Rudnicki, 2009). Pivato et al. (2014) extend this approach, using LES to model the movement of pine trees as simplified flexible cantilever beams. Their model includes the possibility large tree deflections by strong gusts, which Dupont et al. (2010) did not account for in their crop model. Pivato et al.'s model performed well against field observations and more complex small-scale plant models in terms of the instantaneous tree response to gusts.

The direct approaches of Dupont et al. (2010) and Pivato et al. (2014) require the plant architectures to be heavily simplified to be computationally feasible. This is not a major problem for tall, slender trees such as maritime pine, the subject of Pivato et al. (2014). However, decurrent trees, which include many broadleaf species, are structurally more complex and can have modes of vibration across several scales, for example, $f_0 \approx 0.5\,Hz$ in the trunks and a few Hz in the branches (Schindler et al., 2013). Capturing these interactions at the scale of an entire forest would be very demanding computationally. A possible workaround in patchy landscapes is to proceed from the observation that wind velocity spectra at forest edges contain peaks around f_0, the natural frequency of the trees (Dupont et al., 2018). This motion is especially visible in the spanwise direction because the turbulent velocity perturbations are smaller than those in the streamwise direction. From a modeling point of view, the trees' movement transfers energy from the SGS to the smallest resolved scales (Piomelli et al., 1991), a process known as 'backscatter'. In general, backscatter is most apparent where small but energetic eddies are present (Mason & Thomson, 1992), such as around forests and other complex structures. Studies of urban canopy flow provide a template of how backscatter could be incorporated into forest models. For example, O'Neill et al. represent the stochastic effects of backscatter in their LES simulations of the neutral surface layer (O'Neill et al., 2015) and street canyon flow (O'Neill et al., 2016) by incorporating random acceleration fields a_i in the momentum equations. This gives

$$\frac{\partial U_i}{\partial t} = \ldots + f_i + \underbrace{\frac{\partial}{\partial x_i}\left\{ \nu_{SGS}\left(\frac{\partial U_i}{\partial x_j} + \frac{\partial U_j}{x_i} \right) \right\}}_{SGS terms} + a_i, \quad (10)$$

where ν_{SGS} is SGS eddy viscosity and the ellipsis represents the other terms carried over from equation (2b). Here, the Smagorinsky SGS scheme is shown. In principle, this approach could be adopted for an LES of forest canopy flows, ideally with the acceleration terms a_i spaced at frequencies corresponding to the movement of tree parts, while ensuring zero divergence. Selino & Jones (2013) adopt a similar approach for a very different purpose, using synthetic SGS turbulence to improve computer graphical animations of trees moving in wind.

7 Conclusions: fragment-scale models in context

Without a great leap in the understanding of fluid dynamics and the Navier–Stokes equations, it is not possible to simulate all aspects of forest–atmosphere exchange in the turbulent ABL. Numerical models of forest–atmosphere exchange can therefore never act entirely as computational wind tunnels. They are nonetheless an invaluable tool in interpreting observations, and for performing experiments on scales relevant to ecology, commerce, and policy. It is an exciting time to investigate forest–atmosphere exchange. Advances in non-destructive scanning techniques (Liang et al., 2016; Raumonen et al., 2015), computing power, and theory are poised to allow researchers to model exchange in realistic canopies, over large scales, using models capable of resolving turbulence. There is a growing body of high-quality observations from micrometeorological campaigns (Butterworth et al., 2021; Patton et al., 2011), long-term ecosystem monitoring (Hicks & Baldocchi, 2020), and ecosystem-scale FACE experiments (Drake et al., 2016; Hart et al., 2020; Norby et al., 2006) against which models can be tested and improved. Moving beyond idealized cases, and ultimately fulfilling the potential of observational networks and new modeling techniques, requires a concerted effort across scientific disciplines. We conclude by framing progress and outstanding challenges under four overlapping headings.

7.1 Targeted observations in patchy landscapes

The ability of turbulence-resolving models to simulate scalar transport in patchy landscapes is essentially unknown. A major hurdle is that there are few public datasets against which the nascent models can be tested. The observations in the Canopy Horizontal Array Turbulence Study (CHATS) in a walnut orchard are the apogee of surface measurements in a tree dominated landscape (Dupont & Patton, 2012; Patton et al., 2011) and a valuable resource for model developers (Ma & Liu, 2019). However, the CHATS measurements were made in a homogeneous orchard on level ground and are therefore unsuitable for testing models' ability to handle patchiness, species diversity, and undulating topography. More measurements are needed, especially of scalar quantities such as CO_2, water vapor, pollutants, and spores in patchy landscapes. For practical reasons, these measurements may not be on the scale of CHATS. However, existing eddy-covariance and FACE facilities have generated extensive timeseries that may be exploited, especially if combined with experiments of opportunity and targeted observational campaigns around edges, gaps, and hills. For example, further experimental testing will determine the extent to which scalar fluxes reach an approximate equilibrium in patchy landscapes, and whether the chimney effect in the lee of hills is observed in nature as well as in numerical models. Researchers are beginning to incorporate canopy exchange schemes in LES models (Ma & Liu, 2019). However, the schemes are often based on quite coarse exchange models, such as the CLM, which cannot capture all the complex interactions between the turbulent flow, leaf transpiration, and light levels that occur in forests (Huang et al., 2015; D. Kim et al., 2014). Fragment-scale models will eventually require a detailed coupling between the light attenuation, the flow field, and evapotranspiration, supported by field observations.

7.2 Connection to larger scales

Developments in theory and computing capacity are allowing researchers to begin incorporating fragment-scale phenomena into full canopy exchange schemes and mesoscale numerical weather

prediction models (Arthur et al., 2019; Bonan et al., 2018; Ma & Liu, 2019; Shao et al., 2013; Yan et al., 2020). To be computationally feasible, these schemes rely on simplified versions of the forest canopy (Yan et al., 2020), a priori turbulence parameters (Y. Chen et al., 2016), or modifications of MOST with mixing-layer length scales (Bonan et al., 2018). These approximations perform best when the atmosphere is neutral and the surface homogeneous. Further work is needed to determine whether the length scales and approximations can be modified to account for patchy landscapes and a larger range of atmospheric conditions. Robust parametrizations for scalar quantities are particularly difficult to find. Missing theoretical links may become apparent through further testing of LES against high-quality field measurements. Another relatively unexplored approach is to reject the assumption that the scalar statistics should always relate to those of the velocity field. For example, understanding the movement of water vapor around at fragmented forest at dusk is a problem that may not yield to a deterministic, drag-based treatment or approximate vertical turbulence profiles. The geometries of velocity and scalar timeseries are often much less scale-dependent than their accompanying physics (Belušić & Mahrt, 2012; D. Chen et al., 2019; Kang, 2015). Turbulent events in these timeseries can also be clustered by their statistical properties, with no assumption of the underlying physical structures (Kang et al., 2015; Sun et al., 2015). The timeseries of well-chosen turbulence measurements may reveal scale-independent behaviors to parametrize forest–atmosphere exchange in terrain and conditions that are beyond the reach of current approaches.

7.3 Numerically efficient improvements to the forest structure

Laser scanning allows researchers to include detailed, site-specific structural information in their models (Boudreault et al., 2015; Raumonen et al., 2015; D. Wang et al., 2020), and virtual canopy generators can be used to generate realistic forest models from a small number of structural variables (Bohrer et al., 2007). Models incorporating realistic forest structure show very different patterns in gas exchange to those assuming the canopy to be homogeneous (Bohrer et al., 2009; Boudreault et al., 2017; Schlegel et al., 2015). Researchers should include a careful description of the forest morphology in their numerical models, particularly when assessing simulated results against observations, or in forests with a high proportion of edge region. Forest models should account for the streamlining of plants in high wind conditions, particularly around gaps, edges, and clearings. This can be accounted for efficiently in models by incorporating the Vogel number B into the parametrization of the aerodynamic drag f_i. Plant movement at an ecosystem scale can be incorporated through poroelastic and mechanical parametrizations (Dupont et al., 2010; Pivato et al., 2014) or by the inclusion of a stochastic forcing into the momentum equations at a frequency corresponding to plant movement.

7.4 Challenging weather and atmospheric conditions

Numerical models allow low dimensionality experiments that are difficult to perform in the open atmosphere. A common simplification is that of an isolated forest in neutral atmospheric conditions. This removes all aspects of the atmosphere, other than a velocity field that is recycled using periodic boundary conditions. In nature, however, forests are subject to all sorts of weather, climatic, atmospheric conditions. Stability changes quickly in time, such as around dusk, and in space, such as where radiation emission/absorption cause completely different

atmospheric properties within a forest compared with the surroundings. Simulations of the entire ABL will help explore these effects further (Ma & Liu, 2019; Patton et al., 2016; Yan et al., 2020). Local effects around gaps and areas of uneven heating should not be discounted. Further research is needed into the effect of submeso motions on forest–atmosphere exchange. These are difficult to model because they often manifest as intermittent turbulent bursts, but do not result from mixing-layer-type eddies, and therefore must be generated using mesoscale coupling or synthetic turbulence. However, submeso motions are common in the atmospheric conditions that tend to be most problematic for eddy-covariance measurements, such as during stable nights, and discounting their effect from models introduces an unwelcome bias. Rainfall is a significant source of momentum into forests, affecting myriad ecological processes as well as the plants' mechanical response to the flow. Raindrop-induced vortices can carry small particles away from plant surfaces and into the turbulent flow. Wet conditions provide a major unexplored area for numerical investigations of forest–atmosphere exchange because much of the world's forested area is situated in climates where precipitation is common.

Notation

ABL	Atmospheric boundary layer.
ASL	Atmospheric surface layer.
$a(z)$	Layer-wise plant area density.
B	Vogel number.
BIFoR	Birmingham Institute of Forest Research.
(B)VOCs	(Biogenic) volatile organic compounds.
C_d	Drag coefficient.
CLM	Community Land Model.
DNS	Direct numerical simulation.
E_ϕ	Efficiency of particle deposition.
FACE	Free-air carbon dioxide enrichment.
f_i	Aerodynamic drag.

65

f_0	Natural frequency of moving plants.
g	Gravitational acceleration.
h_c	Canopy height.
h_d	Displacement height.
ICR	In-canopy recirculation region.
ISL	Inertial sublayer.
Kt_{u_i}	Kurtosis of the velocity component u_i.
L	Hill half-length.
L_c	Canopy drag length scale.
LES	Large-eddy simulation.
L_s	Shear length scale.
LSM	Lagrangian stochastic modeling.
MOST	Monin–Obukhov similarity theory.
O_d	Diameter of opening.
P	Perturbation pressure.
PAD	Plant area density.
PAI	Plant area index.
Q_{h_c}	Specific flux at the crown top.
RANS	Reynolds-average Navier–Stokes.
$\Re$	Reynolds number.

66

RSL	Roughness sublayer.
SGS	Sub-grid scale.
Sk_{u_i}	Skewness of the velocity component u_i.
S_{ϕ_i}	Source/sink of a scalar quantity ϕ_i.
TKE	Turbulence kinetic energy.
UFP	Ultrafine particles.
U_{h_c}	Mean streamwise wind speed at the crown top.
u_{ι}	Friction velocity.
WRF	Weather Research and Forecasting model.
w_s	Particle settling velocity.
x_A	Adjustment distance.
z_i	Boundary-layer height.
z_0	Roughness length.
α	Attenuation coefficient.
δ_{i3}	Kronecker delta.
θ_v	Virtual potential temperature.
θ_0	Reference temperature.
ν_{SGS}	Sub-grid scale eddy viscosity.
v_ϕ	Dry deposition velocity.
σ_{u_i}	Standard deviation of the velocity component u_i.

τ	Air parcel residence time.
ϕ_l	Resolved local scalar concentration.

8 Appendix A: numerical details of LES model

8.1 Drag parametrization and simulated cases

We simulate flow across different forests, with the presence of the aerial parts of the forests represented using the drag parametrization in equation (6), $f_i = -C_d a(z)|U|\langle u_i \rangle$. We replace the U_i in equation (6) with $\langle u_i \rangle$ here because we do not time average the variables until the post-processing step. We specified a height-averaged sectional drag coefficient $\overline{C}_d =$ ¿ 0.2, a value commonly used in previous studies (Table A1). Figure 9 shows the mean vertical profile of the LAD, $a(z)$, specified across all three cases. The profile $a(z)$ was derived from terrestrial lidar surveys of the BIFoR FACE facility (Hart et al., 2020), using the method in Raumonen et al. (2015), giving PAI ≈ 5.

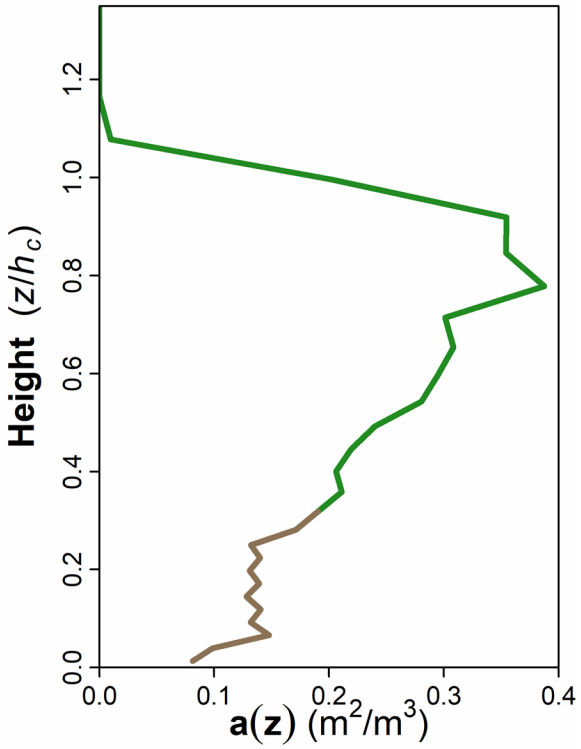

Figure 9. Vertical profile of PAD $a(z)$ (PAI ≈ 5) used in the LES model for Cases 1–3. Coloring indicates that the trunks account for much of the PAD in the lower part of the canopy, and the leaves account for much of the PAD in the upper part of the canopy. The coloring is illustrative only and does not reflect the detailed composition of the BIFoR FACE facility.

We specified three cases:

- **Case 1 –** We apply the distributed-drag method across the entire domain to simulate a continuous, homogeneous forest.

- **Case 2 –** We apply the distributed-drag method over a patch extending 500 m in the streamwise direction, and across the entire domain in the spanwise direction, to simulate flow across a small, isolated forest.
- **Case 3** – As for Case 2 but, for each forested cell, $\overline{C}_d a(z)$ (Case 3) taking a random number (uniformly distributed) within the range $\overline{C}_d a(z)$(Case 2) $\pm 2\%$. This introduces a small spatial stocastic forcing into the momentum equations solved by the LES model via the drag term in equation (6). However, the stochastic forcing does not directly vary with time using this formulation.

8.2 Transport Equations

We solved the transport equations using the LES mode of WRF version 3.6.1 (Skamarock et al., 2008). The WRF model solves discretized forms of the spatially averaged momentum equations using the Runge–Kutta time-integration scheme (Wicker & Skamarock, 2002),

$$\frac{\partial \langle u_i \rangle}{\partial x_i} = 0, \tag{11a}$$

$$\frac{\partial \langle u_i \rangle}{\partial t} + \frac{\partial \langle u_i \rangle \langle u_j \rangle}{\partial x_j} = \frac{-1}{\rho}\frac{\partial \langle p \rangle}{\partial x_i} + \frac{\partial \tau_{ij}}{\partial x_j} + B_i + f_c \epsilon_{ij3}\left(\langle u_j \rangle - U_{g,j}\right) + f_i, \tag{11b}$$

where ρ is the air density;$\langle p \rangle$ is the spatially averaged pressure; τ_{ij} is the kinematic mean stress tensor, which represents the SGS stresses; B_i is the buoyancy force: $B_i = -\delta_{i3} g\theta'/\overline{\theta}$, where $\overline{\theta}$ is the potential temperature for hydrostatic balance, and θ' is the temperature variations with respect to $\overline{\theta}$; f_c is the Coriolis parameter; ϵ_{ij3} is the alternating unit tensor; and $U_{g,j}$ is the geostrophic velocity. Equation (11b) is closed by parametrizing the SGS stress tensor τ_{ij} as

$$\tau_{ij} = -2\nu_{SGS} S_{ij}, \tag{12}$$

$$S_{ij} = \frac{1}{2}\left(\frac{\partial \langle u_i \rangle}{\partial x_j} + \frac{\partial \langle u_j \rangle}{\partial x_i}\right), \tag{13}$$

$$\nu_{SGS} = c_k \sqrt{\langle e_{SGS} \rangle}\left(\Delta x \Delta y \Delta z\right)^{\frac{1}{3}}, \tag{14}$$

where $\langle e_{SGS} \rangle$ is the SGS TKE and $c_k =$ ¿ 0.10 is a modelling constant. The prognostic equation for the evolution of the term $\langle e_{SGS} \rangle$ is,

$$\frac{\partial \langle e_{SGS} \rangle}{\partial t} + \frac{\partial \langle u_j \rangle \langle e_{SGS} \rangle}{\partial x_j} = \nu_{SGS} \frac{\partial}{\partial x_j} \left(\frac{\partial \langle e_{SGS} \rangle}{\partial x_j} \right) + P_r + F - \frac{C_\epsilon \langle e_{SGS} \rangle}{(\Delta x \Delta y \Delta z)^{\frac{1}{3}}}, \quad (15)$$

where P_r represents the shear- and buoyancy-production terms (Skamarock et al., 2008), C_ϵ is the dissipation coefficient (Moeng et al., 2007). The term F is a cascade term, which accounts for additional dissipation of kinetic energy from air–forest interactions at scales smaller than the spatial filter (Shaw & Patton, 2003; Shaw & Schumann, 1992), with

$$F = -2 \overline{C}_d a(z) |U| \langle e_{SGS} \rangle. \quad (16)$$

8.3 Drag parametrization and simulated cases

The simulated domain is 1435 × 1435 × 1000 m in the streamwise, spanwise, and vertical directions, respectively, comprising 287 × 287 × 79 grid cells. The horizontal grid resolution is 5 m in each direction, and the vertical resolution is increased from around 0.67 m in the lower half of the forest to around 60 m at the top of the simulated domain. The mean height of the forest h_c is set to 25 m for each case. For Cases 2 and 3, the upstream edge of the forest is situated approximately 600 m from the inflow edge of the domain (Case 1 is forested across the entire domain). We simulate flow under neutral conditions, with the initial profile of potential temperature θ specified as a constant at 283.15 K at the bottom of the domain (up to $z \approx 475$ m) followed by a linear increase to 291.7 K at the top of the domain. We include a dampening layer of $z \approx 300$ m at the top of the domain to minimize wave reflection (Nottrott et al., 2014). The geostrophic velocity components above the boundary layer top are set to $U_g = -¿6$ m s^{-1} and $V_g = -¿9.3$ m s^{-1}, and this specification yields a mean wind speed of 1.6 m s^{-1} from a flow direction of 343° (approximately a northerly wind) at the crown top ($z = h_c$). We use the meteorological convention where the *x*-direction is aligned west–east and the *y*-direction south–north.

Spin-up was 5 h, with cyclic boundary conditions for all dynamical variables in both horizontal directions. After the spin-up, we ran the simulations for a further 120 min, taking samples at intervals of 3 s. We time-averaged over the latter 100 min (denoted by T) of these samples (*i.e.*, $t_0 = 20$min to $t_0 + T = 120$ min). This process generates a three-dimensional time series of 2000 resolved samples in the form $\langle \phi \rangle (x, y, z, t)$. We derived the resolved turbulent statistics using (a) time averages over the sampling period; and (b) spatial averages along the *y*-direction (L_y= 1435 m), over which the turbulent statistics are homogeneous. For each resolved variable, $\langle \phi \rangle$, the averaging process generates a two-dimensional function,

$$\overline{\Phi}(x, z) = \frac{1}{T L_y} \int_0^{L_y} \int_{t_0}^{t_0 + T} \langle \phi \rangle (x, y, z, t) dt dy, \quad (17)$$

from which we calculate the statistics presented in Figures 5 and 8. The resolved fluctuating component of $\langle\phi\rangle$ around $\overline{\Phi}$ is defined as $\langle\phi'\rangle(x,y,z,t)=\langle\phi\rangle(x,y,z,t)-\overline{\Phi}(x,z)$, with the skewness $Sk_{u_i}=\langle\overline{u_i'^3}\rangle/\sigma_{u_i}^3$ and kurtosis $Kt_{u_i}=\langle\overline{u_i'^4}\rangle/\sigma_{u_i}^4$.

Appendix B: Summary of modeling investigations of flow around forests

Table A1. Chronological summary of highly cited modeling investigations of flow around forests at the fragment scale. PAD and PAI, respectively, refer to the plant area density/index, $a(z)$ is a height-dependent function of the PAD, and C_d is the drag coefficient

Study	Equations/ model	Distribution of PAD as $a(z)$	C_d	PAI range (m^2/m^2)	Additional Features
Shaw & Schumann (1992)	LES	Artificially generated vertical profile for a deciduous forest.	0.15	2, 5	
Dwyer et al. (1997)	LES	Artificially generated vertical profile for a deciduous forest	0.15	2, 5	Numerical setup based on Shaw & Schumann (1992)
Su et al. (1998)	LES	Artificially generated vertical profile for a deciduous forest	0.15	2	Numerical setup based on Shaw & Schumann (1992)
Shaw & Patton (2003)	LES	Artificially generated vertical profile for a deciduous forest	0.15	2	
Watanabe (2004)	LES	Uniform vertical distribution	0.2	2	
Finnigan & Belcher (2004)	Mixing-length closure	Uniform vertical distribution	0.25	≈ 4	Drag parameters are approximations. Analysis is mostly expressed in dimensionless terms
Katul et al. (2006)	Mixing-length closure	Uniform vertical distribution	0.2	3	Investigated carbon dioxide exchange over forested hills
Yang et al. (2006b, a)	LES	Artificially generated vertical profile for a deciduous forest	0.15	2	Numerical setup based on Shaw & Schumann (1992)
Dupont & Brunet (2008a)	LES	Four cases: (1) approximately vertically uniform; (2) sparse trunk space and dense crown; (3) very dense crown and very sparse trunk space; and (4) undergrowth in trunk space	≈ 0.5	2	PAI chosen so that the product $c_d a(z)$ was the same as in Raupach et al. (1987), where PAI ≈ 5
Dupont & Brunet (2008b)	LES	Uniform vertical distribution	0.2	2	Structure of the upstream edge of the forest was varied across seven shapes and densities
Dupont & Brunet (2008c)	LES	Three cases: (1) approximately vertically uniform; (2) sparse trunk space and dense crown; (3) undergrowth in trunk space	0.2	1–5	
Cassiani et al. (2008)	LES	Artificially generated vertical profile for a deciduous forest	0.2	2–8	Forest structure approximately based on that of Duke Forest (Katul & Albertson, 1998)
Sogachev et al. (2008)	RANS	Foliage distribution based on beta probability density function	0.2	0.5–3	Investigated scalar transport around a forest edge
Ross (2008)	LES	Uniform vertical distribution	0.15	5	Simulated flow over forested ridges
Bohrer et al. (2009)	LES	Randomly generated heterogeneous canopy	0.15	1.4–3	1,000 virtual canopies generated for each simulation, with randomized gaps of approximately crown width
Dupont & Brunet (2009)	LES	Artificially generated vertical profile for a deciduous forest	0.2	2, 5	Canopy structure approximately based on deciduous forest reported in Neumann et al. (1989)
Dupont et al. (2011)	LES	Dense canopy with sparse trunk space to approximate pine plantation	0.26	2	Includes five additional cases with the vertical profile gradually relaxed towards a uniform distribution

Edburg et al. (2012)	LES	Artificially generated vertical profile for a deciduous forest	0.5	1	
Schlegel et al. (2012)	LES	Forest dominated by *Picea abies*. PAD varied across simulated domain	0.15	≈ 7.1	PAD distribution derived from terrestrial Lidar
Mueller et al. (2014)	LES	Simplified vertical profiles estimates from observations in a pine plantation and a deciduous forest	0.26	2	Setup taken from Sylvain Dupont et al. (2011) and Hong Bing Su et al. (1998)
Boudreault et al. (2015)	RANS	Forest dominated by *Picea abies*. Frontal area density varied across simulated domain	0.2	≈2.9	Vertical profile derived from aerial lidar scans of the forested area
Xu et al. (2015)	Renormalization Group	Vertical profile from measurements in a forest dominated by spruce and pine	≈ 0.3	3.3	Two-dimensional investigation of stably stratified flow around an idealized forested hill
Kanani-Sühring & Raasch (2015)	LES	Artificially generated vertical profile for a deciduous forest	0.2	1–8	Used LES to investigate scalar transport around a forest edge
Schlegel et al. (2015)	LES	Forest dominated by *Picea abies*. PAD varied across simulated domain	0.15	≈ 7.1	PAD distribution derived from terrestrial lidar. Developed preliminary work in Schlegel et al. (2012)
Ross & Harman (2015)	LES	Uniform vertical distribution	0.25	4	Simulated flow and scalar transport over forested hills
Kanani-Sühring & Raasch (2017)	LES	Artificially generated vertical profile for a deciduous forest	0.2	1–8	Investigated scalar transport in the lee of the forest, with multiple sources and sinks
Yan et al. (2017)	LES	Simplified deciduous trees. Three cases: (1) bluff objects; (2) bluff trunks and porous crowns; (3) fully porous trees	≈0.2	≈ 5	Numerical details couched in terms of bluff objects (e.g. frontal area index) to be compared more easily to wind-tunnel observations in Böhm et al. (2013)
Boudreault et al. (2017)	LES	Two cases: (1) heterogeneous PAD derived from terrestrial lidar; and (2) spatially homogeneous $a(z)$ from averaged data	0.2	6	Heterogeneous case included tapered upstream edge
Chen et al. (2019)	LES	Horizontally homogeneous. Profile derived from leaf area measurements in the Amazon rainforest	0.2	7	Simulated flow and scalar transport over forested hills. PAD profiles generated from observations reported in Tóta et al. (2012) and Fuentes et al. (2016)
Ma & Liu (2019)	LES	Uniform vertical distribution	0.2	2.5	LES coupled with multiple−layer canopy exchange model
Watanabe et al. (2020)	LES (Lattice Boltzmann method)	Uniform vertical distribution	0.2	2	The equations of motion are resolved using the lattice Boltzmann method rather than solving the incompressible Navier–Stokes equations
Ma et al. (2020)	LES	Three cases: (1) vertically uniform (2) sparse trunk space and dense crown; (3) very sparse trunk space and dense crown	0.25	4	LES coupled with a multiple−layer canopy exchange model used to investigate transport of different scalars across a forest edge
Yan et al. (2020)	LES	Profile generated using empirical relationship in Lalic and Mihailovic (2004)	0.15	4.3	LES coupled to the mesoscale Weather Research and Forecasting model. Grid resolution at the mesoscale

Acknowledgments, Samples, and Data

The authors declare no real or perceived financial conflicts of interests. We thank Jian Zhong for help and advice on LES simulations, Eric Casella for his terrestrial laser scans of BIFoR FACE, and the BIFoR FACE operations team for helpful discussions, photography, and drone footage. It is EJB's pleasure to acknowledge the Natural Environment Research Council (NERC) for funding through a CENTA studentship (grant NE/L002493/1). ARMK gratefully acknowledges funding from the JABBS Foundation and NERC (grant NE/S015833/1) in support of this work.

Figure 3c Soil-Science.info on Flickr. "*Pinus taeda* plantation". 21 May 2008. Online image with Creative Common License CC-BY-2.0. https://www.flickr.com/photos/22503286@N06/2512091836

Figure 4(c) -JvL- on Flickr. "Brownsberg jungle path". 22 October 2016. Online image with Creative Common License CC-BY-2.0. https://www.flickr.com/photos/-jvl-/33153976490/

Figure 4(d) R.V. on Flickr. "Forest, British Columbia, Canada". 6 July 2013. Online image with Creative Common License CC-BY-2.0. https://www.flickr.com/photos/bluegruen/9601965057

The WRF-LES data used in this paper, and their supporting R scripts, are available at https://github.com/foresteddy/forest_exchange.

References

Acevedo, O. C., Moraes, O. L. L., Degrazia, G. A., Fitzjarrald, D. R., Manzi, A. O., & Campos, J. G. (2009). Is friction velocity the most appropriate scale for correcting nocturnal carbon dioxide fluxes? *Agricultural and Forest Meteorology*, *149*(1), 1–10. https://doi.org/10.1016/j.agrformet.2008.06.014

Alekseychik, P., Mammarella, I., Launiainen, S., Rannik, Ü., & Vesala, T. (2013). Evolution of the nocturnal decoupled layer in a pine forest canopy. *Agricultural and Forest Meteorology*, *174–175*, 15–27. https://doi.org/10.1016/j.agrformet.2013.01.011

Amiro, B. D. (1990). Comparison of turbulence statistics within three boreal forest canopies. *Boundary-Layer Meteorology*, *51*(1–2), 99–121. https://doi.org/10.1007/BF00120463

Arthur, R. S., Mirocha, J. D., Lundquist, K. A., & Street, R. L. (2019). Using a canopy model framework to improve large-eddy simulations of the neutral atmospheric boundary layer in the weather research and forecasting model. *Monthly Weather Review*, *147*(1), 31–52. https://doi.org/10.1175/MWR-D-18-0204.1

Ashworth, K., Chung, S. H., Griffin, R. J., Chen, J., Forkel, R., Bryan, A. M., & Steiner, A. L. (2015). FORest Canopy Atmosphere Transfer (FORCAsT) 1.0: A 1-D model of biosphere-atmosphere chemical exchange. *Geoscientific Model Development*, *8*(11), 3765–3784. https://doi.org/10.5194/gmd-8-3765-2015

Aubinet, M. (2008). Eddy covariance CO2 flux measurements in nocturnal conditions: An analysis of the problem. *Ecological Applications*, *18*(6), 1368–1378. https://doi.org/10.1890/06-1336.1

Aubinet, M., Feigenwinter, C., Heinesch, B., Bernhofer, C., Canepa, E., Lindroth, A., et al. (2010). Direct advection measurements do not help to solve the night-time CO2 closure problem: Evidence from three different forests. *Agricultural and Forest Meteorology*, *150*(5), 655–664. https://doi.org/10.1016/j.agrformet.2010.01.016

Aubinet, M., Vesala, T., & Papale, D. (2012). *Eddy covariance: a practical guide to measurement and data analysis*. Springer Science & Business Media.

Aylor, D. E., & Flesch, T. K. (2001). Estimating spore release rates using a Lagrangian stochastic simulation model. *Journal of Applied Meteorology*, *40*(7), 1196–1208. https://doi.org/10.1175/1520-0450(2001)040<1196:ESRRUA>2.0.CO;2

Bailey, B. N., & Stoll, R. (2016). The creation and evolution of coherent structures in plant canopy flows and their role in turbulent transport. *Journal of Fluid Mechanics*, *789*, 425–460. https://doi.org/10.1017/jfm.2015.749

Bailey, B. N., Stoll, R., Pardyjak, E. R., & Mahaffee, W. F. (2014). Effect of vegetative canopy architecture on vertical transport of massless particles. *Atmospheric Environment*, *95*, 480–489. https://doi.org/10.1016/j.atmosenv.2014.06.058

Baldocchi, D. D. (2008). TURNER REVIEW No. 15. "Breathing" of the terrestrial biosphere: Lessons learned from a global network of carbon dioxide flux measurement systems. *Australian Journal of Botany*, *56*(1), 1–26. https://doi.org/10.1071/BT07151

Baldocchi, D. D., Falge, E., Gu, L., Olson, R., Hollinger, D., Running, S., et al. (2001). FLUXNET: A New Tool to Study the Temporal and Spatial Variability of Ecosystem-Scale Carbon Dioxide, Water Vapor, and Energy Flux Densities. *Bulletin of the American Meteorological Society*, *82*(11), 2415–2434. https://doi.org/10.1175/1520-0477(2001)082<2415:FANTTS>2.3.CO;2

Bannister, E. J., Cai, X., Zhong, J., & Mackenzie, A. R. (2021). Neighbourhood-scale flow regimes and pollution transport in cities. *Boundary-Layer Meteorology*, *179*(2), 259–289.

Batista, C. E., Ye, J., Ribeiro, I. O., Guimarães, P. C., Medeiros, A. S. S., Barbosa, R. G., et al. (2019). Intermediate-scale horizontal isoprene concentrations in the near-canopy forest atmosphere and implications for emission heterogeneity. *Proceedings of the National Academy of Sciences of the United States of America*, *116*(39), 19318–19323. https://doi.org/10.1073/pnas.1904154116

Belcher, S. E., Jerram, N., & Hunt, J. C. R. (2003). Adjustment of a turbulent boundary layer to a canopy of roughness elements. *Journal of Fluid Mechanics*, *488*(488), 369–398. https://doi.org/10.1017/S0022112003005019

Belcher, S. E., Harman, I. N., & Finnigan, J. J. (2012). The Wind in the Willows: Flows in Forest Canopies in Complex Terrain. *Annual Review of Fluid Mechanics*, *44*(1), 479–504. https://doi.org/10.1146/annurev-fluid-120710-101036

Belušić, D., & Mahrt, L. (2012). Is geometry more universal than physics in atmospheric boundary layer flow? *Journal of Geophysical Research Atmospheres*, *117*(9), 1–10. https://doi.org/10.1029/2011JD016987

Bertrand, R., Aubret, F., Grenouillet, G., Ribéron, A., & Blanchet, S. (2020). Comment on "Forest microclimate dynamics drive plant responses to warming." *Science*, *370*(6520), 1–4. https://doi.org/10.1088/1751-8113/44/8/085201

Bogaert, J., Barima, Y., Mongo, L. I. W., Bamba, I., Mama, A., Toyi, M., & Lafortezza, R. (2011). Forest Fragmentation: Causes, Ecological Impacts and Implications for Landscape Management. In C. Li, R. Lafortezza, & J. Chen (Eds.), *Landscape ecology in forest management and conservation: challenges and solutions for global change* (pp. 273–292). Berlin: Springer. https://doi.org/10.5860/choice.49-2647

Böhm, M., Finnigan, J. J., Raupach, M. R., & Hughes, D. (2013). Turbulence Structure Within and Above a Canopy of Bluff Elements. *Boundary-Layer Meteorology*, *146*(3), 393–419. https://doi.org/10.1007/s10546-012-9770-1

Bohrer, G., Wolosin, M., Brady, R., & Avissar, R. (2007). A virtual canopy generator (V-CaGe) for modelling complex heterogeneous forest canopies at high resolution. In *Tellus, Series B: Chemical and Physical Meteorology* (Vol. 59, pp. 566–576). Blackwell Munksgaard. https://doi.org/10.1111/j.1600-0889.2007.00253.x

Bohrer, G., Katul, G. G., Walko, R. L., & Avissar, R. (2009). Exploring the effects of microscale structural heterogeneity of forest canopies using large-eddy simulations. *Boundary-Layer Meteorology*, *132*(3), 351–382. https://doi.org/10.1007/s10546-009-9404-4

Bonan, G. B., Pollard, D., & Thompson, S. L. (1992). Effects of boreal forest vegetation on global climate. *Nature*, *359*(6397), 716–718. https://doi.org/10.1038/359716a0

Bonan, G. B., Patton, E. G., Harman, I. N., Oleson, K. W., Finnigan, J. J., Lu, Y., & Burakowski, E. A. (2018). Modeling canopy-induced turbulence in the Earth system: A unified parameterization of turbulent exchange within plant canopies and the roughness sublayer (CLM-ml v0). *Geoscientific Model Development*, *11*(4), 1467–1496. https://doi.org/10.5194/gmd-11-1467-2018

Bou-Zeid, E. (2014). Challenging the large eddy simulation technique with advanced a posteriori tests. *Journal of Fluid Mechanics*, *764*, 1–4. https://doi.org/10.1017/jfm.2014.616

Bou-Zeid, E., Anderson, W., Katul, G. G., & Mahrt, L. (2020). The Persistent Challenge of Surface Heterogeneity in Boundary-Layer Meteorology: A Review. *Boundary-Layer Meteorology*, *177*(2), 227–245. https://doi.org/10.1007/s10546-020-00551-8

Boudreault, L. É., Bechmann, A., Tarvainen, L., Klemedtsson, L., Shendryk, I., & Dellwik, E. (2015). A LiDAR method of canopy structure retrieval for wind modeling of heterogeneous forests. *Agricultural and Forest Meteorology*, *201*, 86–97. https://doi.org/10.1016/j.agrformet.2014.10.014

Boudreault, L. É., Dupont, S., Bechmann, A., & Dellwik, E. (2017). How Forest Inhomogeneities Affect the Edge Flow. *Boundary-Layer Meteorology*, *162*(3), 375–400. https://doi.org/10.1007/s10546-016-0202-5

Bright, V. B., Bloss, W. J., & Cai, X. (2013). Urban street canyons: Coupling dynamics, chemistry and within-canyon chemical processing of emissions. *Atmospheric Environment*, *68*, 127–142. https://doi.org/10.1016/j.atmosenv.2012.10.056

Brüchert, F., & Gardiner, B. A. (2006). The effect of wind exposure on the tree aerial architecture and biomechanics of Sitka spruce (Picea sitchensis, Pinaceae). *American Journal of Botany*, *93*(10), 1512–1521. https://doi.org/10.3732/ajb.93.10.1512

Brunet, Y. (2020). Turbulent Flow in Plant Canopies: Historical Perspective and Overview. *Boundary-Layer Meteorology*, *177*(2–3), 315–364. https://doi.org/10.1007/s10546-020-00560-7

Brunet, Y., & Irvine, M. R. (2000). The control of coherent eddies in vegetation canopies: Streamwise structure spacing, canopy shear scale and atmospheric stability. *Boundary-Layer Meteorology*, *94*(1), 139–163. https://doi.org/10.1023/A:1002406616227

Bryan, A. M., Bertman, S. B., Carroll, M. A., Dusanter, S., Edwards, G. D., Forkel, R., et al. (2012). In-canopy gas-phase chemistry during CABINEX 2009: Sensitivity of a 1-D canopy model to vertical mixing and isoprene chemistry. *Atmospheric Chemistry and Physics*, *12*(18), 8829–8849. https://doi.org/10.5194/acp-12-8829-2012

Buccolieri, R., Santiago, J. L., Rivas, E., & Sanchez, B. (2018). Review on urban tree modelling in CFD simulations: Aerodynamic, deposition and thermal effects. *Urban Forestry and Urban Greening*, *31*(July 2017), 212–220. https://doi.org/10.1016/j.ufug.2018.03.003

Butterworth, B. J., Desai, A. R., Metzger, S., Townsend, P. A., Schwartz, M. D., Petty, G. W., et al. (2021). Connecting land–atmosphere interactions to surface heterogeneity in CHEESEHEAD19. *Bulletin of the American Meteorological Society*, *102*(2), E421–E445. https://doi.org/10.1175/BAMS-D-19-0346.1

Canadell, J. G., & Raupach, M. R. (2008). Managing forests for climate change mitigation. *Science*, *320*(5882), 1456–1457. https://doi.org/10.1126/science.1155458

Cassiani, M., Katul, G. G., & Albertson, J. D. (2008). The Effects of Canopy Leaf Area Index on Airflow Across Forest Edges: Large-eddy Simulation and Analytical Results, *126*, 433–460. https://doi.org/10.1007/s10546-007-9242-1

Cava, D., & Katul, G. G. (2008). Spectral short-circuiting and wake production within the canopy trunk space of an alpine hardwood forest. *Boundary-Layer Meteorology*, *126*(3), 415–431. https://doi.org/10.1007/s10546-007-9246-x

Cava, D., Mortarini, L., Giostra, U., Acevedo, O., & Katul, G. (2019). Submeso Motions and Intermittent Turbulence Across a Nocturnal Low-Level Jet: A Self-Organized Criticality Analogy. *Boundary-Layer Meteorology*, *172*(1), 17–43. https://doi.org/10.1007/s10546-019-00441-8

Chaudhari, A., Conan, B., Aubrun, S., & Hellsten, A. (2016). Numerical study of how stable stratification affects turbulence instabilities above a forest cover: Application to wind energy. *Journal of Physics: Conference Series*, *753*(3). https://doi.org/10.1088/1742-6596/753/3/032037

Chen, B., Chamecki, M., & Katul, G. G. (2019). Effects of topography on in-canopy transport of gases emitted within dense forests. *Quarterly Journal of the Royal Meteorological Society*, *145*(722), 2101–2114. https://doi.org/10.1002/qj.3546

Chen, D., Hu, F., Xu, J., & Liu, L. (2019). Long-range correlation analysis among non-stationary passive scalar series in the turbulent boundary layer. *Physica A: Statistical Mechanics and Its Applications*, *517*, 290–296. https://doi.org/10.1016/j.physa.2018.09.094

Chen, L., Liu, C., Zhang, L., Zou, R., & Zhang, Z. (2017). Variation in Tree Species Ability to Capture and Retain Airborne Fine Particulate Matter (PM2.5). *Scientific Reports*, *7*(1), 1–11. https://doi.org/10.1038/s41598-017-03360-1

Chen, Y., Ryder, J., Bastrikov, V., McGrath, M. J., Naudts, K., Otto, J., et al. (2016). Evaluating the performance of land surface model ORCHIDEE-CAN v1.0 on water and energy flux estimation with a single-and multi-layer energy budget scheme. *Geoscientific Model Development*, *9*(9), 2951–2972. https://doi.org/10.5194/gmd-9-2951-2016

Chiesa, M., Bignotti, L., Finco, A., Marzuoli, R., & Gerosa, G. (2019). Size-resolved aerosol fluxes above a broadleaved deciduous forest. *Agricultural and Forest Meteorology*, *279*(June), 107757. https://doi.org/10.1016/j.agrformet.2019.107757

Cionco, R. M. (1965). A Mathematical Model for Air Flow in a Vegetative Canopy. *Journal of Applied Meteorology*. https://doi.org/10.1175/1520-0450(1965)004<0517:ammfaf>2.0.co;2

Cionco, R. M. (1978). Analysis of canopy index values for various canopy densities. *Boundary-Layer Meteorology*, *15*(1), 81–93. https://doi.org/10.1007/BF00165507

Crandall, S. G., & Gilbert, G. S. (2017). Meteorological factors associated with abundance of airborne fungal spores over natural vegetation. *Atmospheric Environment*, *162*, 87–99. https://doi.org/10.1016/j.atmosenv.2017.05.018

Crockatt, M. E., & Bebber, D. P. (2015). Edge effects on moisture reduce wood decomposition rate in a temperate forest. *Global Change Biology*, *21*(2), 698–707. https://doi.org/10.1111/gcb.12676

Cucchi, V., Meredieu, C., Stokes, A., Berthier, S., Bert, D., Najar, M., et al. (2004). Root anchorage of inner and edge trees in stands of Maritime pine (Pinus pinasterAit.) growing in different podzolic soil conditions. *Trees - Structure and Function*, *18*(4), 460–466. https://doi.org/10.1007/s00468-004-0330-2

Dal Maso, M., Kulmala, M., Lehtinen, K. E. J., ŇMkelä, J. M., Aalto, P., & O'Dowd, C. D. (2002). Condensation and coagulation sinks and formation of nucleation mode particles in coastal and boreal forest boundary layers. *Journal of Geophysical Research Atmospheres*, *107*(19). https://doi.org/10.1029/2001JD001053

Drake, J. E., Macdonald, C. A., Tjoelker, M. G., Crous, K. Y., Gimeno, T. E., Singh, B. K., et al. (2016). Short-term carbon cycling responses of a mature eucalypt woodland to gradual stepwise enrichment of atmospheric CO2 concentration. *Global Change Biology*, *22*(1), 380–390. https://doi.org/10.1111/gcb.13109

Dupont, S., & Brunet, Y. (2008a). Edge flow and canopy structure: A large-eddy simulation study. *Boundary-Layer Meteorology*, *126*(1), 51–71. https://doi.org/10.1007/s10546-007-9216-3

Dupont, S., & Brunet, Y. (2008b). Impact of forest edge shape on tree stability: A large-eddy simulation study. *Forestry*, *81*(3), 299–315. https://doi.org/10.1093/forestry/cpn006

Dupont, S., & Brunet, Y. (2008c). Influence of foliar density profile on canopy flow: A large-eddy simulation study. *Agricultural and Forest Meteorology*, *148*(6–7), 976–990. https://doi.org/10.1016/j.agrformet.2008.01.014

Dupont, S., & Brunet, Y. (2009). Coherent structures in canopy edge flow: A large-eddy simulation study. *Technical Reports*, *630*, 93–128. https://doi.org/10.1017/S0022112009006739

Dupont, S., & Patton, E. G. (2012). Influence of stability and seasonal canopy changes on micrometeorology within and above an orchard canopy: The CHATS experiment. *Agricultural and Forest Meteorology*, *157*, 11–29. https://doi.org/10.1016/j.agrformet.2012.01.011

Dupont, S., Gosselin, F. P., Py, C., De Langre, E., Hemon, P., & Brunet, Y. (2010). Modelling waving crops using large-eddy simulation: Comparison with experiments and a linear stability analysis. *Journal of Fluid*

Mechanics, *652*, 5–44. https://doi.org/10.1017/S0022112010000686
Dupont, S., Bonnefond, J. M., Irvine, M. R., Lamaud, E., & Brunet, Y. (2011). Long-distance edge effects in a pine forest with a deep and sparse trunk space: In situ and numerical experiments. *Agricultural and Forest Meteorology*, *151*(3), 328–344. https://doi.org/10.1016/j.agrformet.2010.11.007
Dupont, S., Défossez, P., Bonnefond, J. M., Irvine, M. R., & Garrigou, D. (2018). How stand tree motion impacts wind dynamics during windstorms. *Agricultural and Forest Meteorology*, *262*, 42–58. https://doi.org/10.1016/j.agrformet.2018.06.022
Dwyer, M. J., Patton, E. G., & Shaw, R. H. (1997). Turbulent kinetic energy budgets from a large-eddy simulation of airflow above and within a forest canopy. *Boundary-Layer Meteorology*, *84*(1), 23–43. https://doi.org/10.1023/A:1000301303543
Edburg, S. L., Stock, D., Lamb, B. K., & Patton, E. G. (2012). The Effect of the Vertical Source Distribution on Scalar Statistics within and above a Forest Canopy. *Boundary-Layer Meteorology*, *142*(3), 365–382. https://doi.org/10.1007/s10546-011-9686-1
Fahrig, L. (2003). Effects of Habitat Fragmentation on Biodiversity. *Annual Review of Ecology, Evolution, and Systematics*, *34*, 487–515. https://doi.org/10.1146/annurev.ecolsys.34.011802.132419
Finnigan, J. J. (1979a). *Turbulence in Waving Wheat: I Mean Statistics and Honami*. *Boundary-Layer Meteorology* (Vol. 16). https://doi.org/10.1007/BF03335367
Finnigan, J. J. (1979b). Turbulence in waving wheat: II. Structure of Momentum Transfer. *Boundary-Layer Meteorology*, *16*(2), 213–236. https://doi.org/10.1007/bf02350512
Finnigan, J. J. (1985). Turbulent transport in flexible plant canopies. In B. B. Hicks & B. A. Hutchinson (Eds.), *The Forest-Atmosphere Interaction* (pp. 443–480). Dordrecht: Reidel. https://doi.org/10.1007/978-94-009-5305-5_28
Finnigan, J. J. (2000). Turbulence in Plant Canopies. *Annual Review of Fluid Mechanics*, *32*, 519–571.
Finnigan, J. J., & Belcher, S. E. (2004). Flow over a hill covered with a plant canopy. *Quarterly Journal of the Royal Meteorological Society*, *130*(596), 1–29. https://doi.org/10.1256/qj.02.177
Finnigan, J. J., & Brunet, Y. (1995). Turbulent airflow in forests on flat and hilly terrain. In M. P. Coutts & J. Grace (Eds.), *Wind and Trees* (pp. 3–40). Cambridge, UK: Cambridge University Press. https://doi.org/10.1017/cbo9780511600425.002
Finnigan, J. J., & Shaw, R. H. (2008). Double-averaging methodology and its application to turbulent flow in and above vegetation canopies. *Acta Geophysica*, *56*(3), 534–561. https://doi.org/10.2478/s11600-008-0034-x
Finnigan, J. J., Shaw, R. H., & Patton, E. G. (2009). Turbulence structure above a vegetation canopy. *Journal of Fluid Mechanics*, *637*, 387–424. https://doi.org/10.1017/S0022112009990589
Finnigan, J. J., Harman, I. N., Ross, A. N., & Belcher, S. E. (2015). First-order turbulence closure for modelling complex canopy flows. *Quarterly Journal of the Royal Meteorological Society*, *141*(692), 2907–2916. https://doi.org/10.1002/qj.2577
Finnigan, J. J., Ayotte, K., Harman, I. N., Katul, G. G., Oldroyd, H., Patton, E. G., et al. (2020). Boundary-Layer Flow Over Complex Topography. *Boundary-Layer Meteorology*, *177*(2–3), 247–313. https://doi.org/10.1007/s10546-020-00564-3
Fisher, R. A., & Koven, C. D. (2020). Perspectives on the Future of Land Surface Models and the Challenges of Representing Complex Terrestrial Systems. *Journal of Advances in Modeling Earth Systems*, *12*(4). https://doi.org/10.1029/2018MS001453
Fleischbein, K., Wilcke, W., Goller, R., Boy, J., Valarezo, C., Zech, W., & Knoblich, K. (2005). Rainfall interception in a lower montane forest in Ecuador: Effects of canopy properties. *Hydrological Processes*, *19*(7), 1355–1371. https://doi.org/10.1002/hyp.5562
Foken, T. (2006). 50 years of the Monin-Obukhov similarity theory. *Boundary-Layer Meteorology*, *119*(3), 431–447. https://doi.org/10.1007/s10546-006-9048-6
Forkel, R., Klemm, O., Graus, M., Rappenglück, B., Stockwell, W. R., Grabmer, W., et al. (2006). Trace gas exchange and gas phase chemistry in a Norway spruce forest: A study with a coupled 1-dimensional canopy atmospheric chemistry emission model. *Atmospheric Environment*, *40*, 28–42. https://doi.org/10.1016/j.atmosenv.2005.11.070
Fowler, D., Pilegaard, K., Sutton, M. A., Ambus, P., Raivonen, M., Duyzer, J., et al. (2009). Atmospheric composition change: Ecosystems-Atmosphere interactions. *Atmospheric Environment*, *43*(33), 5193–5267. https://doi.org/10.1016/j.atmosenv.2009.07.068
Friedlander, S. K. (2000). Smoke, dust and haze: Fundamentals of aerosol dynamics. Oxford University Press, New York, USA.
Froelich, N., Croft, H., Chen, J. M., Gonsamo, A., & Staebler, R. M. (2015). Trends of carbon fluxes and climate

over a mixed temperate-boreal transition forest in southern Ontario, Canada. *Agricultural and Forest Meteorology*, *211–212*, 72–84. https://doi.org/10.1016/j.agrformet.2015.05.009

Fuentes, J. D., Lerdau, M. T., Atkinson, R., Baldocchi, D. D., Bottenheim, J. W., Ciccioli, P., et al. (2000). Biogenic Hydrocarbons in the Atmospheric Boundary Layer: A Review. *Bulletin of the American Meteorological Society*, *81*(7), 1537–1575. https://doi.org/10.1175/1520-0477(2000)081<1537:BHITAB>2.3.CO;2

Fuentes, J. D., Wang, D., Bowling, D. R., Potosnak, M., Monson, R. K., Goliff, W. S., & Stockwell, W. R. (2007). Biogenic hydrocarbon chemistry within and above a mixed deciduous forest. *Journal of Atmospheric Chemistry*, *56*(2), 165–185. https://doi.org/10.1007/s10874-006-9048-4

Fuentes, J. D., Chamecki, M., Dos Santos, R. M. N., Von Randow, C., Stoy, P. C., Katul, G. G., et al. (2016). Linking meteorology, turbulence, and air chemistry in the amazon rain forest. *Bulletin of the American Meteorological Society*, *97*(12), 2329–2342. https://doi.org/10.1175/BAMS-D-15-00152.1

Gadde, S. N., Stieren, A., & Stevens, R. J. A. M. (2021). Large-Eddy Simulations of Stratified Atmospheric Boundary Layers: Comparison of Different Subgrid Models. *Boundary-Layer Meteorology*, *178*(3), 363–382. https://doi.org/10.1007/s10546-020-00570-5

Gao, W., Shaw, R. H., & Paw U, K. T. (1989). Observation of Organized Structure in Turbulent Flow within and above a Forest Canopy. In *Boundary Layer Studies and Applications* (pp. 349–377). Springer Netherlands. https://doi.org/10.1007/978-94-009-0975-5_22

Gaylord, B. P., & Denny, M. W. (1997). Flow and flexibility. *Journal of Experimental Biology*, *200*, 3141–3164.

Gerken, T., Chamecki, M., & Fuentes, J. D. (2017). Air-Parcel Residence Times Within Forest Canopies. *Boundary-Layer Meteorology*, *165*, 29–54. https://doi.org/10.1007/s10546-017-0269-7

Gleicher, S. C., Chamecki, M., Isard, S. A., Pan, Y., & Katul, G. G. (2014). Interpreting three-dimensional spore concentration measurements and escape fraction in a crop canopy using a coupled Eulerian-Lagrangian stochastic model. *Agricultural and Forest Meteorology*, *194*, 118–131. https://doi.org/10.1016/j.agrformet.2014.03.020

Gosselin, F. P. (2019). Mechanics of a plant in fluid flow. *Journal of Experimental Botany*, *70*(14), 3533–3548. https://doi.org/10.1093/jxb/erz288

Gosselin, F. P., & de Langre, E. (2009). Destabilising effects of plant flexibility in air and aquatic vegetation canopy flows. *European Journal of Mechanics, B/Fluids*, *28*(2), 271–282. https://doi.org/10.1016/j.euromechflu.2008.06.003

Gosselin, F. P., De Langre, E., & MacHado-Almeida, B. A. (2010). Drag reduction of flexible plates by reconfiguration. *Journal of Fluid Mechanics*, *650*(May 2014), 319–341. https://doi.org/10.1017/S0022112009993673

Gromke, C. (2018). Wind tunnel model of the forest and its Reynolds number sensitivity. *Journal of Wind Engineering and Industrial Aerodynamics*, *175*(August 2017), 53–64. https://doi.org/10.1016/j.jweia.2018.01.036

Grylls, T., Suter, I., & van Reeuwijk, M. (2020). Steady-State Large-Eddy Simulations of Convective and Stable Urban Boundary Layers. *Boundary-Layer Meteorology*. https://doi.org/10.1007/s10546-020-00508-x

Haddad, N. M., Brudvig, L. A., Clobert, J., Davies, K. F., Gonzalez, A., Holt, R. D., et al. (2015). Habitat fragmentation and its lasting impact on Earth's ecosystems. *Science Advances*, *1*(2). https://doi.org/10.1126/sciadv.1500052

Hari Prasad, K. B. R. R., Venkata Srinivas, C., Venkateswara Naidu, C., Baskaran, R., & Venkatraman, B. (2016). Assessment of surface layer parameterizations in ARW using micro-meteorological observations from a tropical station. *Meteorological Applications*, *23*(2), 191–208. https://doi.org/10.1002/met.1545

Harman, I. N., Böhm, M., Finnigan, J. J., & Hughes, D. (2016). Spatial Variability of the Flow and Turbulence Within a Model Canopy. *Boundary-Layer Meteorology*, *160*(3), 375–396. https://doi.org/10.1007/s10546-016-0150-0

Hart, K. M., Curioni, G., Blaen, P., Harper, N. J., Miles, P., Lewin, K. F., et al. (2020). Characteristics of free air carbon dioxide enrichment of a northern temperate mature forest. *Global Change Biology*, *26*(2), 1023–1037. https://doi.org/10.1111/gcb.14786

Heinesch, B., Yernaux, M., & Aubinet, M. (2007). Some methodological questions concerning advection measurements: A case study. *Boundary-Layer Meteorology*, *122*(2), 457–478. https://doi.org/10.1007/s10546-006-9102-4

Hicks, B. B., & Baldocchi, D. D. (2020). Measurement of Fluxes Over Land: Capabilities, Origins, and Remaining Challenges. *Boundary-Layer Meteorology*, *177*(2–3), 365–394. https://doi.org/10.1007/s10546-020-00531-y

Hinds, W. C. (1999). *Aerosol technology: properties, behavior, and measurement of airborne particles* (Second). Hoboken: John Wiley & Sons.

Hirons, A. D., & Thomas, P. A. (2018). *Applied tree biology*. Chichester: Wiley Blackwell.
Holmes, N. S., & Morawska, L. (2006). A review of dispersion modelling and its application to the dispersion of particles: An overview of different dispersion models available. *Atmospheric Environment*, *40*(30), 5902–5928. https://doi.org/10.1016/j.atmosenv.2006.06.003
Howes, F. A., & Whitaker, S. (1985). The spatial averaging theorem revisited. *Chemical Engineering Science*, *40*(8), 1387–1392. https://doi.org/10.1016/0009-2509(85)80078-6
Huang, C. W., Chu, C. R., Hsieh, C. I., Palmroth, S., & Katul, G. G. (2015). Wind-induced leaf transpiration. *Advances in Water Resources*, *86*, 240–255. https://doi.org/10.1016/j.advwatres.2015.10.009
Inagaki, A., Letzel, M. O., Raasch, S., & Kanda, M. (2006). The impact of the surface heterogeneity on the energy imbalance problem using LES. *Journal of the Meteorological Society of Japan*, *84*(1), 187–198. https://doi.org/10.2208/prohe.49.343
Inoue, E. (1955). 'Studies of Phenomena of Waving Plants ('Honami') Caused by Wind. Part 1. Mechanism and Characteristics of Waving Plants Phenomena (in Japanese). *J. Agric. Meteorol*, *11*, 18–22.
Inoue, E. (1963). On the Turbulent Structure of Airflow within Crop Canopies. *Journal of the Meteorological Society of Japan. Ser. II*, *41*(6), 317–326. https://doi.org/10.2151/jmsj1923.41.6_317
Jacobson, M. Z. (2005). *Fundamentals of Atmospheric Modeling* (Second). Cambridge, UK: Cambridge University Press. https://doi.org/https://doi.org/10.1017/CBO9781139165389
Janhäll, S. (2015). Review on urban vegetation and particle air pollution - Deposition and dispersion. *Atmospheric Environment*, *105*, 130–137. https://doi.org/10.1016/j.atmosenv.2015.01.052
Kaimal, J. C., & Finnigan, J. J. (1994). *Atmospheric boundary layer flows—their structure and measurement*. New York: Oxford University Press. https://doi.org/10.16085/j.issn.1000-6613.2012.02.016
Kanani-Sühring, F., & Raasch, S. (2015). Spatial Variability of Scalar Concentrations and Fluxes Downstream of a Clearing-to-Forest Transition: A Large-Eddy Simulation Study. *Boundary-Layer Meteorology*, *155*, 1–27. https://doi.org/10.1007/s10546-014-9986-3
Kanani-Sühring, F., & Raasch, S. (2017). Enhanced Scalar Concentrations and Fluxes in the Lee of Forest Patches: A Large-Eddy Simulation Study. *Boundary-Layer Meteorology*, *164*(1), 1–17. https://doi.org/10.1007/s10546-017-0239-0
Kang, Y. (2015). Detection, Classification and Analysis of Events in Turbulence Time Series. *Bulletin of the Australian Mathematical Society*, *91*(3), 521–522. https://doi.org/10.1017/S0004972715000106
Kang, Y., Belušić, D., & Smith-Miles, K. (2015). Classes of structures in the stable atmospheric boundary layer. *Quarterly Journal of the Royal Meteorological Society*, *141*(691), 2057–2069. https://doi.org/10.1002/qj.2501
Katul, G. G., & Albertson, J. D. (1998). An investigation of higher-order closure models for a forested canopy. *Boundary-Layer Meteorology*, *89*(1), 47–74. https://doi.org/10.1023/A:1001509106381
Katul, G. G., Mahrt, L., Poggi, D., & Sanz, C. (2004). One-and two-equation models for canopy turbulence. *Boundary-Layer Meteorology*, *113*, 81–109.
Katul, G. G., Finnigan, J. J., Poggi, D., Leuning, R., & Belcher, S. E. (2006). The influence of hilly terrain on canopy-atmosphere carbon dioxide exchange. *Boundary-Layer Meteorology*, *118*(1), 189–216. https://doi.org/10.1007/s10546-005-6436-2
Katul, G. G., Grönholm, T., Launiainen, S., & Vesala, T. (2011). The effects of the canopy medium on dry deposition velocities of aerosol particles in the canopy sub-layer above forested ecosystems. *Atmospheric Environment*, *45*(5), 1203–1212. https://doi.org/10.1016/j.atmosenv.2010.06.032
Katul, G. G., Oren, R., Manzoni, S., Higgins, C., & Parlange, M. B. (2012). Evapotranspiration: A process driving mass transport and energy exchange in the soil-plant-atmosphere-climate system. *Reviews of Geophysics*, *50*(3). https://doi.org/10.1029/2011RG000366
Katul, G. G., Cava, D., Siqueira, M., & Poggi, D. (2013). Scalar Turbulence within the Canopy Sublayer. In J. G. Venditti, J. L. Best, M. Church, & R. J. Hardy (Eds.), *Coherent Flow Structures at Earth's Surface* (pp. 73–96). Chichester, UK.
Khan, B., Banzhaf, S., Chan, E., Forkel, R., Kanani-Sühring, F., Ketelsen, K., et al. (2020). Development of an atmospheric chemistry model coupled to the PALM model system 6.0: Implementation and first applications. *Geoscientific Model Development Discussions*, (x), 1–34. https://doi.org/10.5194/gmd-2020-286
Kim, D., Oren, R., Oishi, A. C., Hsieh, C. I., Phillips, N., Novick, K. A., & Stoy, P. C. (2014). Sensitivity of stand transpiration to wind velocity in a mixed broadleaved deciduous forest. *Agricultural and Forest Meteorology*, *187*, 62–71. https://doi.org/10.1016/j.agrformet.2013.11.013
Kim, S., Park, H., Gruszewski, H. A., Schmale, D. G., & Jung, S. (2019). Vortex-induced dispersal of a plant pathogen by raindrop impact. *Proceedings of the National Academy of Sciences of the United States of America*, *116*(11), 4917–4922. https://doi.org/10.1073/pnas.1820318116

Klaassen, W., Van Breugel, P. B., Moors, E. J., & Nieveen, J. P. (2002). Increased heat fluxes near a forest edge. *Theoretical and Applied Climatology*, *72*(3–4), 231–243. https://doi.org/10.1007/s00704-002-0682-8

Koizumi, A., Motoyama, J. ichi, Sawata, K., Sasaki, Y., & Hirai, T. (2010). Evaluation of drag coefficients of poplar-tree crowns by a field test method. *Journal of Wood Science*, *56*(3), 189–193. https://doi.org/10.1007/s10086-009-1091-8

Kruijt, B., Malhi, Y., Lloyd, J., Nobre, A. D., Miranda, A. C., Pereira, M. G. P., et al. (2000). Turbulence statistics above and within two Amazon rain forest canopies. *Boundary-Layer Meteorology*, *94*(2), 297–331. https://doi.org/10.1023/A:1002401829007

Kulmala, M., Dal Maso, M., Mäkelä, J. M., Pirjola, L., Väkevä, M., Aalto, P., et al. (2001). On the formation, growth and composition of nucleation mode particles. *Tellus, Series B: Chemical and Physical Meteorology*, *53*(4), 479–490. https://doi.org/10.3402/tellusb.v53i4.16622

Kulmala, M., Riipinen, I., Sipilä, M., Manninen, H. E., Petäjä, T., Junninen, H., et al. (2007). Toward direct measurement of atmospheric nucleation. *Science*, *318*(5847), 89–92. https://doi.org/10.1126/science.1144124

Kunert, N., Aparecido, L. M. T., Higuchi, N., Santos, J. dos, & Trumbore, S. (2015). Higher tree transpiration due to road-associated edge effects in a tropical moist lowland forest. *Agricultural and Forest Meteorology*, *213*, 183–192. https://doi.org/10.1016/j.agrformet.2015.06.009

Kwak, K. H., & Baik, J. J. (2014). Diurnal variation of NOx and ozone exchange between a street canyon and the overlying air. *Atmospheric Environment*, *86*(x), 120–128. https://doi.org/10.1016/j.atmosenv.2013.12.029

Kwak, K. H., Baik, J. J., Ryu, Y. H., & Lee, S. H. (2015). Urban air quality simulation in a high-rise building area using a CFD model coupled with mesoscale meteorological and chemistry-transport models. *Atmospheric Environment*, *100*, 167–177. https://doi.org/10.1016/j.atmosenv.2014.10.059

Lalic, B., & Mihailovic, D. T. (2004). An empirical relation describing leaf-area density inside the forest for environmental modeling. *Journal of Applied Meteorology*, *43*(4), 641–645.

De Langre, E. (2008). Effects of Wind on Plants. *Annu. Rev. Fluid Mech*, *40*, 141–168. https://doi.org/10.1146/annurev.fluid.40.111406.102135

De Langre, E. (2019). Plant vibrations at all scales: A review. *Journal of Experimental Botany*, *70*(14), 3521–3531. https://doi.org/10.1093/jxb/erz209

Lee, X., & Black, T. A. (1993). Atmospheric turbulence within and above a Douglas-fir stand. Part I: Statistical properties of the velocity field. *Boundary-Layer Meteorology*, *64*(1–2), 149–174. https://doi.org/10.1007/BF00705666

Lefsky, M. A., Cohen, W. B., Acker, S. A., Parker, G. G., Spies, T. A., & Harding, D. (1999). Lidar remote sensing of the canopy structure and biophysical properties of Douglas-fir western hemlock forests. *Remote Sensing of Environment*, *70*(3), 339–361. https://doi.org/10.1016/S0034-4257(99)00052-8

Legg, B. J., Raupach, M. R., & Coppin, P. A. (1986). Experiments on scalar dispersion within a model plant canopy, part III: An elevated line source. *Boundary-Layer Meteorology*, *35*(3), 277–302. https://doi.org/10.1007/BF00123645

Lelieveld, J., Butler, T. M., Crowley, J. N., Dillon, T. J., Fischer, H., Ganzeveld, L., et al. (2008). Atmospheric oxidation capacity sustained by a tropical forest. *Nature*, *452*(7188), 737–740. https://doi.org/10.1038/nature06870

Lemone, M. A., Angevine, W. M., Bretherton, C. S., Chen, F., Dudhia, J., Fedorovich, E., et al. (2019). 100 Years of Progress in Boundary Layer Meteorology. *Meteorological Monographs*, *59*(1), 9.1-9.85. https://doi.org/10.1175/AMSMONOGRAPHS-D-18-0013.1

Li, Q., & Bou-Zeid, E. (2019). Contrasts between momentum and scalar transport over very rough surfaces. *Journal of Fluid Mechanics*, 32–58. https://doi.org/10.1017/jfm.2019.687

Liang, X., Kankare, V., Hyyppä, J., Wang, Y., Kukko, A., Haggrén, H., et al. (2016). Terrestrial laser scanning in forest inventories. *ISPRS Journal of Photogrammetry and Remote Sensing*, *115*, 63–77. https://doi.org/10.1016/j.isprsjprs.2016.01.006

Liao, J., Wang, T., Wang, X., Xie, M., Jiang, Z., Huang, X., & Zhu, J. (2014). Impacts of different urban canopy schemes in WRF/Chem on regional climate and air quality in Yangtze River Delta, China. *Atmospheric Research*, *145–146*, 226–243. https://doi.org/10.1016/j.atmosres.2014.04.005

Lin, M., Katul, G. G., & Khlystov, A. (2012). A branch scale analytical model for predicting the vegetation collection efficiency of ultrafine particles. *Atmospheric Environment*, *51*, 293–302. https://doi.org/10.1016/j.atmosenv.2012.01.004

Lin, X., Chamecki, M., Katul, G. G., & Yu, X. (2018). Effects of leaf area index and density on ultrafine particle deposition onto forest canopies: A LES study. *Atmospheric Environment*, *189*, 153–163. https://doi.org/10.1016/j.atmosenv.2018.06.048

Litschike, T., & Kuttler, W. (2008). On the reduction of urban particle concentration by vegetation - A review. *Meteorologische Zeitschrift*, *17*(3), 229–240. https://doi.org/10.1127/0941-2948/2008/0284

Ma, Y., & Liu, H. (2019). An Advanced Multiple-Layer Canopy Model in the WRF Model With Large-Eddy Simulations to Simulate Canopy Flows and Scalar Transport Under Different Stability Conditions. *Journal of Advances in Modeling Earth Systems*, *11*, 2330–2351. https://doi.org/10.1029/2018MS001347

Ma, Y., Liu, H., Liu, Z., Yi, C., & Lamb, B. K. (2020). Influence of Forest-Edge Flows on Scalar Transport with Different Vertical Distributions of Foliage and Scalar Sources. *Boundary-Layer Meteorology*, *174*(1), 99–117. https://doi.org/10.1007/s10546-019-00475-y

Magnago, L. F. S., Rocha, M. F., Meyer, L., Martins, S. V., & Meira-Neto, J. A. A. (2015). Microclimatic conditions at forest edges have significant impacts on vegetation structure in large Atlantic forest fragments. *Biodiversity and Conservation*, *24*(9), 2305–2318. https://doi.org/10.1007/s10531-015-0961-1

Mahrt, L. (2000). Surface heterogeneity and vertical structure of the boundary layer. *Boundary-Layer Meteorology*, *96*(1–2), 33–62. https://doi.org/10.1023/A:1002482332477

Mahrt, L. (2014). Stably stratified atmospheric boundary layers. *Annual Review of Fluid Mechanics*, *46*(July), 23–45. https://doi.org/10.1146/annurev-fluid-010313-141354

Maitani, T. (1979). An observational study of wind-induced waving of plants. *Boundary-Layer Meteorology*, *16*(3), 49–65. https://doi.org/10.1007/BF03335354

Makar, P. A., Staebler, R. M., Akingunola, A., Zhang, J., McLinden, C., Kharol, S. K., et al. (2017). The effects of forest canopy shading and turbulence on boundary layer ozone. *Nature Communications*, *8*(May), 1–14. https://doi.org/10.1038/ncomms15243

Margairaz, F., Pardyjak, E. R., & Calaf, M. (2020). Surface Thermal Heterogeneities and the Atmospheric Boundary Layer: The Relevance of Dispersive Fluxes. *Boundary-Layer Meteorology*, *175*(3), 369–395. https://doi.org/10.1007/s10546-020-00509-w

Mason, P. J., & Thomson, D. J. (1992). Stochastic backscatter in large-eddy simulations of boundary layers. *Journal of Fluid Mechanics*, *242*(28), 51–78. https://doi.org/10.1017/S0022112092002271

Massman, W. J., & Lee, X. (2002). Eddy covariance flux corrections and uncertainties in long-term studies of carbon and energy exchanges. *Agricultural and Forest Meteorology*, *113*, 121–144.

Maurer, K. D., Bohrer, G., Kenny, W. T., & Ivanov, V. Y. (2015). Large-eddy simulations of surface roughness parameter sensitivity to canopy-structure characteristics. *Biogeosciences*, *12*(8), 2533–2548. https://doi.org/10.5194/bg-12-2533-2015

Mavroidis, I., Andronopoulos, S., & Bartzis, J. G. (2012). Computational simulation of the residence of air pollutants in the wake of a 3-dimensional cubical building. The effect of atmospheric stability. *Atmospheric Environment*, *63*, 189–202. https://doi.org/10.1016/j.atmosenv.2012.09.032

McHugh, I. D., Beringer, J., Cunningham, S. C., Baker, P. J., Cavagnaro, T. R., MacNally, R., & Thompson, R. M. (2017). Interactions between nocturnal turbulent flux, storage and advection at an "ideal" eucalypt woodland site. *Biogeosciences*, *14*(12), 3027–3050. https://doi.org/10.5194/bg-14-3027-2017

Moeng, C. H., Dudhia, J., Klemp, J., & Sullivan, P. P. (2007). Examining Two-Way Grid Nesting for Large Eddy Simulation of the PBL Using the WRF Model. https://doi.org/10.1175/MWR3406.1

Moltchanov, S., Bohbot-Raviv, Y., & Shavit, U. (2011). Dispersive Stresses at the Canopy Upstream Edge. *Boundary-Layer Meteorology*, *139*(2), 333–351. https://doi.org/10.1007/s10546-010-9582-0

Moltchanov, S., Bohbot-Raviv, Y., Duman, T., & Shavit, U. (2015). Canopy edge flow: A momentum balance analysis. *Water Resources Research*, *51*(4). https://doi.org/10.1002/2014WR015397

Monin, A. S., & Obukhov, A. M. (1954). Osnovnye zakonomernosti turbulentnogo pere- meshivanija v prizemnom sloe atmosfery (Basic Laws of Turbulent Mixing in the Atmo- sphere Near the Ground). *Akademii Nauk SSSR Geofizicheskii Institut Trudy*, *24*(151), 163–187.

Monteith, J. L., & Unsworth, M. H. (2008). *Principles of Environmental Physics* (Fourth). Oxford: Academic Press . Retrieved from http://elsevier.com/locate/permissions,

Morse, A. P., Gardiner, B. A., & Marshall, B. J. (2002). Mechanics controlling trubulence developement across a forest edge. *Boundary-Layer Meteorology*, *103*(103), 227–251.

Mortensen, D. A., Rauschert, E. S. J., Nord, A. N., & Jones, B. P. (2009). Forest Roads Facilitate the Spread of Invasive Plants. *Invasive Plant Science and Management*, *2*(3), 191–199. https://doi.org/10.1614/ipsm-08-125.1

Moser, R. D., Haering, S. W., & Yalla, G. R. (2021). Statistical Properties of Subgrid-Scale Turbulence Models. *Annual Review of Fluid Mechanics*, *53*(1), 255–286. https://doi.org/10.1146/annurev-fluid-060420-023735

Mueller, E., Mell, W., & Simeoni, A. (2014). Large eddy simulation of forest canopy flow for wildland fire modeling. *Canadian Journal of Forest Research*, *44*(12), 1534–1544. https://doi.org/10.1139/cjfr-2014-0184

Murena, F., Di Benedetto, A., D'Onofrio, M., & Vitiello, G. (2011). Mass Transfer Velocity and Momentum Vertical Exchange in Simulated Deep Street Canyons. *Boundary-Layer Meteorology*, *140*(1), 125–142. https://doi.org/10.1007/s10546-011-9602-8

Murena, Fabio. (2012). Monitoring and modelling carbon monoxide concentrations in a deep street canyon: Application of a two-box model. *Atmospheric Pollution Research*, *3*(3), 311–316. https://doi.org/10.5094/APR.2012.034

Nebenführ, B., & Davidson, L. (2015). Large-Eddy Simulation Study of Thermally Stratified Canopy Flow. *Boundary-Layer Meteorology*, *156*(2), 253–276. https://doi.org/10.1007/s10546-015-0025-9

Neumann, H. H., Den Hartog, G., & Shaw, R. H. (1989). Leaf area measurements based on hemispheric photographs and leaf-litter collection in a deciduous forest during autumn leaf-fall. *Agricultural and Forest Meteorology*, *45*(3–4), 325–345. https://doi.org/10.1016/0168-1923(89)90052-X

Nicoll, B. C., & Ray, D. (1996). Adaptive growth of tree root systems in response to wind action and site conditions. *Tree Physiology*, *16*(11–12), 891–898. https://doi.org/10.1093/treephys/16.11-12.891

Niinemets, Ü. (2010). Mild versus severe stress and BVOCs: thresholds, priming and consequences. *Trends in Plant Science*, *15*(3), 145–153. https://doi.org/10.1016/j.tplants.2009.11.008

Norby, R. J., Wullschleger, S. D., Gunderson, C. A., Johnson, D. W., & Ceulemans, R. (1999). Tree responses to rising CO2 in field experiments: Implications for the future forest. *Plant, Cell and Environment*, *22*(6), 683–714. https://doi.org/10.1046/j.1365-3040.1999.00391.x

Norby, R. J., Wullschleger, S. D., Hanson, P. J., Gunderson, C. A., Tschaplinski, T. J., & Jastrow, J. D. (2006). CO2 Enrichment of a Deciduous Forest: The Oak Ridge FACE Experiment. In J. Nösberger, S. P. Long, R. J. Norby, M. Stitt, G. R. Hendrey, & H. Blum (Eds.), *Managed Ecosystems and CO2. Ecological Studies (Analysis and Synthesis)* (Vol. 187, pp. 231–251). Berlin: Springer. https://doi.org/10.1007/3-540-31237-4_13

Norros, V., Rannik, Ü., Hussein, T., Petäjä, T., Vesala, T., & Ovaskainen, O. (2014). Do small spores disperse further than large spores? *Ecology*, *95*(6), 1612–1621. https://doi.org/10.1890/13-0877.1

Nottrott, A., Kleissl, J., & Keeling, R. (2014). Modeling passive scalar dispersion in the atmospheric boundary layer with WRF large-eddy simulation. *Atmospheric Environment*, *82*, 172–182. https://doi.org/10.1016/j.atmosenv.2013.10.026

Oke, T. R. (1988). The urban energy balance. *Progress in Physical Geography*, *12*(4), 471–508. https://doi.org/10.1177/030913338801200401

Oleson, K. W., Lawrence, D. M., Bonan, G. B., Drewniak, B., Huang, M., Charles, D., et al. (2013). Technical Description of version 4.5 of the Community Land Model (CLM). *NCAR/TN-503+STR NCAR Technical Note*, (July).

Oliphant, A. J. (2012). Terrestrial Ecosystem-Atmosphere Exchange of CO2, Water and Energy from FLUXNET; Review and Meta-Analysis of a Global in-situ Observatory. *Geography Compass*, *6*(12), 689–705. https://doi.org/10.1111/gec3.12009

Pace, R., & Grote, R. (2020). Deposition and Resuspension Mechanisms Into and From Tree Canopies: A Study Modeling Particle Removal of Conifers and Broadleaves in Different Cities. *Frontiers in Forests and Global Change*, *3*(March), 1–12. https://doi.org/10.3389/ffgc.2020.00026

Pan, Y., Chamecki, M., & Isard, S. A. (2014). Large-eddy simulation of turbulence and particle dispersion inside the canopy roughness sublayer. *J. Fluid Mech*, *753*, 499–534. https://doi.org/10.1017/jfm.2014.379

Pan, Y., Follett, E., Chamecki, M., & Nepf, H. M. (2014). Strong and weak, unsteady reconfiguration and its impact on turbulence structure within plant canopies. *Physics of Fluids*, *26*(10), 105102. https://doi.org/10.1063/1.4898395

Patton, E. G., & Finnigan, J. J. (2012). Canopy Turbulence. In *Handbook of Environmental Fluid Dynamics, Volume One* (pp. 311–328). CRC Press. https://doi.org/10.1201/b14241-28

Patton, E. G., & Katul, G. G. (2009). Turbulent pressure and velocity perturbations induced by gentle hills covered with sparse and dense canopies. *Boundary-Layer Meteorology*, *133*(2), 189–217. https://doi.org/10.1007/s10546-009-9427-x

Patton, E. G., Horst, T. W., Sullivan, P. P., Lenschow, D. H., Oncley, S. P., Brown, W. O. J., et al. (2011). The canopy horizontal array turbulence study. *Bulletin of the American Meteorological Society*, *92*(5), 593–611. https://doi.org/10.1175/2010BAMS2614.1

Patton, E. G., Sullivan, P. P., Shaw, R. H., Finnigan, J. J., & Weil, J. C. (2016). Atmospheric stability influences on coupled boundary layer and canopy turbulence. *Journal of the Atmospheric Sciences*, *73*(4), 1621–1647. https://doi.org/10.1175/JAS-D-15-0068.1

Paul-Limoges, E., Wolf, S., Eugster, W., Hörtnagl, L., & Buchmann, N. (2017). Below-canopy contributions to ecosystem CO2 fluxes in a temperate mixed forest in Switzerland. *Agricultural and Forest Meteorology*, *247*,

582–596. https://doi.org/10.1016/j.agrformet.2017.08.011
Peñuelas, J., & Staudt, M. (2010). BVOCs and global change. *Trends in Plant Science*, *15*(3), 133–144. https://doi.org/10.1016/j.tplants.2009.12.005
Petroff, A., Mailliat, A., Amielh, M., & Anselmet, F. (2008). Aerosol dry deposition on vegetative canopies. Part I: Review of present knowledge. *Atmospheric Environment*, *42*(16), 3625–3653. https://doi.org/10.1016/j.atmosenv.2007.09.043
Pfeifer, M., Lefebvre, V., Peres, C. A., Banks-Leite, C., Wearn, O. R., Marsh, C. J., et al. (2017). Creation of forest edges has a global impact on forest vertebrates. *Nature*, *551*(7679), 187–191. https://doi.org/10.1038/nature24457
Philips, D. A., Rossi, R., & Iaccarino, G. (2013). Large-eddy simulation of passive scalar dispersion in an urban-like canopy. *Journal of Fluid Mechanics*, *723*, 404–428. https://doi.org/10.1017/jfm.2013.135
Pierce, J. R., Leaitch, W. R., Liggio, J., Westervelt, D. M., Wainwright, C. D., Abbatt, J. P. D., et al. (2012). Nucleation and condensational growth to CCN sizes during a sustained pristine biogenic SOA event in a forested mountain valley. *Atmospheric Chemistry and Physics*, *12*(7), 3147–3163. https://doi.org/10.5194/acp-12-3147-2012
Piomelli, U., Cabot, W. H., Moin, P., & Lee, S. (1991). Subgrid-scale backscatter in turbulent and transitional flows. *Physics of Fluids A*, *3*(7), 1766–1771. https://doi.org/10.1063/1.857956
Pivato, D., Dupont, S., & Brunet, Y. (2014). A simple tree swaying model for forest motion in windstorm conditions. *Trees - Structure and Function*, *28*(1), 281–293. https://doi.org/10.1007/s00468-013-0948-z
Poggi, D., Porporato, A., Ridolfi, L., Albertson, J. D., & Katul, G. G. (2004). THE EFFECT OF VEGETATION DENSITY ON CANOPY SUB-LAYER TURBULENCE. *Boundary-Layer Meteorology*, *111*, 565–587.
Poggi, D., Katul, G. G., Finnigan, J. J., & Belcher, S. E. (2008). Analytical models for the mean flow inside dense canopies on gentle hilly terrain. *Quarterly Journal of the Royal Meteorological Society*, *134*(634 A), 1095–1112. https://doi.org/10.1002/qj.276
Pryor, S. C., Barthelmie, R. J., Sørensen, L. L., Larsen, S. E., Sempreviva, A. M., Grönholm, T., et al. (2008). Upward fluxes of particles over forests: When, where, why? *Tellus, Series B: Chemical and Physical Meteorology*, *60 B*(3), 372–380. https://doi.org/10.1111/j.1600-0889.2008.00341.x
Pugh, T. A. M., Mackenzie, A. R., Langford, B., Nemitz, E., Misztal, P. K., & Hewitt, C. N. (2011). The influence of small-scale variations in isoprene concentrations on atmospheric chemistry over a tropical rainforest. *Atmospheric Chemistry and Physics*, *11*(9), 4121–4134. https://doi.org/10.5194/acp-11-4121-2011
Py, C., De Langre, E., & Moulia, B. (2006). A frequency lock-in mechanism in the interaction between wind and crop canopies. *Journal of Fluid Mechanics*, *568*, 425–449. https://doi.org/10.1017/S0022112006002667
Queck, R., Bernhofer, C., Bienert, A., & Schlegel, F. (2016). The TurbEFA Field Experiment—Measuring the Influence of a Forest Clearing on the Turbulent Wind Field. *Boundary-Layer Meteorology*, *160*(3), 397–423. https://doi.org/10.1007/s10546-016-0151-z
Ramos-Rivera, J., Rahardjo, H., Tsen-Tieng, D. L., Xuefeng, N., & King, F. Y. (2020). Mechanical response of the real tree root architecture under lateral load. *Canadian Journal of Forest Research*, *50*(7), 595–607. https://doi.org/10.1139/cjfr-2019-0332
Ramos, F. M., Bolzan, M. J. A., Sá, L. D. A., & Rosa, R. R. (2004). Atmospheric turbulence within and above an Amazon forest. *Physica D: Nonlinear Phenomena*, *193*(1–4), 278–291. https://doi.org/10.1016/j.physd.2004.01.026
Rap, A., Scott, C. E., Reddington, C. L., Mercado, L., Ellis, R. J., Garraway, S., et al. (2018). Enhanced global primary production by biogenic aerosol via diffuse radiation fertilization. *Nature Geoscience*, *11*(9), 640–644. https://doi.org/10.1038/s41561-018-0208-3
Raumonen, P., Casella, E., Calders, K., Murphy, S., Åkerblom, M., & Kaasalainen, M. (2015). Massive-scale tree modelling from TLS data. *ISPRS Annals of the Photogrammetry, Remote Sensing and Spatial Information Sciences*, *2*(3W4), 189–196. https://doi.org/10.5194/isprsannals-II-3-W4-189-2015
Raupach, M. R., & Shaw, R. H. (1982). Averaging procedures for flow within vegetation canopies. *Boundary-Layer Meteorology*, *22*(1), 79–90. https://doi.org/10.1007/BF00128057
Raupach, M. R., Coppin, P. A., & Legg, B. J. (1986). Experiments on scalar dispersion within a model plant canopy part I: The turbulence structure. *Boundary-Layer Meteorology*, *35*(1–2), 21–52. https://doi.org/10.1007/BF00117300
Raupach, M. R., Bradley, E. F., & Ghadiri, H. (1987). *A wind tunnel investigation into the aerodynamic effect of forest clearings on the nesting of Abbott's booby on Christmas Island* (Vol. 2). Canberra, Australia. https://doi.org/10.4225/08/587521fe26b7f
Raupach, M. R., Antonia, R. A., & Rajagopalan, S. (1991). Rough-wall turbulent boundary layers. *Applied*

Mechanics Reviews, *44*(1).
Raupach, M. R., Finnigan, J. J., & Brunet, Y. (1996). Coherent Eddies and Turbulence in Vegetation Canopies: The Mixing-Layer Analogy. *Boundary-Layer Meteorology 25th Anniversary Volume, 1970–1995*, 351–382. https://doi.org/10.1007/978-94-017-0944-6_15
Reynolds, A. M. (2012). Incorporating sweeps and ejections into Lagrangian stochastic models of spore trajectories within plant canopy turbulence: Modeled contact distributions are heavy-tailed. *Phytopathology*, *102*(11), 1026–1033. https://doi.org/10.1094/PHYTO-01-12-0002
Richardson, A. D., Keenan, T. F., Migliavacca, M., Ryu, Y., Sonnentag, O., & Toomey, M. (2013). Climate change, phenology, and phenological control of vegetation feedbacks to the climate system. *Agricultural and Forest Meteorology*, *169*, 156–173. https://doi.org/10.1016/j.agrformet.2012.09.012
Riitters, K., Wickham, J., Neill, R. O., Jones, B., Ecology, S. C., & Dec, N. (2000). Global-Scale Patterns of Forest Fragmentation. *Conservation Ecology*, *4*(2), 1–24.
Riutta, T., Slade, E. M., Morecroft, M. D., Bebber, D. P., & Malhi, Y. (2014). Living on the edge: Quantifying the structure of a fragmented forest landscape in England. *Landscape Ecology*, *29*(6), 949–961. https://doi.org/10.1007/s10980-014-0025-z
Rominger, J. T., & Nepf, H. M. (2011). Flow adjustment and interior flow associated with a rectangular porous obstruction. *Journal of Fluid Mechanics*, *680*, 636–659. https://doi.org/10.1017/jfm.2011.199
Ross, A. N. (2008). Large-eddy Simulations of Flow Over Forested Ridges, *128*, 59–76. https://doi.org/10.1007/s10546-008-9278-x
Ross, A. N., & Harman, I. N. (2015). The Impact of Source Distribution on Scalar Transport over Forested Hills. *Boundary-Layer Meteorology*, *156*(2), 211–230. https://doi.org/10.1007/s10546-015-0029-5
Rozema, W., Bae, H. J., Moin, P., & Verstappen, R. (2015). Minimum-dissipation models for large-eddy simulation. *Physics of Fluids*, *27*(8). https://doi.org/10.1063/1.4928700
Russell, E. S., Liu, H., Gao, Z., Lamb, B., & Wagenbrenner, N. (2016). Turbulence dependence on winds and stability in a weak-wind canopy sublayer over complex terrain. *Journal of Geophysical Research*, *121*(19), 11502–11515. https://doi.org/10.1002/2016JD025057
Sabatini, F. M., Burrascano, S., Keeton, W. S., Levers, C., Lindner, M., Pötzschner, F., et al. (2018). Where are Europe's last primary forests? *Diversity and Distributions*, *24*(10), 1426–1439. https://doi.org/10.1111/ddi.12778
Schindler, D., Fugmann, H., Schönborn, J., & Mayer, H. (2012). Coherent response of a group of plantation-grown Scots pine trees to wind loading. *European Journal of Forest Research*, *131*(1), 191–202. https://doi.org/10.1007/s10342-010-0474-0
Schindler, D., Schönborn, J., Fugmann, H., & Mayer, H. (2013). Responses of an individual deciduous broadleaved tree to wind excitation. *Agricultural and Forest Meteorology*, *177*, 69–82. https://doi.org/10.1016/j.agrformet.2013.04.001
Schlegel, F., Stiller, J., Bienert, A., Maas, H. G., Queck, R., & Bernhofer, C. (2012). Large-Eddy Simulation of Inhomogeneous Canopy Flows Using High Resolution Terrestrial Laser Scanning Data. *Boundary-Layer Meteorology*, *142*(2), 223–243. https://doi.org/10.1007/s10546-011-9678-1
Schlegel, F., Stiller, J., Bienert, A., Maas, H. G., Queck, R., & Bernhofer, C. (2015). Large-Eddy Simulation Study of the Effects on Flow of a Heterogeneous Forest at Sub-Tree Resolution. *Boundary-Layer Meteorology*, *154*(1), 27–56. https://doi.org/10.1007/s10546-014-9962-y
Schmid, M. F., Lawrence, G. A., Parlange, M. B., & Giometto, M. G. (2019). Volume Averaging for Urban Canopies. *Boundary-Layer Meteorology*, *173*(3), 349–372. https://doi.org/10.1007/s10546-019-00470-3
Schmidt, M., Jochheim, H., Kersebaum, K. C., Lischeid, G., & Nendel, C. (2017, January 15). Gradients of microclimate, carbon and nitrogen in transition zones of fragmented landscapes – a review. *Agricultural and Forest Meteorology*. Elsevier B.V. https://doi.org/10.1016/j.agrformet.2016.10.022
Schneider, F. D., Kükenbrink, D., Schaepman, M. E., Schimel, D. S., & Morsdorf, F. (2019). Quantifying 3D structure and occlusion in dense tropical and temperate forests using close-range LiDAR. *Agricultural and Forest Meteorology*, *268*(December 2018), 249–257. https://doi.org/10.1016/j.agrformet.2019.01.033
Scholes, R. J. (2017). Taking the Mumbo Out of the Jumbo: Progress Towards a Robust Basis for Ecological Scaling. *Ecosystems*, *20*(1), 4–13. https://doi.org/10.1007/s10021-016-0047-2
Schröttle, J., & Dörnbrack, A. (2013). Turbulence structure in a diabatically heated forest canopy composed of fractal Pythagoras trees. *Theoretical and Computational Fluid Dynamics*, *27*(3–4), 337–359. https://doi.org/10.1007/s00162-012-0284-8
Schuepp, P. H. (1993a). Tansley Leaf Review boundary. *New Phytologist*, *125*(3), 477–507.
Schuepp, P. H. (1993b). Tansley Review No. 59 Leaf boundary layers. *New Phytologist*, *125*(3), 477–507.

https://doi.org/10.1111/j.1469-8137.1993.tb03898.x
Schymanski, S. J., & Or, D. (2016). Wind increases leaf water use efficiency. *Plant Cell and Environment*, *39*(7), 1448–1459. https://doi.org/10.1111/pce.12700
Seinfeld, J. H., & Pandis, S. N. (2016). *Atmospheric chemistry and physics: from air pollution to climate change* (Third). John Wiley & Sons.
Selino, A., & Jones, M. D. (2013). Large and small eddies matter: Animating trees in wind using coarse fluid simulation and synthetic turbulence. *Computer Graphics Forum*, *32*(1), 75–84. https://doi.org/10.1111/j.1467-8659.2012.03232.x
Shao, Y., Liu, S., Schween, J. H., & Crewell, S. (2013). Large-Eddy Atmosphere-Land-Surface Modelling over Heterogeneous Surfaces: Model Development and Comparison with Measurements. *Boundary-Layer Meteorology*, *148*(2), 333–356. https://doi.org/10.1007/s10546-013-9823-0
Sharkey, T. D., Singsaas, E. L., Vanderveer, P. J., & Geron, C. (1996). Field measurements of isoprene emission from trees in response to temperature and light. *Tree Physiology*, *16*(7), 649–654. https://doi.org/10.1093/treephys/16.7.649
Sharma, A., & García-Mayoral, R. (2020a). Scaling and dynamics of turbulence over sparse canopies. *Journal of Fluid Mechanics*, *888*. https://doi.org/10.1017/jfm.2019.999
Sharma, A., & García-Mayoral, R. (2020b). Turbulent flows over dense filament canopies. *Journal of Fluid Mechanics*, *888*. https://doi.org/10.1017/jfm.2020.27
Shaw, R. H., & Patton, E. G. (2003). Canopy element influences on resolved- and subgrid-scale energy within a large-eddy simulation. In *Agricultural and Forest Meteorology* (Vol. 115, pp. 5–17). https://doi.org/10.1016/S0168-1923(02)00165-X
Shaw, R. H., & Schumann, U. (1992). Large-eddy simulation of turbulent flow above and within a forest. *Boundary-Layer Meteorology*, *61*(1–2), 47–64. https://doi.org/10.1007/BF02033994
Shaw, R. H., & Tavangar, J. (1983). Structure of the Reynolds Stress in the Canopy Layer. *Journal of Climate and Applied Meteorology*, *22*, 1922–1931. Retrieved from papers3://publication/uuid/5BAB6D15-DD1E-4002-B055-1E869ECC9992
Shralman, B. I., & Siggia, E. D. (2000). Scalar turbulence. *Nature*, *405*(6787), 639–646. https://doi.org/10.1038/35015000
Skamarock, W. C., Klemp, J. B., Dudhia, J. B., Gill, D. O., Barker, D. M., Duda, M. G., et al. (2008). *A description of the Advanced Research WRF Version 3, NCAR Technical Note TN-475+STR*. *Technical Report*. https://doi.org/10.5065/D68S4MVH
Smagorinsky, J. (1963). General Circulation Experiments with the Primitive Equations: 1. The Basic Experiment. *Monthly Weather Revieweather Review*, *91*(3), 99–164. https://doi.org/10.1126/science.12.306.731-a
Sogachev, A., Leclerc, M. Y., Zhang, G., Rannik, Ü., & Vesala, T. (2008). CO2 fluxes near a forest edge: A numerical study. *Ecological Applications*, *18*(6), 1454–1469. https://doi.org/10.1890/06-1119.1
Speck, O. (2003). Field measurements of wind speed and reconfiguration in Arundo donax (Poaceae) with estimates of drag forces. *American Journal of Botany*, *90*(8), 1253–1256. https://doi.org/10.3732/ajb.90.8.1253
Spracklen, D. V., Carslaw, K. S., Kulmala, M., Kerminen, V. M., Mann, G. W., & Sihto, S. L. (2006). The contribution of boundary layer nucleation events to total particle concentrations on regional and global scales. *Atmospheric Chemistry and Physics*, *6*(12), 5631–5648. https://doi.org/10.5194/acp-6-5631-2006
Spracklen, D. V., Bonn, B., & Carslaw, K. S. (2008). Boreal forests, aerosols and the impacts on clouds and climate. *Philosophical Transactions of the Royal Society A: Mathematical, Physical and Engineering Sciences*, *366*(1885), 4613–4626. https://doi.org/10.1098/rsta.2008.0201
Stępalska, D., & Wołek, J. (2009). Intradiurnal periodicity of fungal spore concentrations (Alternaria, Botrytis, Cladosporium, Didymella, Ganoderma) in Cracow, Poland. *Aerobiologia*, *25*(4), 333–340. https://doi.org/10.1007/s10453-009-9137-3
Stoy, P. C., Mauder, M., Foken, T., Marcolla, B., Boegh, E., Ibrom, A., et al. (2013). A data-driven analysis of energy balance closure across FLUXNET research sites: The role of landscape scale heterogeneity. *Agricultural and Forest Meteorology*, *171–172*, 137–152. https://doi.org/10.1016/j.agrformet.2012.11.004
Stull, R. B. (1988). *An Introduction to Boundary Layer Meteorology*. Dordrecht: Kluwer Academic Publishers. https://doi.org/10.1007/978-94-009-3027-8
Stull, R. B. (1991). Static stability - an update. *Bulletin - American Meteorological Society*, *72*(10), 1521–1529.
Stull, R. B. (2006). The Atmospheric Boundary Layer. In J. M. Wallace & P. V Hobbs (Eds.), *Atmospheric science: an introductory survey* (Second, Vol. 92, pp. 375–418). London: Elsevier.
Su, H. B., Schmid, H. P., Vogel, C. S., & Curtis, P. S. (2008). Effects of canopy morphology and thermal stability on mean flow and turbulence statistics observed inside a mixed hardwood forest. *Agricultural and Forest*

Meteorology, *148*(6–7), 862–882. https://doi.org/10.1016/j.agrformet.2007.12.002

Su, Hong Bing, Shaw, R. H., Pawu, K. T., Moeng, C. H., & Sullivan, P. P. (1998). Turbulent statistics of neutrally stratified flow within and above a sparse forest from large-eddy simulation and field observations. *Boundary-Layer Meteorology*, *88*(3), 363–397. https://doi.org/10.1023/A:1001108411184

Sun, J., Mahrt, L., Banta, R. M., & Pichugina, Y. L. (2012). Turbulence regimes and turbulence intermittency in the stable boundary layer: During CASES-99. *Journal of the Atmospheric Sciences*, *69*(1), 338–351. https://doi.org/10.1175/JAS-D-11-082.1

Sun, J., Nappo, C. J., Mahrt, L., Belušic, D., Grisogono, B., Stauffer, D. R., et al. (2015). Review of wave-turbulence interactions in the stable atmospheric boundary layer. *Reviews of Geophysics*, *53*(3), 956–993. https://doi.org/10.1002/2015RG000487

Szendrei, Z., & Rodriguez-Saona, C. (2010). A meta-analysis of insect pest behavioral manipulation with plant volatiles. *Entomologia Experimentalis et Applicata*, *134*(3), 201–210. https://doi.org/10.1111/j.1570-7458.2009.00954.x

Tadrist, L., Saudreau, M., Hémon, P., Amandolese, X., Marquier, A., Leclercq, T., & de Langre, E. (2018). Foliage motion under wind, from leaf flutter to branch buffeting. *Journal of the Royal Society Interface*, *15*(142). https://doi.org/10.1098/rsif.2018.0010

Taubert, F., Fischer, R., Groeneveld, J., Lehmann, S., Müller, M. S., Rödig, E., et al. (2018). Global patterns of tropical forest fragmentation. *Nature*, *554*(7693), 519–522. https://doi.org/10.1038/nature25508

Telewski, F. W. (2009). Wind-induced physiological and developmental responses in trees. In *Wind and Trees* (pp. 237–263). Cambridge University Press. https://doi.org/10.1017/cbo9780511600425.015

Telewski, F. W., & Pruyn, M. L. (1998). Thigmomorphogenesis: A dose response to flexing in Ulmus americana seedlings. *Tree Physiology*, *18*(1), 65–68. https://doi.org/10.1093/treephys/18.1.65

Thom, A. S. (1971). Momentum absorption by vegetation. *Quarterly Journal of the Royal Meteorological Society*, *097*(414), 414–428. https://doi.org/10.1256/smsqj.41403

Tóta, J., Roy Fitzjarrald, D., & Da Silva Dias, M. A. F. (2012). Amazon rainforest exchange of carbon and subcanopy air flow: Manaus LBA SiteA complex terrain condition. *The Scientific World Journal*, *2012*. https://doi.org/10.1100/2012/165067

Villani, M. G., Schmid, H. P., Su, H. B., Hutton, J. L., & Vogel, C. S. (2003). Turbulence statistics measurements in a northern hardwood forest. *Boundary-Layer Meteorology*, *108*(3), 343–364. https://doi.org/10.1023/A:1024118808670

Virot, E., Amandolese, X., & Hémon, P. (2013). Fluttering flags: An experimental study of fluid forces. *Journal of Fluids and Structures*, *43*, 385–401. https://doi.org/10.1016/j.jfluidstructs.2013.09.012

Visakorpi, K., Gripenberg, S., Malhi, Y., Bolas, C., Oliveras, I., Harris, N., et al. (2018). Small-scale indirect plant responses to insect herbivory could have major impacts on canopy photosynthesis and isoprene emission. *New Phytologist*, *220*(3), 799–810. https://doi.org/10.1111/nph.15338

Vogel, C. S. (1968). " Sun Leaves " and " Shade Leaves ": Differences in Convective Heat Dissipation Author (s): Steven Vogel Published by : Ecological Society of America Stable URL : http://www.jstor.org/stable/1934517 . *Ecology*, *49*(6), 1203–1204.

Vogel, C. S. (1989). *Drag and Reconfiguration of Broad Leaves in High Winds*. *Journal of Experimental Botany* (Vol. 40). Retrieved from https://academic.oup.com/jxb/article-abstract/40/8/941/605983

Vogel, C. S. (2009). Leaves in the lowest and highest winds: Temperature, force and shape: Tansley review. *New Phytologist*, *183*(1), 13–26. https://doi.org/10.1111/j.1469-8137.2009.02854.x

Vogel, C. S. (2020). *Life in Moving Fluids: The Physical Biology of Flow-Revised and Expanded Second Edition*. Princeton University Press.

Wang, B., Shugart, H. H., & Lerdau, M. T. (2017). An individual-based model of forest volatile organic compound emissions—UVAFME-VOC v1.0. *Ecological Modelling*, *350*, 69–78. https://doi.org/10.1016/j.ecolmodel.2017.02.006

Wang, D., Momo Takoudjou, S., & Casella, E. (2020). LeWoS: A universal leaf-wood classification method to facilitate the 3D modelling of large tropical trees using terrestrial LiDAR. *Methods in Ecology and Evolution*, *11*(3), 376–389. https://doi.org/10.1111/2041-210X.13342

Watanabe, T. (2004). Large-eddy simulation of coherent turbulence structures associated with scalar ramps over plant canopies. *Boundary-Layer Meteorology*, *112*(2), 307–341. https://doi.org/10.1023/B:BOUN.0000027912.84492.54

Watanabe, T., Shimoyama, K., Kawashima, M., Mizoguchi, Y., & Inagaki, A. (2020). Large-Eddy Simulation of Neutrally-Stratified Turbulent Flow Within and Above Plant Canopy Using the Central-Moments-Based Lattice Boltzmann Method. *Boundary-Layer Meteorology*, *176*(1), 35–60. https://doi.org/10.1007/s10546-

020-00519-8
Way, D. A., & Pearcy, R. W. (2012). Sunflecks in trees and forests: From photosynthetic physiology to global change biology. *Tree Physiology*, *32*(9), 1066–1081. https://doi.org/10.1093/treephys/tps064
Webb, V. A., & Rudnicki, M. (2009). A linear analysis of the interaction between the atmosphere and an underlying compliant plant canopy. *Boundary-Layer Meteorology*, *133*(1), 93–111. https://doi.org/10.1007/s10546-009-9417-z
Wharton, S., Ma, S., Baldocchi, D. D., Falk, M., Newman, J. F., Osuna, J. L., & Bible, K. (2017). Influence of regional nighttime atmospheric regimes on canopy turbulence and gradients at a closed and open forest in mountain-valley terrain. *Agricultural and Forest Meteorology*, *237–238*, 18–29. https://doi.org/10.1016/j.agrformet.2017.01.020
Whitaker, S. (1973). The transport equations for multi-phase systems. *Chemical Engineering Science*, *28*(1), 139–147. https://doi.org/10.1016/0009-2509(73)85094-8
Whitmore, T. C. (1989). Canopy Gaps and the Two Major Groups of Forest Trees. *Ecology*, *70*(3), 536–538.
Wicker, L. J., & Skamarock, W. C. (2002). Time-splitting methods for elastic models using forward time schemes. *Monthly Weather Review*, *130*(8), 2088–2097. https://doi.org/10.1175/1520-0493(2002)130<2088:TSMFEM>2.0.CO;2
Wilson, K., Goldstein, A., Falge, E., Aubinet, M., Baldocchi, D. D., Berbigier, P., et al. (2002). Energy balance closure at FLUXNET sites. *Agricultural and Forest Meteorology*, *113*(1–4), 223–243. https://doi.org/10.1016/S0168-1923(02)00109-0
Wilson, N. R., & Shaw, R. H. (1977). A higher order closure model for canopy flow. *Journal of Applied Meteorology*, *16*(11, Nov.1977), 1197–1205. https://doi.org/10.1175/1520-0450(1977)016<1197:ahocmf>2.0.co;2
With, K. A. (2002). The landscape ecology of invasive spread. *Conservation Biology*, *16*(5), 1192–1203. https://doi.org/10.1046/j.1523-1739.2002.01064.x
Wohlfahrt, G., Anfang, C., Bahn, M., Haslwanter, A., Newesely, C., Schmitt, M., et al. (2005). Quantifying nighttime ecosystem respiration of a meadow using eddy covariance, chambers and modelling. *Agricultural and Forest Meteorology*, *128*(3–4), 141–162. https://doi.org/10.1016/j.agrformet.2004.11.003
Wolfe, G. M., Thornton, J. A., Mckay, M., & Goldstein, A. (2011). Forest-atmosphere exchange of ozone: sensitivity to very reactive biogenic VOC emissions and implications for in-canopy photochemistry. *Atmos. Chem. Phys*, *11*, 7875–7891. https://doi.org/10.5194/acp-11-7875-2011
Xu, X., Yi, C., & Kutter, E. (2015). Stably stratified canopy flow in complex terrain. *Atmospheric Chemistry and Physics*, *15*(13), 7457–7470. https://doi.org/10.5194/acp-15-7457-2015
Yan, C., Huang, W. X., Miao, S., Cui, G., & Zhang, Z.-S. (2017). Large-Eddy Simulation of Flow Over a Vegetation-Like Canopy Modelled as Arrays of Bluff-Body Elements. *Boundary-Layer Meteorology*, *165*, 233–249. https://doi.org/10.1007/s10546-017-0274-x
Yan, C., Miao, S., Liu, Y., & Cui, G. (2020). Multiscale modeling of the atmospheric environment over a forest canopy. *Science China Earth Sciences*. https://doi.org/10.1007/s11430-019-9525-6
Yang, B., Raupach, M. R., Shaw, R. H., U, K. T. P., & Morse, A. P. (2006). Large-eddy simulation of turbulent flow across a forest edge. Part I: Flow statistics. *Boundary-Layer Meteorology*, *120*(3), 377–412. https://doi.org/10.1007/s10546-006-9057-5
Yang, B., Morse, A. P., Shaw, R. H., & Paw U, K. T. (2006). Large-eddy simulation of turbulent flow across a forest edge. Part II: Momentum and turbulent kinetic energy budgets. *Boundary-Layer Meteorology*, *121*(3), 433–457. https://doi.org/10.1007/s10546-006-9083-3
Yue, W., Parlange, M. B., Meneveau, C., Zhu, W., van Hout, R., Katz, J., et al. (2007). Large-eddy simulation of plant canopy flows using plant-scale representation, *124*, 183–203. https://doi.org/10.1007/s10546-007-9173-x
Zellweger, F., De Frenne, P., Lenoir, J., Vangansbeke, P., Verheyen, K., Bernhardt-Römermann, M., et al. (2020). Forest microclimate dynamics drive plant responses to warming. *Science*, *368*(6492), 772 LP – 775. https://doi.org/10.1126/science.aba6880
Zeng, P., & Takahashi, H. (2000). A first-order closure model for the wind flow within and above vegetation canopies. *Agricultural and Forest Meteorology*, *103*(3), 301–313. https://doi.org/10.1016/S0168-1923(00)00133-7
Zeri, M., Rebmann, C., Feigenwinter, C., & Sedlák, P. (2010). Analysis of periods with strong and coherent CO2 advection over a forested hill. *Agricultural and Forest Meteorology*, *150*(5), 674–683. https://doi.org/10.1016/j.agrformet.2009.12.003
Zhao, F., Yang, X., Schull, M. A., Román-Colón, M. O., Yao, T., Wang, Z., et al. (2011). Measuring effective leaf area index, foliage profile, and stand height in New England forest stands using a full-waveform ground-based

lidar. *Remote Sensing of Environment*, *115*(11), 2954–2964. https://doi.org/10.1016/j.rse.2010.08.030
Zhong, J., Cai, X., & Bloss, W. J. (2016). Coupling dynamics and chemistry in the air pollution modelling of street canyons: A review. *Environmental Pollution*, *214*, 690–704. https://doi.org/10.1016/j.envpol.2016.04.052
Zhong, J., Nikolova, I., Cai, X., Mackenzie, A. R., & Harrison, R. M. (2018). Modelling traffic-induced multicomponent ultrafine particles in urban street canyon compartments: Factors that inhibit mixing. *Environmental Pollution*, *238*, 186–195. https://doi.org/10.1016/j.envpol.2018.03.002
Zhu, J., Zhang, G., Wang, G. G., Yan, Q., Lu, D., Li, X., & Zheng, X. (2015). On the size of forest gaps: Can their lower and upper limits be objectively defined? *Agricultural and Forest Meteorology*, *213*, 64–76. https://doi.org/10.1016/j.agrformet.2015.06.015
Zohner, C. M., Mo, L., Pugh, T. A. M., Bastin, J.-F., & Crowther, T. W. (2020). Interactive climate factors restrict future increases in spring productivity of temperate and boreal trees. *Global Change Biology*, *26*(7), 4042–4055. https://doi.org/10.1111/gcb.15098